

Accepted Manuscript

Selenium Nanomaterials: An Overview of Recent Developments in Synthesis, Properties and Potential Applications

Savita Chaudhary, Ahmad Umar, S.K. Mehta

PII: S0079-6425(16)30030-5

DOI: <http://dx.doi.org/10.1016/j.pmatsci.2016.07.001>

Reference: JPMS 407

To appear in: *Progress in Materials Science*

Received Date: 9 August 2014

Revised Date: 30 May 2015

Accepted Date: 6 July 2016



Please cite this article as: Chaudhary, S., Umar, A., Mehta, S.K., Selenium Nanomaterials: An Overview of Recent Developments in Synthesis, Properties and Potential Applications, *Progress in Materials Science* (2016), doi: <http://dx.doi.org/10.1016/j.pmatsci.2016.07.001>

This is a PDF file of an unedited manuscript that has been accepted for publication. As a service to our customers we are providing this early version of the manuscript. The manuscript will undergo copyediting, typesetting, and review of the resulting proof before it is published in its final form. Please note that during the production process errors may be discovered which could affect the content, and all legal disclaimers that apply to the journal pertain.

Selenium Nanomaterials: An Overview of Recent Developments in Synthesis, Properties and Potential Applications

Savita Chaudhary^{a,*,\$}, Ahmad Umar^{b,c,*,\$} and S.K. Mehta^a

^a*Department of Chemistry and Centre of Advanced Studies in Chemistry, Panjab University, Chandigarh 160014, India*

^b*Promising Centre for Sensors and Electronic Devices (PCSED), Najran University, P.O. Box 1988, Najran 11001, The Kingdom of Saudi Arabia*

^c*Department of Chemistry, College of Science and Arts, Najran University, P.O. Box 1988, Najran 11001, The Kingdom of Saudi Arabia*

***Dr Savita Chaudhary**
E-mail: schaudhary@pu.ac.in

***Prof. Ahmad Umar**
E-mail: ahmadumar786@gmail.com

Tel.: +966-534574597

\$Both authors contributed equally to this work

Abstract

Advances in science and nanotechnology have facilitated the development of new methods for the preparation of pure selenium as selenium nanomaterials. They offer remarkable potential for technological applications in the fields of medicine, diagnostics, therapeutics, toxicology, electronics, catalysis and so on. Moreover, selenium nanomaterials also find applications in photographic exposure metres, rectifiers, signal emitting devices and transmitting devices, because of their unique structural, optical and electronic properties. This study describes a detailed advanced report on the synthesis, assembly, characterization and various applications of selenium nanomaterials. In addition, relevant synthesis methods, properties, challenges and opportunities associated with selenium nanomaterials are also presented.

Keywords: Selenium nanomaterials, Synthesis; electronic; optical properties; therapeutic; diagnostic

Contents:**1. Introduction****2. Historical developments of selenium****3. Synthesis of selenium nanomaterials**

3.1. Photocatalytic synthesis

3.2. Pulsed laser ablation method

3.3. Vapour deposition technique

3.4. Electrochemical methods

3.5. Biosynthetic method

3.6. Hydrothermal and Solvothermal techniques

3.7. Synthesis in a constrained environment

3.7.1. Using polymers

3.7.2. Surfactant-mediated synthesis

3.8. Microwave-assisted synthesis

3.9. Other methods

4. Properties of selenium nanomaterials

4.1. Shape and structure of selenium nanomaterials

4.2. Catalytic properties

4.3. Electrochemical properties

4.4. Optical properties

4.4.1. Quantum Mechanical Treatments

4.5. Thermal Properties

5. . Toxicity of selenium nanomaterials

- 5.1. Effect of Se nanoparticles on cytotoxicity assays
- 5.2. Significance of dose
- 5.3. Effect of morphology
- 5.4. Effect of size
- 5.5. Value of functionalization

6. Potential applications of selenium nanomaterials

- 6.1. Diagnostics and therapy
- 6.2. Antagonistic effect of selenium on minerals
- 6.3. Electronic applications of selenium nanomaterials
- 6.4. Selenium nanoparticle-based DMFCs
- 6.5. Selenium nanomaterials for chemical sensor applications

7. Summary and future prospects**Acknowledgements****References****Authors Biographies****Schemes****Figures****Tables**

1. Introduction

Selenium (Se), an element of the chalcogenide group, has been extensively used in various industries such as medicinal,^{1–4} chemical,⁵ electrical and electronics,⁶ ceramic,⁷ metallurgical,^{8–10} and glass making.^{11–14} Used widely for the fabrication of pigments,¹¹ selenium has also been utilized for the compounding of rubber,¹⁵ manufacturing of rectifiers,¹⁶ and as an alloying element to improve the machinability of copper alloys and stainless steel.^{17,18} Electrical resistance changes under light irradiation were first found in selenium in 1873.^{19,20} Se is also considered an important material for laser printing, photovoltaic cells, fuel cells, X-ray instruments and so on.^{21–24} Notably, a trace amount of selenium is essential for proper cellular and metabolic functioning in all animals,²⁵ and various studies have revealed the health-endorsing properties of selenium.^{26,27} It efficiently advances the restorative competence and selectivity of anticancer drugs,²⁸ and has many useful applications in nutritional complement drugs.²⁹ Because of its biological importance, selenium is comprehensively used in pharmaceutics,^{30–39} and is also considered one of the important constituents for regulating spermatogenesis, whose deficiency may have adverse effects on sperm quality.^{40–42} In addition, selenium has also been revealed as a crucial component in the fields of agriculture and horticulture.³⁰

Recent advances in nanotechnology have facilitated the production of pure selenium as selenium nanoparticles.^{31–35} The strong electron-contributing tendency of selenium is significantly enhanced in the nanoscale.^{36,37} Photostability and decreased photo-assisted deterioration have directed the use of selenium nanoparticles in photocatalysis.³⁸ Selenium is also used for generating chemically doped, industrially significant materials.⁴¹

This study focuses on the recent advances in the synthesis, assembly, characterization and applications of selenium nanomaterials prepared by various techniques. Furthermore, the roles of various physiochemical characteristics, such as particles shapes and sizes, anisotropy, exterior surface area and functionalization, on the electronic, catalytic and biological properties of Se nanomaterials are extensively reviewed. Finally, various potential applications of Se nanomaterials, such as in diagnostics and therapy, electronic devices, catalysts, chemical sensors and other specific applications, are presented.

2. Historical developments of selenium

The position of Se in the periodic table explains its biological interfaces with sulphur, arsenic and its neighbour phosphorus.^{43,44} Scientific investigation on Se was started way back in 1817 at Uppsala University, Sweden, and the first report on its dual character was published by Berzelius in 1818.^{45,46} Afterwards, numerous studies^{18,29,47–53} demonstrated the development of selenium research and the discoveries that have shaped the current knowledge in this field. Bock and Stadtman⁵⁴ laid the foundation by studying seleno-cysteins, while a narrative description of seleno-proteins was given by Flohe^{55,56} in *The Labour Pains of Biochemical Selenology: The History of Selenoproteins Biosynthesis*. Previous studies primarily highlighted the potential uses of Se for human health or examined the toxicities of Se compounds.^{57, 58} However, in this study, we review the recent information on the synthesis, characterization, properties and various applications of Se nanoparticles. This study provides a complete summary of Se nanoparticles from their growth to applications in various high-technological areas of science and technology.

3. Synthesis of selenium nanomaterials

Because of its colloidal nature, synthetic routes for the preparation of Se nanomaterials are quite complicated, and it is still quite challenging to produce mono-disperse Se nanomaterials with adjusted size. Further, the complicated synthetic routes also restrict their commercialization.^{59–61}

The synthesis techniques can be broadly divided into three main groups:

- (i) Physical processes,
- (ii) Chemical techniques and
- (iii) Solid-state syntheses.

The literature revealed that various architectures of Se nanomaterials can be prepared via specific synthesis techniques; therefore, by using precise synthesis techniques, particular morphologies of Se nanomaterials can be obtained.

3.1. Photocatalytic synthesis

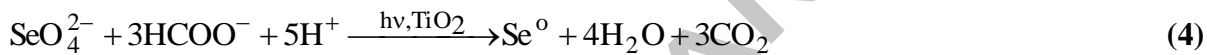
Photocatalytic synthesis is an important technique to produce size-controlled Se nanoparticles at ambient temperatures. The literature reveals that such photocatalytic reactions safely occur within a few seconds with high controllability over the sizes of produced nanoparticles.^{62–71} The most important characteristic of the photocatalytic processes is that the inorganic wastes produced during the course of reactions are converted into less-toxic side products.

Triantis et al.⁶² used the photocatalytic process for the production of selenium nanoparticles using polyoxometalate (POM) anions (**Fig. 1**). The unique redox properties of POM, because of the presence of various oxygen-bridged metal clusters, support the liberation of electrons in distinct steps without undergoing any kind of disintegration, as shown in the equations presented below.^{63–69}

.....**Figure 1**.....

It was also observed that under irradiation conditions, with controlled pH, the POM anions acted as powerful oxidants for selenium salt (Na_2SeO_3). Triantis et al.⁶² presented detailed investigations on various experimental factors such as reactant concentrations, ionic strength and the nature of POM on the growth of selenium nanoparticles.

Nguyen et al.⁷⁰ investigated the photocatalytic synthesis of Se nanoparticles via reduction of Se(IV) and Se(VI) ions using commercially available TiO_2 powders (Millennium PC-500 and PC50) as photocatalysts. The corresponding chemical reactions are described by the following chemical equations:



In brief, as a photocatalyst, TiO_2 can reduce metal salts to their elemental form, and then be readily recovered.⁷¹ The increased surface area of the photocatalyst enhances the particle formation process. The correlation between the photoreduction rates and increased adsorption was also monitored when comparing the photoreduction of two ions. Moreover, the method improves the conversion of organic contaminants into their less-toxic states.⁷² TiO_2 -supported photocatalysis of selenium salts, therefore, is favourable for nanoparticle synthesis at ambient conditions. Unfortunately, the major problem in this process is the generation of heterogeneous particles in an individual reaction. In order to overcome this drawback, a few size-controlling strategies were presented by altering the reaction conditions.^{69,73} Yang et al.⁷³ demonstrated the size-controlled synthesis of Se nanoparticles via the reduction of selenious acid (H_2SeO_3) by ultraviolet (UV) irradiation of tungsto-silicate acid ($\text{H}_4\text{SiW}_{12}\text{O}_{40}$, TSA) solution. During the reactions, the TS ions were formed as a subset of POMs of Keggin structure with common

prescription as $(XM_{12}O_{40})^{(8-n)-}$, where M represents the element W or Mo, X denotes heteroatoms such as P, Si and Ge and n refers to the valencies of X. In these reactions, the TSA played dual roles: reducing and stabilizing the formed particles.

Yang et al.⁷³ also studied the distinctive catalytic activities of the as-synthesized Se nanoparticles by investigating the decolourization of Congo red dye in the presence of UV light. They observed that the as-synthesized Se nanoparticles catalyse the reaction more effectively. In addition, particle size has a significant effect on the decolourization of dyes, and it was observed that the rate of decolourization decreases with larger particles. This fact can be explained by the smaller total surface area.^{74,75} Thus, particle size is an important parameter for improving highly competent Se-supported catalysts for decolourization of dyes.

Maldotti⁷⁶ conducted a study on photo-induced processes. The as-synthesized nanoparticles were efficiently used in the oxidation of fine chemicals under mild conditions for water treatment, photodynamic bactericidal inactivation or photodynamic therapy. The generation, diffusion and reactivity of reactive oxygen species (ROS), and particularly of singlet oxygen (1O_2) in these nanostructured materials were also discussed by Maldotti. Shi et al.⁷⁷ presented the photocatalytic synthesis of Se nanotubes, nanowires, nanobelts, nanorods and nanoflakes. Recently, Fujishima et al.⁷⁸ have synthesized Se quantum dots (QDs) using a current doubling-induced two-step photocatalytic deposition (CD-2PD). The as-synthesized Se QDs were used for removing organic pollutants from water under UV and visible light irradiations.

O'Connor and co-workers⁷⁹ investigated the synthesis of Se nanocrystals via a photocatalytic process and demonstrated that the process has a significant impact on the exciton dynamics of the nanoparticles. Youn et al.⁸⁰ used the combinations of phase transition and

photocatalytic reactions to prepare size-controlled Se and Se carbon nanotubes (CNTs) and nanocomposites.

3.2. Pulsed laser ablation method

Recently, the use of pulsed laser ablation method for preparing Se nanoparticles/QDs has received much attention.^{81–88} Quintana et al.⁸¹ synthesized Se nanoparticles using a YAG laser with a harmonic wavelength of 532 nm. The experimental conditions were as follows: power density = 10^8 W/cm², pulse rate = 10 ns and spot dimension = 2 mm². The corresponding size, shape and density of Se nanoparticles can be easily controlled by modifying the reaction parameters, such as energy density, substrate temperature and laser pulses, during the course of synthesis. Jiang et al.⁸² reported a direct and scalable process for the synthesis of highly pure trigonal selenium (t-Se) nanorods of different sizes by using a Nd:YAG laser (Quantary DCR 130) with wavelength and pulse duration of 1064 nm and 7 ns, respectively. It was observed that the reaction temperature has a significant effect on the morphologies. This method was helpful in describing reaction conditions for the formation of Se nanorods on the walls of the quartz tube. By decreasing the temperature from 300°C to room temperature, three different morphologies were found: micro-sized Se rods at 300°C, nanorods (20–300 nm) at 220–110°C and small nanoparticles (≤ 10 nm) at $< 110^\circ\text{C}$. During the synthesis, no catalyst, additive, or template was used, and hence the Se nanomaterials produced are highly purity.

Yu et al.⁸⁹ synthesized a heterogeneous mixture of Li₂Se–Sb₂Se₃ nanocomposite using a 355-nm laser beam with repetition rate of 10 Hz at 45°. The corresponding distance between the target and substrate was 4 cm with a pulse width of 10 ns. The obtained nanocomposite exhibited excellent reversibility in the de-lithiation and lithiation processes with voltage ranging from 1.7

to 3.5 V. Morales and Lieber^{90a} combined the laser ablation process with the vapour–liquid–solid (VLS) method to prepare high-density Se nanowires with diameter and length ranging from 3 to 9 nm and 1 to 30 μm , respectively. Mendivil et al.^{90b} used fundamental (1064 nm) and second harmonic (532 nm) outputs from a Q-switched Nd:YAG laser to produce nanocomposites of Cu, In, Ga and Se in various liquid solutions. The corresponding effects of laser fluence and ablation wavelengths were also studied to optimize the product.

Singh et al.⁹¹ demonstrated the preparation of Se QDs using laser-based melting/vaporization of water-dispersed larger particles (**Fig. 2**). The irradiation time has a significant impact on the size, shape, energy levels, surface defects and phase structures of particles. The mechanism was correlated with reduction of surface energy of large particles into QDs with laser beam.

-----Figure 2-----

Selenium–tungsten (Se–W) nanocomposites were also prepared using a shadow masked pulsed laser deposition technique.⁹² The comparison of synthetic parameters including deposition rate and ion bombardment dose suggested that an ion-to-atom ratio of 0.1 was optimum for particle synthesis.

Jeong et al.⁹³ used KrF excimer with wavelength and pulse width of 248 nm 30 ns, respectively, to prepare nanocomposites of Cu, In and Se. This method resolved the problem of interstitial site formation during the reaction process. The transition metal dichalcogenide nanocomposites were also synthesized by using a wavelength, energy density, pulse energy and repetition rate of 1064 nm, $\sim 20 \text{ J/cm}^2$, $\sim 50 \text{ mJ}$ and 25 Hz, respectively.⁹⁴ Recently, an electro-optically Q-switched Nd:yttrium–aluminium–garnet laser with a harmonic wavelength of 1.06 μm has been used with a spot dimension, pulse duration, repetition rate and pulse energy of ~ 7.5

J/cm², 15 ns, ~25 Hz and 30 mJ to prepare nanocomposites of Mo, Ni, C and Se.⁹⁵ The modified process has a significant impact on the degree of crystallization of Mo and Se phases with better control over the shape, size and surface properties of the as-generated nanoparticles.

3.3. Vapour deposition technique

The desired shapes and sizes of pure Se and their corresponding nanocomposites have also been synthesized by chemical vapour deposition (CVD) technique.^{96–108} Ren et al.¹⁰⁹ described the growth of Se nanowires from bulk powder under argon gas atmosphere. The temperature and the nature of catalysts such as Cu, Fe, Ni and Si have a significant impact on the nucleation rate of the nanowires (**Fig. 3**).

-----Figure 3-----

Various diameters of Se nanowires, for example, 75, 83 and 90 nm, were generated at different temperatures such as 750, 850 and 950°C, respectively. The thermodynamics of the system was analysed by Gibbs–Thompson formula:

$$r_c = \frac{v_\sigma}{kT} \left(\ln \frac{P}{P_s} \right)^{-1}, \quad (5)$$

where r_c is the critical radius of a nucleus, which corresponds to the molecular volume, k is the Boltzmann constant, P is the pressure of the reaction site, T is the temperature and v_σ is the surface specific energy of the nucleus. It is apparent from this equation that the critical radius of the nucleus decreases with increasing reaction temperature. The uniform nucleation rate was assessed using the following equation:

$$N = 4\pi r_c^2 \Phi n_s \exp\left(\frac{-\Delta G^*}{KT}\right), \quad (6)$$

where Φ is the atom impingement flux, n_s is the site of nucleation and ΔG^* denotes the energy barrier to the nucleation. A comparison of Eqs. 5 and 6 shows that the solid phase with a larger nuclei and higher coalescence rate was formed at higher temperature.

Cao et al.¹¹⁰ explained the growth and characterization of single-crystalline ultrathin t-Se nano-ribbons (thickness of approximately 15 nm and length up to several hundreds of micrometres) towards c-axis. This approach was also appropriate for the growth of crystalline and pure Se-based nanocomposites with modified sizes and composition. Cho et al.¹¹¹ developed a non-vacuum deposition process for the preparation of Cu, In and Se nanocomposites using hybrid ink. The as-prepared material exhibits a higher stress relief and diminished crack deflection properties. Uhl et al.¹¹² also used the non-vacuum chemical deposition technique to prepare highly porous nanocomposites of Se with Cu, In and Ga. The obtained composites exhibit a higher solar energy conversion efficiency of approximately 5.8%.

3.4. Electrochemical methods

Electrochemical method is one of the well-accepted environmentally friendly approaches for the synthesis of Se nanomaterials with high selectivity. Hodes's group significantly contributed to the synthesis of size- and shape-controlled semiconducting QDs on metal substrates using the electrodeposition process in non-aqueous solutions.^{113–116} In addition, the temperature and current densities have also influenced the morphologies of the as-prepared materials.^{117–124}

Zhang et al.¹²⁵ synthesized the single-crystalline Se nanotubes over the exterior surface of Au electrode in the presence of cetyltrimethyl ammonium bromide (CTAB) by cyclic voltammetric technique. The nanotubes were generated by the reduction of Se(IV) to Se(0) in the presence of colloidal templates of CTAB. Being positively charged, the radicals of CTAB united with the

anionic species of Se reactants HSeO^{3-} or SeO_3^{2-} and formed the joint radicals. These combined radicals provide the electron pathway for the reduction process over the electrode surface. The concentration of surfactant plays a significant role in the modification of morphology of the particles from spherical to rod-shaped. These morphological changes of particles can be explained based on rod-shaped micelle development of CTAB at higher concentration. The corresponding growth of Se particles occurred through the deposition of nanoparticles at the electrode tip.¹²⁶ As the concentration of Se atoms increases, they tend to adsorb at the circumferential peripheries because of the increased free energy over these sites.¹²⁷

The under-potential depositions of Cd over Se particles were studied by Cabral et al.¹²⁸ via electrochemical process. The generated particles could efficiently be used for various future electronic, laser and solar cell devices. Zhao et al.¹²⁹ prepared W-doped Co–Se nanocomposites with high catalytic efficiency for oxygen reduction. Recently, Saji and Lee¹³⁰ have studied the electrochemical behaviour of Se nanoparticles using the electrochemical atomic layer epitaxy (ECALE) technique. Mahmoodi et al.¹³¹ investigated the AC electrokinetic behaviour of Se nanoparticles. The as-used electrochemical strategy was identified as one of the useful methods for separation, alignment and positioning of microscopic objects. Furthermore, the low working voltage, minimum effect on electrolysis and chemical reactions have made this technique more useful for generating Se nanoparticles.¹³² Dembinska et al.¹³³ investigated the improvement in the oxygen-reducing activities of fuel cells by using Ru- and Ir-based Se nanocomposites. These fuel cells represent better alternative sources of electrochemical energy and also possess the ability to reduce oxygen over higher potentials, with a relatively more negative potential than the standard platinum as catalyst. Gao et al.¹³⁴ reported the synthesis and catalytic role of Se nanocomposites in energy conversion and storage devices. Liu and co-workers¹³⁵ performed a

detailed analysis of synthetic parameters such as size, ligand and composition on the band gap modification of electrochemically generated nanocomposites. Such methods have provided more information on the electroactive species and their electronic behaviour in the particles. The schematic variation of electron removal from valence band and the corresponding injection of electron in conduction bands are depicted in **Scheme 1**.

-----**Scheme 1**-----

This is a very simple, cost-effective and facile technique, in which tuneable sizes, compositions, surface structure and properties of specific nanomaterials can be varied by controlling the reaction parameters. Moreover, modifications in electrochemical reactions can also affect the productivity and yield of particles.

3.5. Biosynthetic method

Biosynthesis is a facile, safe, biocompatible, eco-friendly and recyclable way of preparing Se nanomaterials. The properties, size and morphology of nanoparticles can be easily controlled by changing the incubation temperature, pH, reaction time, metal ion concentrations and the quantity of organic material. At present, various microorganisms, such as bacteria, yeast, fungi and some biofriendly agents, have been considered as eco-friendly green nanofactories for the fabrication of Se nanomaterials. Selenium occurs in multiple oxidation states, for example, +6 and +4, 0 or -2. The toxicity of respective states depends on the rate of solubility in water and their bio-accessibility.^{136,137} Elemental or red amorphous Se and selenate (SeO_4^{2-})/selenite (SeO_3^{2-}) ions possess remarkably high water solubility. Amongst the classified selenium species, selenite (SeO_3^{2-}) reduction has been the subject of significant consideration for microbial reduction, because of its high lethal activity.¹³⁸⁻¹⁴⁰

Se-respiring bacteria such as *Sulfurospirillum barnesii*, *Bacillus selenitireducens* and *Selenihalanaerobacter shriftii* were used by Oremland et al.¹⁴¹ to prepare structurally different low band gap Se nanoparticles as compared to chemically synthesized Se. Synthesis of m-Se nanoparticles under ambient temperature, pressure and pH conditions was carried out on a large scale by Wang et al.¹⁴² using the *Bacillus subtilis* microbes. The protein and other biomolecules excreted from *B. subtilis* are responsible for the stability of the as-formed particles. The synthesized particles were used for the production of Horseradish peroxidase (HRP) biosensor with higher electrocatalytic activity for the reduction of H₂O₂, because of the excellent bonding ability and biocompatibility of nanomaterials.

Yadav et al.¹⁴³ carried out the biosynthesis of Se nanoparticles using the aerobic bacterium *Pseudomonas aeruginosa* (SNT1). Dungan et al.¹⁴⁴ reported the growth of Se nanostructures with *Stenotrophomonas maltophilia*. These nanoparticles were also prepared using *Enterobacter taylorae*.¹⁴⁵ The biotransformation of selenium in the culture medium of *Enterobacter cloacae* cells generated Se⁰ with diameter <0.1 μm.¹⁴⁶ The probability of vesicular method for the bioconversion of Se⁰ was calculated by Kessi group.¹⁴⁷ Switer-Blum et al.¹⁴⁸ inspected the development of small nanospheres of Se on the cell surface of a Gram-positive rod, the *Bacillus selenireducens* strain MLSIO. Aerobic biosynthesis using *Bacillus cereus* from coalmine soil was carried out by Dhanjal and Cameotra.¹⁴⁹ The activity of the soluble fraction of selenite ion was also reduced after incubation. This phenomenon is described based on the non-specific reduction of the ions by the reductase protein(s) associated with the bacterial membranes.

Anaerobic biogenesis using *Shewanella sp. HN-41* was conducted by Tam et al.¹⁵⁰ The reaction parameters such as duration of reaction, preliminary amount of biomass and selenite quantity have a direct effect on particle size. Under aerobic conditions, Bajaj et al.¹⁵¹ reported the

formation of spherical Se^0 nanoparticles using *Duganella sp* and *Agrobacterium sp* from Se-laden soil of Punjab, India. *Tetrathiobacter kashmirensis* strain CA1 was used by Hunter and Manter¹⁵² for the bio-reduction of selenite to elemental red selenium.

The effects of liquefied oxygen on the removal of extracellular Se have also been examined by using *Saccharomyces cerevisiae*.¹⁵³ The comparative results of aerobic and anaerobic conditions on particle formation clearly point towards the necessity of an oxygen-restricted atmosphere for selenite reduction. The extraction of *in vivo*-synthesized particles was also achieved for the first time by using the vesicle-like structures in micro-aerophilic surroundings.¹⁵³ The *S. maltophilia* strain SELTE02 from rhizospheric soil of *Astragalus bisulcatus* has also shown a significant conversion of selenite (SeO_3^{2-}) to elemental selenium (Se^0) under ambient conditions. The as-generated elemental Se nanoparticles have a higher tendency of being accumulated in the cell protoplasm or the extracellular legroom.¹⁵⁴ Mishra et al.¹⁵⁵ performed an experiment for the reduction of selenite to red elemental Se by *Bacillus megaterium* strains isolated from Bhitarkanika mangrove soil. The strains were incubated for 6 h for the bio-reduction of sodium selenite pentahydrate using *Pseudomonas alcaliphila* (Fig. 4).¹⁵⁶ By varying the incubation time from 6 to 12 h, the sizes were easily increased from 50 to 500 nm. The formation of larger Se particles was explained by the classical Ostwald ripening phenomenon.

-----Figure 4-----

Dobias et al.¹⁵⁷ investigated a comprehensive analysis of a protein extracted from *Escherichia coli* for the synthesis of nanoparticles. The changes in the concentration of proteins had a considerable effect on the shapes and sizes of nanoparticles. The purpose of their study was to identify the significant proteins that participated in the bio-mineralization of Se and other metals

and their binding modes, and to extend their protocols for commercial needs. Kaur et al.^{158a} presented a simple method for the synthesis of highly crystalline nanobars and amorphous nanospheres of Se from an aqueous solution containing bovine serum albumin (BSA). The unfolded stretched form of BSA efficiently produced Se particles. The uncovered hydrophobic surface of unfolded form of protein was capable of providing a higher surface activity for the crystalline growth of nanoparticles (**Fig. 5**). By adjusting the concentration of BSA, the collections of fine multifaceted bars became apparent (**Fig. 5b**) with a standard aspect ratio of 4.7 ± 1.8 . The block arrows in **Figure 5c** indicate the occurrence of conjugated BSA (BSAc) over the outer surface of Se nanoparticles. Stability was achieved by the surface covering of proteins (**Fig. 5d**). Recently, Kalishwaralal and co-workers^{158b} have also used BSA and keratin to produce size-controlled Se nanoparticles at ambient reaction conditions. The as-produced nanoparticles can potentially protect the cardiomyoblasts and zebrafish embryos against ethanol-induced oxidative stress.

-----Figure 5-----

An exponential increase in the application of bio-attuned agents such as amino acids and sugar for the preparation of Se nanomaterials has also been observed. For instance, Se particles with a mean diameter of 80–220 nm were generated by mild heating of aqueous solution of L-cysteine, which acts as both a capping and reducing agent.^{159,160} The concentration variation of L-cysteine to Na₂SeO₃ exhibits a significant effect on the diameter and morphology of the as-synthesized nano-Se. A remarkable advantage of the as-synthesized nano-Se was its superior stability when diffused in the reaction solutions, which indicates its potential medical applications. Similarly, particles with 20–80 nm were synthesized in 30 min under ambient conditions using glucose as a reducing agent.¹⁶¹ Chen et al.¹⁶² proposed a simple process to

synthesize size-controlled nano-Se by mixing *Undaria pinnatifida* polysaccharides to the redox system of selenite and ascorbic acid. The effect of molecular weights of different saccharides on the growth, morphology and agglomeration rate (**Table 1**) of nanoparticles in liquid state was studied by Bai et al.¹⁶³

-----**Table 1**-----

The corresponding stabilization order was *Eucheuma striatum* sulphated polysaccharide (ESSP) > sucrose > glucose. The mechanism was described by using the hydrogen bonding capabilities of oligosaccharide with the as-synthesized Se particles. For glucose, spherical particles with a mean diameter of 100–500 nm were obtained, whereas for 1.0% sucrose sol, dendritic type particles were generated. Elliptical and rod-shaped particles with average sizes of 10–20 and 100–200 nm were synthesized with 0.1% and 1% chitosan. The non-toxic, biofriendly properties of highly soluble heme protein, that is, Cytochrome *c*₃, was used by Abdelouas et al.¹⁶⁴ to prepare Se nanowires. The electron transfer ability and stability towards chemical modification enhance the utility of Cytochrome *c*₃ for the preparation of Se nanoparticles (**Fig. 6**). In a separate report, L-L-ascorbic acid was used by Peng et al.^{164b} to produce graphene oxide-encapsulated Se nanoparticles. The as-synthesized nanocomposites exhibit a higher utility in high-power lithium–selenium battery cathode.

-----**Figure 6**-----

The dual functionality of stabilization and morphological control of hyper-branched polysaccharide (HBP) extracted from the sclerotia of *Pleurotus tuber-regium* and *Rhizoma Panacis Japonici* was used by Zhang et al.¹⁶⁵ to prepare spherical Se particles (**Fig. 7**). The template effect of HBP leads to the formation of water-dispersible Se nanoparticles. The availability of active sites over HBP provides a better platform for the reduction of Se salts to

their elemental state. This method provides a simple approach for the generation of organic–inorganic hybrid composites, with high bio-tunability and biodegradability.^{166,167}

-----**Figure 7**-----

Se particles with high anti-mutagenic activities towards UV-induced DNA disorder of isolated lymphocytes were prepared using the plant extract of *Spirulina platensis*.¹⁶⁸ Mendoza-Reséndez and co-workers¹⁶⁹ prepared the spherical, twinned and disc-shaped Ag–Se nanocomposites by varying the concentration of the extracts of red fruit *Piquin pepper* (*Capsicum annuum var. aviculare*). The sugar chains of the cell surface were used to prepare less-toxic and biocompatible QDs of Zn–Se nanocomposite.¹⁷⁰ Se nanocomposites with Cd and Zn were obtained at room temperature using protein extract from *Rhodobacter sphaeroides R26*.¹⁷¹ Because of the associated potential advantages, the biosynthetic methods are one of the promising approaches to prepare biofriendly and biocompatible particles with desired shape and size for various biotechnological applications.

3.6. Hydrothermal and Solvothermal Techniques

The use of hydrothermal approaches for preparing semiconducting nanoparticles with special attention to elemental Se has been reviewed previously.^{172–179} The cost-effective novel hydrothermal approach is also capable of influencing the morphology of the generated particles. For instance, Lu et al.¹⁷⁹ prepared nanobelts, wires and one-dimensional (1D) structures of Se at ambient reaction conditions using the hydrothermal approach (Fig. 8). The corresponding method does not involve any type of template for the stabilization of particles.¹⁸⁰ During the synthesis, extended helical chains are also formed using the covalent bonds among Se atoms. The chain axes are capable of promoting the overlapping of the vertical boundaries of the

hexagonal unit cells. The as-synthesized particles acquire their metallic character because of the decreasing distance between the Se–Se atoms within the chains.

-----**Figure 8**-----

Ding et al.¹⁸¹ studied the effect of solvents, such as CS₂, ethanol, benzene and pyridine, on the morphological developments of single-crystalline β-physic monoclinic and rod-shaped t-Se crystals of nanomaterials. The changes in the morphologies were associated with the selective solubility of different solvents in different Se species. The effect of reaction conditions on the polymer-assisted hydrothermal method was used to synthesize uniform nanorod bundles of t-Se. The low stability of α-Se resulted in the delayed formation of t-Se (after 2 h). The phenomenal changes were clearly demonstrated by the existence of dark grey samples on the internal boundary of the autoclave. In another report, Liu et al.¹⁸² studied the effect of ethanol, benzene, pyridine, ethylenediamine (en), toluene and carbon tetrachloride on the growth of Se nanomaterials under solvothermal conditions. Microtubular brown precipitates with a higher ability to coalesce were obtained for ethylenediamine (en).

Zhang et al.¹⁸³ explained the effect of sonication rate on the growth mechanism of Se nanotubes (**Fig. 9**). The crystalline phases of the as-obtained particles were different from the particles generated by the refluxing process. The growth of the circumferential edge was modified by a 3-min sonication after 20 h of hydrothermal treatment (**Fig. 9c, d**). Long nanotubes were obtained by sonicating the sample for approximately 30 min without any adsorbed particles on the surface (**Fig. 9e**). Single-crystalline t-Se nanobelts were produced on a large scale by Xia et al.¹⁸⁴ The prepared Se nanomaterials were used for the fabrication of photosensitive and photovoltaic nanodevices. Nanorods and nanowires of t-Se were obtained by the thermal decomposition of [(CH₃)₄N]₄Ge₄Se₁₀¹⁸⁵ using the following reaction:



-----Figure 9-----

The major difference in this strategy is the use of selenide ion as a source material for the synthesis, whereas the previous methods described in the literature used oxyanions with a positive charge on Se as the source material.^{186,187} The reactive sites on the precipitates of t-Se act as a catalyst for the generation of 1D nanorods. This behavioural change has been clearly observed by the colour variations in the reaction media. During the course of the reaction, the red solution became lighter and the resulting darker Se nanorods settled at the bottom.

In a separate experiment, single-crystalline Se nanowires were synthesized from polycrystalline Se powder¹⁸⁸ via hydrothermal process at 150°C for 24 h. The development of Se single crystals along the *c*-axis was categorized as bonded growth, while the crystal growth perpendicular to the *c*-axis has a layered growth phenomenon (on the (001) face).¹⁸⁹ This method serves as a suitable and efficient way of synthesizing single-crystalline Se nanowires in a large scale.¹⁹⁰

Chen et al. demonstrated the effect of reaction temperature and nature of reducing agents on the size, shape and distribution of particles.¹⁹¹ Amine-based compounds assist the crystal-phase changes from amorphous to t-Se by stimulating the nebulous ring of Se. The new t-Se microspheres were also synthesized by a simple solution-phase approach at a low temperature of 150°C for 20 h.¹⁹² The abilities of the as-formed α -Se nanoparticles to coalesce prompt the formation of microspheres (**Scheme 2B**). The external surface of the particles became smooth

with time (**Scheme 2C**). As the reaction temperature increases, the solubility of α -Se nanoparticles was enhanced. Free Se atoms were generated during the reaction, which acted as catalyst for the growth of crystalline t-Se nuclei (**Scheme 2D**).

-----**Scheme 2**-----

This method was categorized as a solid–solution–solid transformation. The broken structures generated along the reaction were gradually repaired by the crystal growth mechanism. A butterfly-like microstructure of t-Se was obtained from elemental state via a solvothermal and aging route by Zeng et al.¹⁹³ The opposing directional growth of hexagonal rods results in the formation of a butterfly-like microstructure. Ray et al.¹⁹⁴ prepared Se nanowires using less-toxic, low-cost reagents by a customized hydrothermal reaction process. The as-generated nanowires play a significant role in clock reaction. The nanocomposite of Se with Zn and TiO₂ possesses a higher catalytic activity towards the photodegradation of methylene blue (MB).¹⁹⁵ Sobhani and Niasari^{196,197} investigated the effect of different Se sources on the synthesis of Se nanocomposite with Cd and Ni. The natures of capping and reducing agents with an optimized molar ratio of Cd/Se have the ability to produce different sizes and morphologies of nanocomposites. The growth mechanism and higher storage ability of hollow nanospheres of Se nanocomposites with Ni and Fe has been scrutinized by Shi et al.^{198,199} It was observed that the adopted reaction procedure has provided better control on the morphology and size of the prepared nanomaterials. The nanocomposites of Se with Cu, Zn and Sn have also been synthesized by this process, which were further used to fabricate high-efficiency solar cells with a light-to-electricity conversion efficiency of approximately 2.48%.²⁰⁰

In contrast to other approaches, the hydrothermal and solvothermal methods are template-free, and represent a surfactant-less process for the large-scale production of Se nanomaterials

with appropriate compositions, morphologies and sizes. With several advantages, these methods also have several drawbacks such as the requirement of high temperature and pressure and the corresponding difficulties of *in situ* monitoring of growth development of nanomaterials.

3.7. Synthesis in a constrained environment

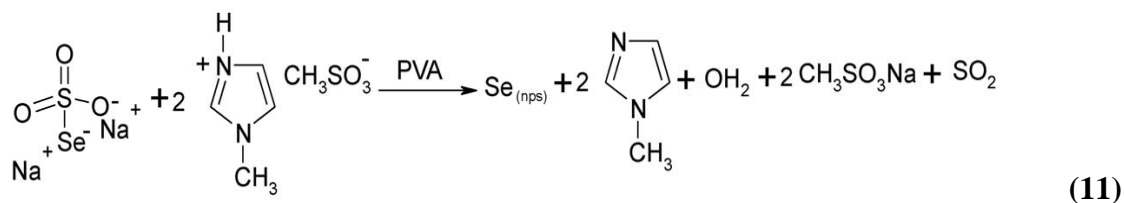
Morphologies and functionalization are the main characteristics for the modification of nanomaterials. Organization of these factors under constrained environments can lead to the formation of specific and innovative nanostructures. Using this, numerous procedures have been developed to synthesize Se nanomaterials with post-synthetic coating with surfactants and polymers.^{201–206}

3.7.1. Using polymers

The use of polymers has been proved as a potential way of providing a constrained environment for the synthesis of Se nanomaterials.^{207–228} The functionalized polymers not only act as a structure-directing agent, but also exhibit a dual behaviour, that is, a stabilizing and reducing agent. In particular, the replicability and organizeable structures of polymers have provided better morphological flexibility and size control. High yields of size- and shape-controlled particles were obtained by radical polymerization of poly-*N,N,N,N* trimethyl methacryloyloxy ethylammonium methyl sulphate P(DMAEMA·DMS) in ethanol solutions.²²⁹ The involvement of *in situ* complex of Se with polymer radical was visualized from absorption spectra. Shah et al.²³⁰ reported the synthesis of size-controlled particles with different vinyl monomers, such as sodium acrylate and acrylamide, N,N'-dimethylene bis-acrylamide (BisAM) and methyl methacrylate. The nucleophilic attack of the anionic species with the β-carbon of the polymeric unit results in the formation of an intermediate of four-membered cyclic ring, which

subsequently releases the Se nanoparticles. The nature of electron-donating and -withdrawing groups on polymers also influenced the efficiency of the process by modulating the electron cloud over C=C in the polymeric monomers. For instance, strong electron-withdrawing group, such as nitrile, in the case of acrylonitrile, has the tendency to reduce the electron cloud, while the presence of an electron-donating group, such as methyl, in the case of methyl methacrylate, enhances the electron concentration around the C=C, and hence hinders the nucleophilic attack. The effect of resonance stabilization of carboxylate anion has also been observed for sodium acrylate. The presence of an additional double bond in bis-acrylamide monomer makes the reaction more effective. The effect of α -methyl styrene monomer on the synthesis of Se nanoparticles has also been assessed. The incomplete solubility of α -methyl styrene hinders the rate of formation of nanoparticles. Moreover, the absorption maxima transfer towards red and the peak intensity decreases with the increase of the nanoparticle size.²³¹ The concentration effect of sodium selenosulphate was also investigated to examine its effect on the sizes of the obtained particles. Shah et al.²³² used polyvinyl alcohol (PVA) for the stabilization of 100–300-nm Se nanoparticles under ambient conditions. The stability was examined by the development of orange/red particles in the presence of PVA, whereas reddish-black elemental Se powder was precipitated out in its absence.

The potential capacity of ionic liquid with sodium selenosulphate in the presence of PVA was studied by Langi et al.²³³ for preparing 75–100-nm spherical nanoparticles. The acidic nature of the ionic liquid, ($[\text{Hmim}]^+\text{CH}_3\text{SO}_3^-$), helps the generation of small nanoparticles by releasing proton in PVA, as illustrated in the following equation²²².



This method does not require harsh reaction conditions for preparing Se particles.^{234,235} Zhang et al.²³⁶ used poly(2-hexadecyloxyaniline) monomers to synthesize crystalline Se nanoparticles without any additional oxidizing or reducing agent for the completion of reaction. Valueva et al.²³⁷ performed detailed molecular optics and spectrophotometric characterizations of Se nanoparticles synthesized by using various nonionic polymeric matrices of polyvinylpyrrolidone (PVP); oxyethylated cellulose; cationic polyelectrolyte: poly-*N,N,N,N*-trimethyl methacryloyloxy ethyl ammonium methyl sulphate; anionic poly electrolytes: poly-2-acrylamido-2-methylpropanesulphonic acid and polymethacrylic acid. By adjusting the concentrations of representative polymeric matrices, particle sizes can be easily controlled from 100 to 250 nm. The concentration and temperature variations result in the bathochromic shift in the absorption band of the as-prepared Se nanoparticles in the presence of polymers.²³⁸

Song et al.²³⁹ produced uniform and amorphous 100-nm capped Se particles via the reduction of selenious acid solution with hydrazine hydrate in the presence of PVP. The polarity of the dispersion media played a significant role in the phase transformation of the as-prepared particles. It was found that n-butyl alcohol has a higher tendency to transfer the a-Se nanoparticles along the liquid–liquid interface between water and n-butyl alcohol (**Fig. 10**). The shape evolution and crystallization at this interface resulted in the formation of crystalline nanorods. The enrichment of nanoparticles with an amphiphilic character at the interface has led to the phase transformation and crystallization of nanomaterials. These polymer-based methods have the ability to stabilize Se nanoparticles and hence provided a low-cost solution-based

technique to control the morphology and composition of nanomaterials. In addition, the electrocatalytic performance of the as-prepared nanomaterials has also been modified by varying the concentration of the precursors, reagents and stabilizing agents, as well as reaction conditions under the ambient temperature.^{240–242}

-----Figure 10-----

3.7.2. Surfactant-mediated synthesis

The applications of surfactants have extended from the traditional domain of cleaning to being used as structural directing agents for controlling the morphologies of nanostructured materials. Surfactants have the ability to manage the dimensions of nanoparticles. During the growth phase, the surfactants adsorbed reversibly on the exterior surface of the nanoparticles and provided a template, which stabilizes the particles and controls their growth.^{243, 244} The synthesis of Se nanoparticles in surfactant media was carried out in the late 1990s,²⁴⁵ and afterwards, several reports appeared in the literature.^{246–250} Johnson et al.²⁴⁶ fabricated 40–3000-Å Se particles in AOT reverse micelles by adjusting the water-to-surfactant molar ratio (ω). A comprehensive investigation on the change of precipitation rate with concentration was also studied, and it was found that a concentration of 2.0×10^{-3} M was needed to confirm the spectra, whereas for $\leq 5.0 \times 10^{-4}$ M, the particles remained in the form of suspension.

A rapid and convenient approach for the preparation of Se nanoparticles by the microemulsion method was proposed by Liu et al.²⁴⁷ The experimental results demonstrated that the concentration of HCl and reaction temperature have considerable control on the morphologies of the prepared nanomaterials. Se nanorods can be prepared using 2.0-mol/L HCl solution, whereas the chain-like Se nanoparticles were obtained with 3.0-mol/l HCl solution. The morphological changes were explained based on the rate of reaction in HCl media. By using 3.0-

mol/l HCl solution, the reaction occurred instantly and the formed particles led to the formation of nanorods. The as-formed spherical particles have a tendency to grow in a chain form by stacking the nanocrystals in the same direction. For 2.0-mol/l HCl solution, stranded rods of Se accumulated with tiny spherical particles and the corresponding weak nanorods have a tendency to promote growth by joining the particles.

Zhang et al.²⁴⁸ prepared submicrotubes of single-crystalline t-Se by using polyoxyethylene (20) sorbitan monolaurate (Tween 20) as surfactant. An analogous method was also used to prepare submicrotubes of Te and other anisotropic materials. The behavioural aspects of different nonionic surfactants of Span and other Tween series were also used to synthesize Se tubes (**Fig. 11**) by using the above-described method. The concentrations of surfactants have a direct impact on the morphology, size and electrical charges on the surface of nanotubes.

----- **Figure 11** -----

The solution-phase progression of nanoparticles was carried out by using the reduction of aqueous selenious acid with NaBH₄ in the water core of Triton X-100. The micelle of nonionic surfactant offers potential stability to prevent agglomeration, and hence enhances the catalytic activity towards the decolourization of MB.²⁴⁹ The degradation of MB in H₂O, Black Se and TX-100-stabilized Se nanoparticles is depicted in **Figure 12**.

----- **Figure 12** -----

Ma et al.²⁵⁰ demonstrated the synthesis of single-crystalline nanobelts and wires of Se in the colloidal assemblies of poly(oxyethylene(20)) octadecyl ether (C₁₈EO₂₀) and poly(oxyethylene(10)) dodecyl ether (C₁₂EO₁₀), respectively. The distinctive differences in the absorption spectra for nanowires and nanobelts clearly show the variations for the two different

morphologies of Se. Lin and Wang²⁵¹ analysed the effect of surfactant concentration and the starting reactants on the size and morphologies of particles by absorption techniques.

Zhang et al.²⁵² proposed a fast and controlled method for the preparation of nanotubes in colloidal assemblies of the cationic surfactant CTAB. The mechanism of formation was explained based on the effective adsorption of negatively charged selenious acid on the surface of the positively charged CTAB micelles via electrostatic interactions. The concentration of CTAB has a significant effect on the morphological changes in Se nanoparticles.²⁵³⁻²⁵⁵ The inherent configuration of t-Se seeds has the ability to allow spontaneous expansion of particles along *c*-axis. By contrast, the growth of t-Se seeds via the micellar process was restricted by the insufficiency of a-Se in solution. The enhanced solubility of functionalized Se in CTAB micelles resulted in the existence of a higher quantity of a-Se over the polar covering of micelles.²⁵⁶ The adsorption of extra Se atoms at the edges of t-Se resulted in the generation of t-Se nanotubes (**Fig. 13**). An et al.²⁵⁷ showed the use of anionic surfactant sodium dodecyl sulphate (SDS) to synthesize nanowires with adjustable size and shape.

-----Figure 13-----

Although several studies on the use of surfactants for the growth of nanomaterials are reported in the literature, the utilization of aqueous surfactants for the preparation of Se nanomaterials is still limited. The spontaneous self-coalescent aptitudes of nanoparticles into larger particles have posed a significant challenge in the synthesis process. By considering the aforementioned points, Mehta et al.²⁰¹⁻²⁰³ reported the synthesis and stabilization of nanoparticles in aqueous solution of CTAB and AOT. The surfactant presented a distinctive environment for inorganic reactions. These micellar assemblies provided steric stabilization to nanoparticles and inhibit their aggregation tendency. The major improvement of this method is the use of ambient reaction

conditions with better control over the morphologies of the particles. Moreover, the ability of compartmentalization of these assemblies provides a direct control over the ground-state transition and product states. The reaction dimensionalities were also controlled by varying the composition of the surfactant. The existence of surfactant monomers in the solution reduces the susceptibility of Se nanoparticles to accumulate and provide hydrophobicity to the nanomaterials. The distinct adsorption properties of Se nanoparticles in surfactant solutions illustrate a vital confirmation for their application in photo-electronic devices.^{258–263} A summary of various approaches for the synthesis of Se nanomaterials is presented in **Table 2**.

-----**Table 2** -----

3.8. Microwave-assisted synthesis

The use of microwave irradiation in synthetic chemistry is a well-established process, in which the reaction mixtures are rapidly heated, leading to the formation of nanomaterials. Very small particle sizes with narrow size distributions were prepared by this technique.

Olivas and Donard²⁶⁴ described the growth of Se particles in HCl media under microwave method. An open-centred mono-type microwave oven, Microdigest A-301 (2450 MHz, maximum power 200 W) (Prolabo, France), was used for the reduction of Se salt. The sample was situated in the waveguide, from which the highest concentration of microwave power was targeted over the sample. A modified process with the TX32 programmer also provided a direct control over the reproducibility of the microwave power in the range of 20–200 W. The morphology of the particles directly depended on the exposure periods of the microwave. The resultant loss due to volatilization was also prevented by using a refluxing unit in the instruments. The requirement of a small quantity of reagents is an added advantage of this technique. Zhu and Hu²⁶⁵ demonstrated the growth of Se with different morphologies by using

an economic, fast and easy microwave-polyol method. Kolachi et al.²⁶⁶ reported the extraction of Se in aqueous media from medicinal plants using microwave-assisted conventional extraction methods. The total and residual Se in medicinal plants was determined by electrothermal atomic absorption spectrometry. The Se contents in aqueous extract of medicinal plants were found in the range of 1.09–2.23 µg/g, corresponding to 21–33% of total Se contents. A comparison of microwave-assisted extraction (ME) and conventional methods for the determination of Se is presented in **Table 3**. Recently, Yan et al.²⁶⁷ have reported the synthesis and characterization of nanocomposites of Se with Cu, Zn and Sn by this method. Detailed studies revealed that the synthesized nanocomposites possess amendable band gaps with higher photovoltaic activities. On the contrary, Se nanocomposites with Ag,²⁶⁸ Cu and In were also prepared via microwave-enhanced aqueous methods.^{269–271}

-----**Table 3** -----

3.9. Other methods

In addition to the above-described synthetic methods, other methods were used for the synthesis of Se nanomaterials. Gao et al.²⁷² introduced a simple procedure for the synthesis of single-crystalline monoclinic nanowires using a solution–solid augmentation process. This technique was found to be associated with the reduction of sodium selenite with glutathione (GSH), which has an increased tendency to respond towards sodium selenite via generating selenodiglutathione (GSSeSG), which gradually decomposes to produce Se molecules and diglutathione (GSSG).

Zhang et al.²⁷³ reported the carbothermal chemical vapour deposition (CTCVD) route to prepare t-Se nanowires and ribbons by evaporating the combined mixture of dynamic carbon (C) and Se powder. In this process, the Se precursor was reduced by carbon. The corresponding

mixture was further evaporated and purified to obtain 1D Se nanostructures. These nanostructures exhibit enhanced optical properties with large hypsochromic shifts. A solution-based method for the synthesis of Se nanoparticles by reducing selenious acid with ascorbic acid in the presence of silk fibroin was reported by Xia.²⁷⁴ Silk fibroin has a natural, potential medicinal suitability for drug design. The as-extracted silk fibroin can control the growth and stabilization of nanoparticles. Porous flower- and apple-like microstructures of Se were prepared on a commercial scale by selecting Zn and Ni foils.²⁷⁵ These foils provided an effective deposition substrate to perform the reduction reaction between selenious salt and N₂H₄.H₂O (**Fig. 14**). The complex coordinating agent ethylenediaminetetraacetic acid (EDTA) provided the particles with more stability. The morphology of the particles was varied by regulating the experimental parameters. The coordinating abilities of Zn/Ni ions released from the foils have a noteworthy function in managing the porous morphology with different shapes for the final products. The liberation of N₂ via the decomposition of N-containing molecules is accountable for the generation of pores in the Se particles. The as-formed particles exhibit high hydrogen storage efficiencies.

-----**Figure 14**-----

A new synthetic approach using silver nanoparticles was studied by Jiang et al.²⁷⁶ for the synthesis of trigonal nanowires at ambient conditions. The prepared wires possess covered tips with a diameter and length of 23 and approximately 100 nm, respectively. The method does not involve any harmful chemicals, and does not require any external stabilizing agent or sonochemical treatment. The as-prepared nanomaterials show considerable applications in photo- and thermal conductors. Redman et al.²⁷⁷ synthesized Se nanoparticles using cathodic

electrodeposition process from an air- and water-stable ionic liquid. The as-synthesized products were used as potential material for producing efficient and high-sensitive sensors.

4. Properties of selenium nanomaterials

The morphologies, physical properties and sizes of nanomaterials depended on several reaction parameters, including synthesis techniques, starting materials, use of surfactants/additives, reaction temperature, pH of the solution, choice of substrates, reaction time, reaction media and nature of solvent. The as-prepared nanomaterials were characterized by various techniques such as field emission scanning electron microscopy (FESEM), transmission electron microscopy (TEM), energy dispersive spectroscopy (EDS), X-ray diffraction (XRD), X-ray photoelectron spectroscopy (XPS), low-energy electron diffraction (LEED) and selected-area electron diffraction (SAED).

4.1. Shape and structure of selenium nanomaterials

SEM and TEM measurements revealed the shape, size, agglomeration and distribution of nanomaterials on the substrate surface. The comprehensive analysis conducted by TEM and SEM measurements is considered as a standard paradigm in most of the size- and shape-dependent studies of nanoparticles.^{171–176} The agglomeration behaviour of Se nanoparticles during wet chemical synthesis was studied by Shah et al.²⁷⁸ using structural analysis methods. The rate of aggregation increases during extraction and drying. Xi et al.²⁷⁹ performed the time-dependent (2–25 h) SEM analysis to investigate the growth of t-Se nanotubes (**Fig. 15**). Within a reaction time of 2 h and temperature of 100°C, different types of morphologies with average diameter of 10 nm were created (**Fig. 15a**). SAED patterns also verify the development of t-Se nanocrystals prepared via the reduction of Na₂SeO₃ by NaCHO₂. By increasing the reaction time,

t-Se nanotubes were converted into sphere-like microparticles with average diameter ranging from 1 to 3 μm (**Fig. 15b**). After 8 h, the mass of the particle grows linearly to generate nanorods (arrows in **Figure 15c**) on the external surface of spherical microparticles. The visualization of grooves with length between 0.3 and 2 μm and diameter of approximately 250 nm revealed the presence of hollow structures (**Fig. 15d**). By increasing the reaction time to 14 h, the shapes of the particles mainly include nanogrooves (~40%) and sphere-like particles (~40%) together with small (~20%) intermediate nanotubes with unsealed ends (**Fig. 15e, f and g**). Small prongs of inclusive nanotubes were produced after 20 h (**Fig. 15h**). Eventually, as the hydrothermal reaction time reached 25 h, the majority of the product was converted into ideal nanotubes (**Fig. 15i**).

-----**Figure 15**-----

XRD analysis was done to examine the crystalline phases of the as-prepared nanomaterials.²⁸⁰⁻^{289,179,180} Singh et al.⁹¹ investigated the effect of laser irradiation on the diffraction patterns of nanoparticles (**Fig. 16**). In the absence of laser effect, mainly β -Se was obtained, with lattice parameters of 9.05, 9.07 and 11.61 and corresponding diffraction reflections at $2\theta = 23.523^\circ$, 29.87° , 41.36° , 43.89° , 45.40° , 51.66° , 56.13° and 61.66° .²⁹⁰ On the contrary, in the presence of laser radiations, Se QDs were produced with diffraction peaks at $2\theta = 20.54^\circ$, 21.9° , 24.7° and 28.8° . These changes suggest a better packing and higher stability of particles under laser light (**Fig. 16B**).

-----**Figure 16**-----

The composition, purity and morphology of nanoparticles were also examined by EDS,^{291,292} XPS²⁹³ and direct current plasma atomic emission spectroscopy (DCP-AES) or inductively coupled plasma atomic emission spectroscopy (ICP-AES).^{249,233} The anisotropic morphological

changes in Se nanowires were clearly visualized by using a combination of SAED and HRTEM techniques.²⁹⁴ Particles have the affinity to grow along [001] direction, with distinct lattice spacings of approximately 0.5, 0.37 and 0.29 nm, which further correspond to the (001), (100) and (101) planes of t-Se, respectively. The presence of globular 200-nm Se nanostructures was examined by Zhang et al.¹⁶⁵ with and without HBP (**Fig. 17**).

-----**Figure 17**-----

Johnson et al.²⁴⁶ conducted a SANS analysis to study the sizes and shapes of nanoparticles in the colloidal assemblies of AOT. XPS experiments have also been conducted by Rodrigues et al.²⁹⁵ to investigate the atomic composition of the near-surface region of Se/Se-based nanoparticles (**Fig. 18**). The observed XPS spectra showed significant structural variations with an intense peak at approximately 291.8 eV for C 1s and -61eV for 3d core-level bindings of Se. The results clearly revealed the covering of SeO_2 layers with the amorphous carbon. Similarly, Song et al.²³⁹ carried out the structural characterizations of Se nanoparticles by using XPS analysis. The spectra displayed a well-defined peak at 54.9 eV, which corresponds to the Se 3d binding energy. The purity of the product was also determined by the absence of an absorption peak of SeO_2 . Furthermore, the observed spectra do not show any corresponding peaks of the polymeric moiety used for the synthesis of Se nanoparticles.

-----**Figure 18**-----

Large micrometre range bamboo-raft-like single-crystalline super-structures of Se were reported by Song et al.²⁹⁶ using solvothermal approach by reducing SeO_2 with ethylene alcohol in the presence of cellulose acetate (**Fig. 19**). The corresponding ends of these rafts were not smooth, rather possess tooth-like structures resembling bamboo strips, which are arranged next to each other (**Fig. 19b–e**).

-----Figure 19-----

Needle-shaped nanocomposites (100–400 nm) of Se with Cu and In were also prepared by Dong et al.²⁹⁷ Shi and co-workers⁷⁷ observed the anisotropic ring-like and Mobius strips-like morphologies of Se nanocomposites with Te and Ni. The nanosheets of organochalcogenides were prepared by Gao et al.¹³⁴ Xiao et al.²⁹⁸ examined the effects of reducing agents and Se precursors on the morphology and application in solar and memory devices of nanoparticles.²⁹⁹ The effect of solvents on the photo-assisted transformation of metal selenide into Se nanowires was also studied (**Fig. 20**).³⁰⁰ Dimethyl sulphoxide (DMSO) removes the organic ligands attached on the surface of nanomaterials and generates surface trap sites for photo-induced charge carriers. Kumar et al.³⁰¹ demonstrated the effect of pH, incubation time and temperature on the synthesis of nanorods and wires by reducing selenious acid with hydroquinone in the presence of Daxad 11G.

-----Figure 20-----***4.2. Catalytic properties***

Se has also been attracting much attention as a platinum-free, methanol-tolerant cathode material, and it also possesses high stability and electrocatalytic activity towards major responses in fuel cells generated by the electrochemical oxidation of hydrogen and other organic substances. These cells integrated various types of reactions, including the hydrogen oxidation reaction (HOR), formic acid oxidation, oxygen reduction reaction (ORR), ethanol oxidation reaction (EOR) and methanol oxidation reaction (MOR). A ruthenium chalcogenide, Ru_xSe_y, was first reported by Alonso-Vante et al.³⁰² for preparing a platinum-free, methanol-tolerant cathode material with high ORR activity. Conventional direct methanol fuel cells (DMFCs) have low

activity because of the deposition of methanol inside the polymer electrolyte membrane, which further results in a reduced cell voltage performance of the catalyst. However, the high methanol tolerance aptitude of Se nanoparticles makes them selective cathode materials for the ORR. Inukai et al.³⁰³ conducted a detailed study on the ORR activity of Se/Ru-based materials using in situ spectroscopic measurements. A highly advanced in situ synchrotron X-ray fluorescence spectroscopy was used to study the oxidation state of Se and the corresponding environment of Se/Ru nanoparticle catalyst during ORR. The reoxidation of Se was also achieved by using the 800-mV electrode potential. The mechanistic behaviour of ORR activity of Se–Ru nanoparticles was further verified by the extended X-ray absorption fine structure (EXAFS) technique. The results of the analysis showed that Se–O bond were not formed during the ORR activity. Gilleo et al.³⁰⁴ successfully synthesized extremely porous Ru/Se/C electrocatalysts using a template-based method. The catalytic action of the as-prepared Ru/Se/C catalysts for the oxygen reduction response was also confirmed in an oxygen-saturated solution at ambient conditions. Rodrigues et al.²⁹⁵ studied the catalytic performance of carbon-supported ruthenium-based catalysts (Ru/C) in selenious acid. The presence of Se enhances the performance of the catalyst without affecting the kinetic properties, such as Tafel gradient, and hydrogen peroxide production. In this reference, Le Rhun and Alonso-Vante³⁰⁵ suggested the preparation of a new catalytically active complex of Se with Ru with the general formula of RuSe_x . The high surface area and enhanced catalytic activity of Se make it useful for the decolourization of dyes in the presence of UV light.³⁰⁶ The progress of dye decolourization was observed via the reduction of UV absorbance intensities at 488 nm. The degradation kinetics and rate of reaction were also monitored with and without nanoparticles by evaluating the absorbance as a function of time.³⁰⁷ Se is also known for its strong photoconductive properties. Chiou and Hsu³⁰⁸ studied the controlled electron–hole

reunion effect through the charge relocation progression in Se nanoparticles.^{309,310} These assumptions were established for evaluating the light-to-energy translational competence of Se nanoparticles for practical applications. Currently, modification of nanoparticles with bismuth sulphides has produced enhanced catalytic activity towards the removal of MB under visible light irradiation ($\lambda > 400$ nm).³¹¹ Higher capability of Se in preventing the hole–electron (h+/e-) recombination was also examined for the photocatalytic degradation of trypan blue (TB) dye.³¹² The fundamental mechanism involved for the degradation of dye was mainly because of the production of electrons (e⁻) and holes (h⁺) by irradiating the samples with photon energy higher than the band gap of the photocatalyst. Consequently, electrons are moved towards the conduction band and the corresponding holes reside in valence band. The as-generated electrons were used to reduce oxygen molecules present on the peripheral surface of the photocatalyst, which resulted in the generation of extremely reactive superoxide anions such as AOS and hydroxyl radical (OH[•]) for degrading the dye molecules. The concentrations and morphology of nanoparticles have also affected the degradation of dye molecules.¹⁹⁴ For instance, nanowires induce more time lag to clock reaction (**Fig. 21**).

-----**Figure 21**-----

The catalytic activity of artificial GSH peroxidase was also modified by affecting the thermosensitivity of the enzyme with Se nanoparticles.³¹³ The electron transport efficiency and ORR catalytic activity were also enhanced by using a combination of Se-doped CNTs and graphene particles (**Fig. 22**).³¹⁴ Overall, the catalytic properties of Se nanomaterials were used to enhance the electrocatalytic activity of fuel cells. However, it is still required to increase the activity of nanomaterials for their effective utilization in photocatalysis and other photovoltaic device applications.³¹⁵

-----Figure 22-----**4.3. Electrochemical properties**

The excellent electrochemical properties of Se make it useful in optoelectronic and bio-photonic devices. The diffusive nature of the valence electronic state of Se particles offered better conduction via electron coupling with Au electrode surface.³¹⁶ The concentration of Se-modified Ru particles has a direct effect on the electron transport and ORR activity of the system.³¹⁷ The changes were associated with the development of new active phase because of the inhibition of hydroxide electro-sorption on Ru sites. Chemisorbing ability, oxide reduction hydrogen desorption peak areas as well as the electrochemical surface area (ECSA) of oxygenated species over Pt/Ru-modified catalyst were altered by the introduction of Se nanoparticles.³¹⁸ The electrochemical properties of Se have further been used for the preparation of chemical sensors. Zapp et al.³¹⁹ fabricated an electrochemical sensor for H₂O₂ recognition by using the amino derivatives of Se particles. In this fabricated sensor, a glutathione peroxidase mimetic (GPx) was immobilized on chitosan-graphite (CHI-GN) nanoplatelets by cross-connecting with glyoxal. The existence of H₂O₂ facilitates the catalysis of GSH by using GPx. Systematic reactions were obtained by using GPx (7.4 µg per electrode), CHI-GN (0.10:0.05%, w/v) and 0.1 M Britton–Robinson buffer solution (pH 7.0) including 99.0 µM of GSH. The change in the physical characteristics of Se materials by protecting their morphology or reacting with Cd²⁺, Fe²⁺ or Zn²⁺ precursor to generate II–IV semiconductor material has been currently very important in biosensing applications.¹²⁰

Shih et al.³²⁰ prepared various compositions (Se/Ru_{0.2}, Se/Ru_{0.7} and Se/Ru_{1.1}) of cathode electrocatalysts of Se/Ru core/shell nanoparticles using different concentrations of RuCl₃. Oxidation of MeOH was easily achieved by modifying the electrode with Se/Ru core/shell

nanoparticles. Of the various electrodes, Se/Ru_{1.1} possesses higher stability and activity up to 100 cycles and generates more current density and tolerance towards MeOH poisoning over the potential range from -0.15 to +1.0 V with a scan rate of 50 mV s⁻¹. Electrochemical detection of MeOH was also performed in 0.5 M H₂SO₄/1.0 M MeOH over a similar potential range. The CV curves displayed a peak at approximately 0.45 V in the forward scan from -0.15 to +1.0 V for the oxidation of oxygen-containing species adsorbed on the surface of Se/Ru_{1.1} catalyst.²⁵⁷ The ORR occurred at approximately 0.35 V in the backward scan. The PtRu catalyst was also used as the reference to determine the advantages of Se/Ru_{1.1} catalyst over the traditional catalysts used in DMFCs.³²¹⁻³²³ The solution containing MeOH was produced with a smaller reduction current (~0.75-fold) than the MeOH-free solution. This behavioural change is associated with depolarization over the external surface of the electrode. Zhang et al.³²⁴ demonstrated the electrochemical and photocatalytic activities of Se nanomaterials for fabricating reliable photovoltaic cells. The electron transport efficiency, current density and band potential of Se were also amended by making nanocomposites with other metal ions, which might be good for fuel cell applications.³²⁵

-----Figure 23-----

4.4. Optical properties

The optical properties of Se have significant importance because of their photoconductive, photovoltaic and rectifying behaviour in the presence of visible light. Intrinsic quantum confinement behaviour of Se induces different shape- and size-dependent physical properties in particles. Therefore, numerous studies were conducted to examine the optical properties of Se nanoparticles. Filippo et al.³²⁶ conducted morphology-dependent optical studies of Se. The absorption spectrum of Se microtubes was split into five bands with peaks centred at

385, 445, 540, 665 and 780 nm (**Fig. 24**); however, nanowires exhibited peaks at approximately 354, 452 and 590 nm. The significant red shift in the absorption spectra with peak positions at 375, 460 and 575 nm was also investigated in the presence of anodic alumina membranes.³²⁷ t-Se powder displayed characteristic peaks at 325, 371, 525, 662 and 798 nm. The variations in the numeric values of absorption peak positions of different morphologies depend on the reflectivity measurements in the generated particles.³²⁸

-----**Figure 24**-----

The peaks beyond 540 nm were exclusively attributed to the degree of crystalline precision and interchain interactions of particles towards vertical *c*-axis in t-Se crystal.³²⁹ Singh et al.⁹¹ anticipated the effect of size in UV–Vis absorption spectra as a function of time for laser irradiation (**Fig. 25**). Irradiation for 2 min shifts the bulk Se peaks from 273 and 700 nm to 260 and 558 nm. The peak in the UV region at approximately 260 nm corresponds to the interband and core conversions, while the peak in the visible region signifies the dependable fluctuation of non-dominant electrons from the external surface of the particles.

-----**Figure 25**-----

The presence of polymeric templates also affected the visualization of absorption peak in the UV region.²⁷⁸ On the contrary, the absorption edge at approximately 300 nm showed a significant increase as a function of Se source in comparison to polymer concentration (**Fig. 26**).

-----**Figure 26**-----

Similarly, Stroynk et al.⁹⁸ carried out a detailed spectroscopic analysis of size modification in Se nanoparticles with respect to stabilizing agents. The comparable values of band gap for Se nanoparticles in different stabilizing agents are presented in **Table 4**. The corresponding variations in the values were adequately explained by the presumption of Mie

theory and increase in the Rayleigh scattering from larger particles. However, other synthetic factors, such as the type of stabilizer and its integral constituents, have an insignificant effect on the optical properties of nanoparticles.

-----**Table 4**-----

The helical chain, transverse optical and second-order vibrational modes of t-Se have shown optical variations with characteristic Raman peaks at approximately 233, 145, 438 and 458 cm⁻¹ for different morphologies of Se particles.²⁵⁶ The variation in nanobelts and wires were also observed by absorption spectra in colloidal media. The characteristic peaks at 570, 450 and 346 nm signify the existence of nanowires, whereas those at 590, 452 and 354 nm confirm the existence of nanobelts in the micellar media.³³⁰ The peaks beyond 530 nm were associated with the interchain interactions of t-Se crystals. The shifting of peak from 346 to 354 nm for nanobelts confirms the presence of interchain interactions. The result was further rationalized by considering the higher Ersatz-hexagonal cross sections of t-Se wires than the nanobelts. The distinguishing peaks at 234 and 254cm⁻¹ in Raman spectra point towards the existence of t-Se and m-Se.³³¹ **Table 5** summarizes the shapes, absorption peaks and methods for the synthesis of Se nanostructures.

-----**Table 5**-----

The effect of morphology has also been associated with the colour transformations in the UV–Vis absorption spectra by Li et al. (**Fig. 27**).³³² These spectra display two characteristic bands at 540 and 580 nm. The concentration-dependent bathochromic shift and interchain interaction were analysed from the enhancement of peak intensity at 580 nm. The changes also revealed the gradual formation of homogeneous mono-dispersed spherical particles. The presence of capping

agent and dispersion media has also influenced the position of absorption peaks. For instance, in cellulose media, two peaks were observed at approximately 380 and 630 nm. However, the Se nanowires fabricated with sorbitol displayed two absorbance peaks at 440 and 610 nm.²⁷⁶ Se particles prepared using polygalacturonic acid showed a weak peak at approximately 450 and 600 nm.

-----**Figure 27**-----

The progressive growth of the particles was also observed by using the gradual shift in the absorption spectra over time. The absorption spectra of Se sols as a function of time also showed significant variations with sodium selenosulphate (1.5×10^{-3} mol dm⁻³), BisAM and methyl methacrylate (NaA) monomer (9.0×10^{-2} mol dm⁻³).²³⁰ The existence of different functional groups on the stabilizing agents also produced considerable changes in the absorption behaviour as well as the growth kinetics of nanoparticles. For example, acrylonitrile-, BisAM-, sodium acrylate-, acrylamide- and methyl methacrylate-modified particles showed absorption peaks at 330, 528, 558, 574 and approximately 560 nm, respectively. The sizes of the particles also varied in the same order.

The increased particle sizes displayed bathochromic and hyperchromic shifts with reaction time and concentration of Se source in polymer media (**Fig. 28**).²³² Particles >100 nm were visualized by the existence of peaks at above 300 nm. The confined growth of smaller particles with a higher concentration of a stabilizing agent showed a hypsochromic shift in the absorption spectra (**Fig. 28c**). The concentration of Se also displayed significant variations in peak position for Cu–Se composites.³³³ The spectroscopic effect of Se-related oxygen-deficient centres on the ion-implanted silica nanofilms was also studied elsewhere.^{334–336}

-----**Figure 28**-----

4.4.1. Quantum mechanical treatments

The occupancy of spectral range from 250 to 800 nm makes Se one of the essential materials in optoelectronic devices. The ability of a semiconducting nanoparticle to maintain absorption maxima is dependent on parameters such as band gap, surface morphology and shape. The functionalization of nanoparticle surface with capping agents, concentration of precursors and reducing agents helped to manipulate the absorption properties of nanoparticles. The simplest way of describing the optical properties is the Tauc relation for calculating band gaps. Mehta et al.^{201–206} conducted a detailed study on the effect of concentration of surfactants, reducing agents and precursors on the band gap of Se nanoparticles. The inclination gradient of the straight-line graph of $\ln(\alpha h\nu)$ versus $\ln(h\nu - E_g)$ helps to determine the nature of transition.³²⁸ The band gaps were obtained by extrapolating the straight-line segment of the $(\alpha h\nu)^{1/n}$ versus $h\nu$ graph to the x -axis in AOT, CTAB and TX-100 micellar media (**Fig. 29a–e**). Quantum confinement effect varies the band gap of nanoparticles in comparison to bulk Se (1.7 eV). The agglomeration rate and sizes of the particles were also estimated from the band gaps of different systems (**Fig. 29 e and f**). The obtained results confirmed that the higher concentration of surfactant restricted the growth of particles in contrast to the enhanced agglomeration rate in lower concentration.

-----**Figure 29**-----

The band gap of particles was also affected by the duration of laser irradiation (**Fig. 30 and Table 6**). The comparative role of laser radiations showed that the size and time displayed a second-order exponential decay by using the following function⁹¹:

$$E_g = C + A_1 \exp(-t_1 a) + A_2 \exp(-t_2 a),$$

where $C = 1.746\ 56 \pm 0.008\ 39$, $A_1 = 1.870\ 78 \pm 0.636\ 57$, $t_1 = -3.123\ 41 \pm 0.423\ 88$, $A_2 = 18.479\ 5 \pm 9.200\ 21$ and $t_2 = 0.823\ 22 \pm 0.187\ 61$ for 2–70-nm particles.

-----**Figure 30**-----

-----**Table 6**-----

The effects of reaction media and morphology were investigated by the presence of absorption peaks at approximately 1.777, 2.39 and 3.79 eV, while the polymer solution exhibited a band at 2.69 eV.³³⁷ The concentration of reducing agent (sodium thiosulphate) also showed variation in the band gap and sizes of the nanoparticles (**Fig. 31**). Detailed experimental evidence showed that the higher concentration of reducing agents results in the production of smaller particles via nucleation faster than the growth process.

-----**Figure 31**-----

4.5. Thermal properties

Differential scanning calorimetry (DSC), thermogravimetric analysis (TGA), differential thermal analysis (DTA), thermomechanical analysis (TMA), dynamic mechanical analysis (DMA)/dynamic mechanical thermal analysis (DMTA) and dielectric thermal analysis provide a deeper insight into the effect of morphological variation on the thermal properties of nanoparticles. For instance, endothermic peaks at 220.6, ~221, ~175 and ~70°C correspond to the melting point of the nanorods, bulk t-Se, m-Se and a-Se, respectively (**Fig. 32**).¹⁶² The homogeneity of the particles was determined by the existence of a single narrow DSC peak. The lower values of melting enthalpy were associated with the size variations of the nanoparticles. The DSC curve (curve 2 in **Fig. 32b**) of the nanotubes exhibited an endothermic peak at 224.7°C.²⁵² The mass of the sample remained constant in the temperature range of 100–300°C in TGA analysis; however, heating over 450°C led to a sharp decrease of mass, because of the

sublimation of elemental Se. The crystalline transformations have also been visualized from the enthalpy values for the two.

-----**Figure 32**-----

The presence of polymers and temperature variations during synthesis showed a significant variation in peak shift from 220 to 250°C in the DSC thermogram.²⁷⁵ The spectra also displayed an exothermic transition peak at 81°C with enthalpy of transition equal to 48.4 J/g. These observations were also supported by the X-ray power diffraction (XRPD) results of annealed Se samples at 130°C. In another study, nanoparticles also showed an exothermic transition at 85°C and an endothermic melting peak at 217°C.²³³ Enthalpy of the transition was found to be 21.83 J/g, and the ionic liquid-mediated nanoparticles showed an exothermic transition at 87°C.²³³ Acid-induced synthesis of Se nanoparticles showed an exothermic transition at 93°C in DSC with a transition enthalpy of 50.4 J g⁻¹ and 3–5% weight loss up to 220°C in TGA thermograms.²³⁴ This loss was probably correlated with the evaporation of the adsorbed moisture. The major weight loss started at approximately 300°C, with a peak temperature of approximately 470°C, which corresponds to the vaporization of Se under N₂. These alterations were attributed to the enhancement of crystallinity in the reaction media. However, Song et al.²³⁹ found an endothermic peak at 217.9°C for crystallized Se products synthesized via polymer-based method.

Shin et al.³³⁹ examined the effect of temperature on the morphologies and crystallinity of selenium nanoparticles synthesized using cellulose nanocrystal (CNXL). Hydrolysis of Na₂SeO₃ produced selenious acid (H₂SeO₃) in an acidic CNXL solution (pH ~ 2.7). The corresponding selenious acid had a tendency to allocate isotropically over CNXL colloids. The corresponding heat treatment converts the selenious acid to elemental selenium. The XRD analysis of samples

showed diffraction reflections at $2\theta = 15.1^\circ$, 16.8° , 22.5° and 34.1° for CNXL. The hexagonal phase of Se demonstrated diffraction reflections at 23.7° , 29.8° , 41.4° , 43.9° , 45.5° , 51.8° , 56.3° , 61.9° , 65.2° and 68.6° . The corresponding lattice parameters for Se were $a = 4.367 \text{ \AA}$ and $c = 4.948 \text{ \AA}$ (JCPDS 06-0362). The intensities of the peaks are regularly enhanced by the reaction temperature. The temperature also caused significant changes in size and shape of particles with gradual expansion from 10 to 15 and 20 nm at 120, 140 and 160°C, respectively. The concentration of Se source, sonication and the nature of reaction media also affected the thermophysical and optical properties of Se nanocomposites (Fig. 33).³⁴⁰⁻³⁴³

-----Figure 33-----

5. Toxicity of selenium nanomaterials

Because of the rapidly developing chemo-preventive and chemotherapeutic applications of Se nanoparticles, it is very important to study, in detail, the toxicological properties of Se nanomaterials.^{344,345} A comprehensive evaluation of different parameters that influence the biocompatibility or toxicity of the nanomaterials is critical for secure and prolonged improvement of the growing technologies. However, numerous factors need to be addressed before these nanoparticles can be comprehensively used in the field of medicine. The questions which remain unclear yet are as follows:

- i) What is the relationship between morphology and surface functionalization of nanoparticles and their corresponding *in vivo* activities?
- ii) What is the eventual fate of Se nanomaterial-supported drugs?
- iii) How can Se nanomaterials be metabolized in or removed from the body?

All these questions should be addressed before effectively using Se particles for real medicinal applications. Se toxicity depends on the nature of its existing chemical form.³⁴⁶ In mammals,

inorganic selenites are more lethal than selenate and Se. Seleno-cysteine exhibits adverse toxic effects compared with selenomethionine,³⁴⁷ whereas gray and black elemental forms of Se are biologically inactive and non-toxic in nature. By contrast, the red nano-Se elements have bio-accessibility of approximately 2% compared with selenite, which makes it non-toxic with higher importance in the ecological safety of various types of bacteria.^{348, 349} The average size range of 5–100 nm also enhances the bioavailability, cell propagation, enzyme stimulation and defence against free radicals in rats.^{350, 351} The toxicity rate of the as-prepared Se nanomaterials was lower than that of selenite. Furthermore, it was also observed that sub-Se nanoparticles produced by the light-induced blanching of seleno-merocyanine dye in the presence of BSA have higher selectivity and cytotoxicity towards tumour cells in contrast to normal cells.³⁵² It was mainly explained by the stabilizing action of BSA proteins through *in vitro* size-dependent redox actions³⁵³ on less-toxic Se⁰ than selenite for regulating the selenoenzymes.^{354, 355} The cell viability assay of anastrozole-induced cell death also showed significant improvement in the presence of Se nanoparticles.³⁵⁶ The nano-Se also induced activity for serum alkaline phosphatase (AP) and tartrate-resistant acid phosphatase (TRAP) for different groups of ‘ovariectomized’ rat model (**Table 7A and 7B**).

-----**Table 7**-----

5.1. Effect of Se nanoparticles on cytotoxicity assays

The majority of nano-toxicological research has focused on the detailed investigations of cell culture media. Recently, Kong et al.³⁵⁷ have published detailed cytotoxic inhibitory effects of Se with high bioavailability and low toxicity towards the growth of human prostate LNCaP cancer cells by using a wide viable assay of lung cancer cell A549, androgen-independent

prostate cancer cell DU-145, breast cancer cell MCF-7, embryonic kidney cell HEK-293 and androgen-dependent LNCaP cells (**Fig. 34**).

----- **Figure 34-----**

MTT assay was used to screen the *in vitro* cytotoxic effects of Se nanomaterials on various human cancer cell lines.³⁵⁸ Se nanomaterials exhibited a broad range of inhibitory effect towards A375, CNE2, Hep G2 and MCF-7 cancer cells with IC₅₀ values varying from 3.0 to 14.1 μM. These growth-hindering effects were equivalent to selenite. In addition, nano-Se also possessed less cytotoxicity towards normal cells (Hs68 human fibroblasts) with an IC₅₀ value of 67.9 μM than selenite (22.3 μM). Mahmoudvand et al.³⁵⁹ studied the inhibitory effect of Se nanoparticles on the protoscoleces of *Echinococcus granulosus*. These tapeworms have a significant effect on zoonotic parasitic infection called as cystic echinococcosis (CE).

5.2. Significance of dose

The dosage of nanoparticles also plays an imperative role in nano-toxicology. Wang et al.³⁶⁰ studied the effects of severe fatal doses of SeMet or nano-Se on 100 randomly selected male Kunming mice with body mass between 22 and 24 g. A bolus of SeMet or nano-Se suspended in 0.9% NaCl was administered to the mice orally with different doses. The cumulative mortality rate was increased with dose via the prominent effect on the liver of mice with selenium toxicity. They also analysed the effect of acute lethal doses of SeMet and nano-Se over the hepatic metabolic rates of alanine transaminase (ALT), aspartate aminotransferase (AST) and lactate dehydrogenase (LDH) enzymes released from the liver into the serum. The high rate of accumulation was associated with the removal of Se by SeMet in methionine. Evidently, Se nanoparticles with 36-nm pores have also influenced the accumulation rate and

low toxicity towards tissue as compared with 5-nm SeMet. The smaller SeMet causes more material to pass through membrane and results in irretrievable and serious pathological alterations in the forms of pyknosis and necrosis in liver as compared with hydrophobic and reversible pathological changes for nano-Se.³⁶¹

The linear dependency of cytotoxic behaviour of Se nanoparticles prepared by *Bacillus* sp. MSh-1 was assessed *in vitro* by Shakibaie et al.³⁶² against the fibrosarcoma cell line (HT-1080) at four different doses: 10, 20, 50 and 100 µg ml⁻¹. The viable concentration and anti-invasive properties of cells were also affected by the dose. For instance, 100 µg ml⁻¹ of nanoparticles reduced the viability proportion of the cell line to 50%, whereas 10 µg ml⁻¹ of nanoparticles showed variations up to 80%. The comparative time-dependent cytotoxic effects of nano-Se and SeO₂ on *Leishmania infantum* promastigotes were analysed using MTT assay.³⁶³ Both systems showed cytotoxic effects depending on their dose with IC₅₀ values of 25 and 50 µg/ml for nano-Se and SeO₂, respectively. The viability of the promastigotes also declined with increasing drug dose. The maximum cytotoxic effects were detected for 100-µg/ml concentration of nano-Se as compared with SeO₂. The accumulation rate of nano-Se in livers, gills and muscles of fish was found to be lower than other forms of Se at different time intervals. As a result, equivalent concentration of nano-Se also exhibits higher bioavailability and less toxicity in mice, fish and rats than sodium selenite, selenomethionine and methylselenocysteine.³⁶⁴ Nano-Se showed five times higher lethal activity for medaka fish in terms of LC₅₀ than selenite. It also caused a more intense effect on the oxidative stress in the liver. These investigations also proposed that toxicity of nanoparticles can vary mainly among different species and the assessment of nanotoxicology should be verified for each case individually.

The growth, activities of serum glutathione peroxidase (GSHPx) and retention rate of nano-Se were assessed for 2×4 factorial planning with 0.15-, 0.30-, 0.60- and 1.20-mg/kg dietary product of nano-Se or sodium selenite in maize–soya bean diet.³⁶⁵ The concentration of Se in serum, liver and breast muscle was directly augmented with Se level for each feeder source. The preservation and intestinal transportation rate for the orally or intravenously administered nano-Se were found to be much higher ($p < 0.05$) than selenite, although the intestinal retention of nano-Se was found to be much lower ($p < 0.05$) than selenite.³⁶⁶ The scolicidal activities of protoscoleces of *E. granulosus* measured for 50–500-mg/ml nano-Se for 10, 20, 30 and 60 min.³⁶⁰ It was found that 500-mg/ml particles tend to kill the protoscoleces within 10 min, whereas 250-mg/ml particles killed all protoscoleces after 20 min of exposure. Using 125-mg/ml particles, the percentage of protoscoleces decreased to 41.4%, 73.4%, 86.6% and 100%, whereas for 50-mg/ml particles, the corresponding decreases were 16.2%, 27.8%, 41.6% and 56.5% after 10, 20, 30 and 60 min of exposure, respectively. The peritoneal cavities, haematological, serum parameters and enzymatic activities of cancer cells were also affected by the concentration of nanoparticles³⁶⁶ in mice (**Fig. 35**).

----- **Figure 35** -----

The *in vivo* antitumour efficacy of Se nanoparticles in nude mice bearing HepG2 cancer xenografts was investigated by Sun et al.³⁶⁷ It was found that 11-mercaptoundecanoic acid-functionalized Ru–Se nanocomposites enhance the stability of particles, which will further support cellular uptake with minimum toxicity (**Scheme 3**). The 40-mg/ml modified particles significantly reduced the cell viability and tumour size by approximately 19.7% in 15 days. In addition, the corresponding doses have negligible effect on the body weight loss of the tumour-

bearing mice, which further confirms the specificity of Se towards tumour cells compared with normal tissue (**Fig. 36**).

-----**Scheme 3**-----

-----**Figure 36**-----

The bioavailability and renal and hepatic GPx activities were also affected by pH and dose (4–50 µg/kg) for epigallocatechin-3-gallate-functionalized Se (E-Se) nanoparticles (**Fig. 37**).³⁶⁸ The antioxidant activity of DPPH as scavenging agent and Se with a higher reducing power was assessed by Forootanfar et al.³⁶⁹ for MCF-7 cell lines. The obtained results showed that at a concentration of 200 g/mL, Se nanoparticles and SeO₂ showed scavenging activities of 23.1 ± 3.4% and 13.2 ± 3.1%, respectively. A higher IC₅₀ value of approximately 41.5 ± 0.9 g/mL for nano-Se than that for SeO₂ (6.7 ± 0.8 g/mL) confirmed the lower cytotoxicity of the biogenic Se nanoparticles under physiological conditions (**Fig. 38**). The neurotoxicity of Aβ₄₀ with or without Se nanoparticles also showed a dose-dependent behaviour. The aggregation of Aβ₄₀ significantly reduced at a higher concentration of Se nanoparticles with a higher IC₅₀ value.³⁷⁰

-----**Figure 37**-----

-----**Figure 38**-----

Recently, Faghfuri et al.³⁷¹ have studied the dose-dependent inhibitory effects of Se nanoparticles (<250 nm) on cancer-bearing mice. The growth of tumour cells and increase of mortality rate showed a significant impact with different doses of Se nanoparticles. It was found that 200 µg/day of Se nanoparticles exhibits a higher rate of survival than Se (100 µg/day). Such results will be of use as immunostimulatory agent against dose-dependent growth of tumour. In a separate study, He et al.³⁷² investigated that 0.2 mg Se/kg body weight of male *Sprague–Dawley* (SD) rats produced positive results on their health, whereas concentrations higher than 2.0

mg Se/kg body weight resulted in chronic toxicity to the rats. Nagy et al.³⁷³ studied the comparative role of different sources of Se on kidney toxicity. It was observed that in comparison with sodium selenite and selenate sources, nano-Se was harmless and can be used as food supplements with minimum effect to the normal cells. As a result, nano-Se has significant prospect in the reduction of renal toxicity compared with other Se sources.

5.3. Effect of morphology

The cytotoxic behaviour of various shapes of nano-Se such as spheres, rods, tubes and shuttles was studied by Panchapakesan et al.³⁷⁴ for HeLa cell lines. The anti-propagation- and vacuolization-induced endocytosis of cells were different for different shapes and concentrations of particles. It was found that tubes and shuttles exhibit a modest growth inhibition in contrast to rod- and sphere-shaped Se particles. Cell viability showed a large decrease for 50- $\mu\text{g}/\text{mL}$ nano-Se. Correspondingly, the percentage of apoptosis of HeLa cells in reaction was approximately 40% higher for 100- $\mu\text{g}/\text{ml}$ Se nanospheres. The surface functionalization also affected the size and shape of the particles, which further affected the toxicity.³⁷⁵ The as-fabricated particles exhibited a higher cellular uptake and also induced the reversal of cisplatin (CIS)-induced toxicity in the system (**Figs. 39 and 40**). The antioxidative activity was also amended by using different shapes and amounts of nano-Se.

-----**Figure 39**-----

-----**Figure 40**-----

5.4. Effect of size

Zhang et al.³⁷⁶ reported the effect of different sizes of nano-Se on *in vitro* capturing aptitude for various free radicals, including carbon-centred free radicals from 2,2'-azo-bis-(2-amidinopropane) hydrochloride (AAPH), stable free radical of 1,1-diphenyl-2-picrylhydrazyl

(DPPH), superoxide anion (O_2^-) generated from xanthine/xanthine oxidase (X/XO) system and singlet oxygen (1O_2) produced from haemoporphyrin. The changes produced were attributed to the enhanced surface area exposure of smaller particles on free-radical electron substitution. It was found that nano-Se could directly scavenge the free radicals in a size-reliant manner.³⁷⁷ The sizes and concentrations (0.5–2.0 mg Se/kg) of nanoparticles also affected the blood and liver GST activity for mice fed with supra-dietetic dose of nano-Se (**Fig. 41**).

-----Figure 41-----

Bartůnek et al.³⁷⁸ studied the effect of size variation from 43 to 136 nm on the antimicrobial activities of *E. coli* (Gram-negative bacteria), *Staphylococcus epidermidis* and *Staphylococcus aureus* (Gram-positive bacteria) as model organisms. The surfactant-mobilized Se nanoparticles have significant inhibitory effect on *S. epidermidis* and *S. aureus* with inhibition zones of 3.5 ± 0.5 and 3.0 ± 0.4 mm, respectively, with concentration as low as 2 ppm. The effect of glucan-modified Se nanoparticles with average sizes of 28, 33, 44 and 52 nm also showed controlling effect on the apoptosis of HeLa cells. The anticancer activity of Se nanoparticles is inversely proportional to the size of the particles. Larger the size of the particles, lesser is the bioactivity and lower will be the *in vivo* antitumour activity. On the contrary, generation of ROS is also affected by the size of the particles.³⁷⁹

5.5. Value of functionalization

Functionalization of particles facilitates the dispersion, diffusion, cellular uptake and biological activities of Se in physiological media.^{380,381} The multi-branched, cell-supported contouring approach has the ability to provide valuable means for the improvement of these Se nanomaterials for biomedical purposes. The controlling effects, cytotoxicity and growth

retardation of PEG–selenium nanoparticles (SeNPs) were considerably higher for R-HepG2 cells than HepG2 cells (**Table 8**).³⁰⁴ The cell viability decreases to 75.2%, 34.97%, 17.76% and 14.8% for 2-, 4-, 8- and 16- μ g/ml PEG-modified SeNPs, respectively. Furthermore, it was found that 12 μ g/ml of PEG-modified Se has cell viability of approximately 94.8% and 88.9% after 10–20 min. PEG200-modified Se at 1, 2 and 4 μ g/ml reduced cell viability to 83.5%, 81.2% and 76.2%, respectively, with an IC₅₀ value of 38.2 μ g/ml.

-----**Table 8**-----

The *in vitro* cytotoxic inhibitory effects against A375, MCF-7, HepG2, Colo201 and PC-3 cancer cells with IC₅₀ values ranging from 6.2 to 14.4 μ M were also investigated for 5FU-functionalized SeNPs (**Fig. 42**).^{381a} The current modification of SeNPs has also displayed more selectivity and less cytotoxicity for normal human cells (e.g. Hs68 human fibroblasts, HK-2 proximal tubular cells and MCF-10A human mammary epithelial cells) and bone marrow-derived macrophages (BMM), with the corresponding IC₅₀ values of 67.1, 88.4, 72.7 and 61.3 μ M.

-----**Figure 42**-----

In addition, MCF-10A cells were also used as a replica to observe the effects of 5FU-SeNPs on healthy breast cells as compared with the cancer-affected ones. The results showed that 5FU-SeNPs exhibited a higher cellular uptake and lower cytotoxicity towards MCF-10A (IC = 72.7 μ M) than MCF-7 cells (IC = 6.8 μ M) (**Fig. 43**). The nature of cell also affected the inhibitory effects of Se towards cancer. This selectivity could be partially due to the different protein and gene expression contours of different cells, which further affects the intracellular pathways for respective systems. Currently, the effect of polymer coverage on amending the

surface charges of Se nanoparticles have been analysed by Jain et al.^{381b} Such functionalization significantly enhanced the utilities of Se nanoparticles in bio-remediation.

-----**Figure 43**-----

The combination of antitumour drug irinotecan with nano-Se also showed effective inhibitory effects on tumour growth of HCT-8 cells.³⁸² The 50-μM concentration of nano-Se showed the suppression of tumour cells up to 63%. Only 47% of hepatoma tumour cells (HTCs) were able to survive after the treatment with the combination of irinotecan with nano-Se within 48 h. This combination also produced some effects on the expressions of p53 proteins in the tumour cells and IEC6 rat gut epithelial cells, and further controlled tumour growth. The anticancer effect of Se nanoparticles synthesized using carboxylic group of acetic acid, pyruvic acid and benzoic acid played a concentration-dependent (10–100 μM) inhibitory role against Dalton's lymphoma cells.³⁸³ Se nanoparticles can affect the nuclear morphology and DNA fragmentations of the infected cells and cure the tumour by using low concentrations of Se nanoparticles. The conjugation of Se nanoparticles with folate also showed a higher tendency towards cancer-targeted drug delivery systems than the conventional drugs.³⁸⁴ The modification of Se surface with FA enhanced the cellular uptake of particles and antagonized the effect of multidrug resistance in cancer treatment. The surface functionalization of Se nanoparticles also modulated the inhibition of ABC family of protein expression, which is mainly responsible for drug resistance. In a separate study, Zheng et al.³⁸⁵ investigated the role of polyamidoamine-modified Se nanoparticles against the multidrug resistance. The modified particles can deliver the DDP and siRNA to A549/DDP cells for regulating the expression of P-gp cells, induce cell apoptosis and restrict the growth of tumour.

6. Potential applications of selenium nanomaterials

Se nanomaterials are widely used for various high-technological applications in diagnostics and therapy, electronic devices, catalysis, fuel cells and bio- and environmental remediations.

6.1. Diagnostics and therapy

The lower intrinsic toxicity, high surface area and amendable surface chemistry of Se nanoparticles make it the most promising material in diagnostics, therapy and clinical applications.^{386–388} The use of Se nanoparticles in cancer treatment has made an innovative breakthrough in therapeutics.³⁸⁹ The significant characteristic features of sub-100-nm Se nanoparticles overcome the limitations of customary drug release schemes.³⁹⁰ The high surface area facilitates drug loading with a higher competence to targeted liberation with minimum leakage and side effects. Nano-Se also possessed long-lasting circulation of bioactive particles with enhanced body preservation capacity and permeability.³⁹¹ The external modification of Se nanoparticles presented a better platform to incorporate various curative drugs or bio-macromolecules by covalent or non-covalent conjugation with nanoparticles.³⁹² Jia et al.³⁹³ demonstrated the complexation of water-soluble polysaccharide–protein over Se surface. The higher adsorptive aptitude via NH, C=O, COO⁻ and C–N groups of proteins on Se enhanced the anti-proliferative activity towards lung and breast cancers. The protective action of surface-functionalized Se against UV-induced DNA damage activities was well documented in the literature.^{394a} Recently, Yu et al. have analysed the use of X-ray-responsive Se nanoparticles in the treatment of cancer via chemo-radio therapy technique.^{394b} Se has a direct effect on the enzymatic actions of seleno- and glutathione peroxidase enzymes. Se at supra-dietary doses exhibited a chemo-preventive action by inducing the detoxification of harmful electrophilic compounds by GSH S-transferase enzyme (**Fig. 44**).³⁹⁵

-----Figure 44-----

Se nanoparticles have a tendency to interrupt the activity of estrogen receptor- α (ER α) inside the cancer cells. The protective actions of Se towards *in vivo* and *in vitro* cell injury from free radicals make it useful for preventing the oxidation of DNA. The antimicrobial properties make it significant towards developing a better immune system. Epidemiological, biological and clinical studies on male albino rats showed that Se decreases the risk of prostate, lung and colon cancers.³⁹⁶ The growth of cancerous osteoblasts was also managed by using nano-Se.³⁹⁷ The higher selectivity, caspase activation and mitochondrial dysfunctional activities towards cancer cells improve the remedial competence of Se in anticancer drugs. Vekariya and co-workers³⁹⁸ studied the concentration-dependent inhibitory effect of 40–90-nm particles on the growth of stage I mammary tumour breast cancer MCF-7 cells. Se particles exhibited a higher selectivity for early-stage breast cancer in contrast to the metastatic stage. The antitumour activity of Se is mainly associated with the restraining action on phase I enzymes and stimulation of phase II enzymes (**Fig. 45**). CIS-induced improper redox equilibrium of reproductive organs and nephrotoxicity can be modified by using Se supplementation.³⁹⁹ The brutal degenerative transformations in testicular structures with healed spermatogenesis were also obtained by nano-Se (**Fig. 46**).

-----Figure 45-----**-----Figure 46-----**

Human lung carcinoma cell A549, breast cancer cell MCF-7, androgen-independent prostate cancer cell DU-145 and androgen-dependent LNCaP cells were also treated with these particles by decreasing the regulation of AR protein, which further controls the cell proliferation

in tumours. Nuclear endocytosis increased the apoptotic index of tumour cells by distracting nuclear condensation, DNA disintegration and collapsing of plasma membrane (**Fig. 47**).

-----**Figure 47**-----

The inhibitory effect of Se on the blood vessels carrying oxygen and food to the tumour cells was mainly responsible for the prevention of tumour. Se–Ru composites also possess the restraining effects on fibroblast growth factor (bFGF), which further enhances the angiogenesis of human umbilical vascular endothelial cells (HUVEC). The corresponding fragmentation of DNA and depolarization of mitochondria also induced the concentration-dependent (20–40 μ M) apoptosis of A375 human melanoma cells (**Fig. 48**).⁴⁰⁰

-----**Figure 48**-----

By contrast, the cell cycles of healthy cells were unaffected during exposure, which further confirmed the selectivity of Se particles towards different cells. Sialic acid-modified particles with a lower passive transportation in biological system also showed higher apoptosis towards cancerous HeLa human cervical carcinoma cells. The activation of caspase-3 and subsequent cleavage of poly(ADP-ribose) polymerase (PARP) by DNA fragmentation is responsible for this changes. Se nanoparticles also exhibited significant importance in the anticancerous activities towards Bel7402 and HepG2 human hepato cellular carcinoma cells.⁴⁰¹ Activities of various commercially available anticancerous drugs such as adriamycin and tamoxifen can be enhanced by using nano-Se. The generation of ROS, GSH and thioredoxin was also modulated by Se to treat cancers in intra-peritoneal cavity (**Fig. 49**).³⁶⁵

-----**Figure 49**-----

Tf-functionalized Se particles showed better loading capacity for doxorubicin (DOX), which further affected the growth of MCF-7, HepG2 and A375 cancer cell lines, with IC₅₀ values

ranging from 7.1 to 11.1 μM .⁴⁰² The cellular internalization path was also investigated to visualize the mechanistic process of anticancerous activities of Se nanoparticles (**Fig. 50**). It was found that Tf-Se nanoparticles have the tendency to attach with ferric ions through clathrin-coated vesicles. Furthermore, lipid raft-mediated endocytosis also supported the internalization of nanoparticles with a higher generation of ROS in the tumourous cells. The mitochondria were also affected during ROS generation and supported the apoptosis.

-----**Figure 50**-----

The presented approach to use Tf-Se nanoparticles opens a novel pathway for synergistic treatment of cancer with a higher efficiency and less side effects. The transcriptional activity of androgen receptor by down-regulating its mRNA and protein expression also influenced the growth of prostate LNCaP cancer cells in the presence of Se.⁴⁰³ The activities of Akt kinase also affected the phosphorylation and Mdm2-controlled degradation of androgen receptor. The adhesion force and Young's modulus of cancerous MCF-7 cells were modulated with nano-Se. Particles have an ability to induce the down-regulation and disorganization of trans-membrane CD44 molecules and F-actin (**Fig. 51**). The corresponding effects of particles on respective proteins further affected the tension on the cell side walls and hence decreased the stiffness of cancerous cells.

-----**Figure 51**-----

Se nanoparticles also showed a defensive action against the progression of diabetic nephropathy (DN) in male (SD) rats.⁴⁰⁴ Nano-Se also showed inhibitory effects on the levels of blood urea nitrogen (BUN), creatinine, fibronectin and collagen in diabetic rats. The levels of albumin and heat shock protein (HSP-70) showed effect enhancement in the presence of nano-Se. The kidney of diabetic rats showed modulated apoptotic proteins Bax and Bcl-2 with Se. The obtained

results reveal the therapeutic role of SeNPs in controlling DN by decreasing the oxidative stress and activating cyto-protective protein HSP70 and durability of SIRT1 protein in the species. The anti-biofilm effect of the biogenic SeNPs has also been investigated recently by Shakibaie et al.^{405a} against the clinically isolated bacterial strains of *S. aureus*, *P. aeruginosa* and *Proteus mirabilis*. The average size of Se (80–220 nm) showed approximately 42%, 34.3% and 53.4% inhibition of biofilms in *S. aureus*, *P. aeruginosa* and *P. mirabilis* respectively. Novel selenium-substituted hydroxyapatite nanoparticles (SeHANs) were synthesized by Wang et al.^{405b} as an anticancer agent. The respective blood biochemical analysis showed that the as-synthesized SeHAN group exhibited significantly lower toxicities on the liver and kidney functions.

Alzheimer's disease (AD) is considered as one of the most common disorders worldwide.^{406–409} At present, various diagnostic practices have been proposed for effective cure of AD, among which, the most commonly practiced method is the use of aggregates of amyloid β (A β). Yang et al.³⁷⁰ demonstrated the use of nano-Se to cure AD. The availability of high surface area, less toxicity and better binding ability of Se with A β exhibited a significant effect on the fibrillization of A β_{40} (**Fig. 52**).

-----Figure 52-----

The lysosomal pathway is mainly used for the reduced volume of intracellular A β_{40} aggregates in the presence of Se nanoparticles. The biogenic Se also possessed impending benefits to treat CE or hydatid disease. The amelioration of anastrozole-induced toxicity of bone, brain and kidney was also optimized by using Se in ovariectomized female SD rats.^{410,386} The corresponding inhibitory effects of Se on the activities of brain butyryl cholinesterase and gamma glutamyltransferase were also well documented in the literature.³⁸⁶ Carbendazim-induced oral subchronic testicular toxicity in bucks was also affected in the presence of Se particles.⁴¹¹

Supplementation with Se nanoparticles has a momentous increase in sperm count and minimum oxidative stress parameters in the bucks' testicular tissue. Li et al.⁴¹² investigated the ameliorative role of Se against the hepatic, histopathological, oxidative and apoptosis stress of Cd ions. The ameliorative roles of Se nanoparticles against the anti-inflammatory drug 'aspirin' and organo-phosphorus insecticide 'diazinon' were studied by Mossa and co-workers.⁴¹³ The regeneration of liver structure was also achieved by nano-Se. The protective effects of Se particles were also found on fluoride-induced variations in certain mice brain enzymes.^{414–417} The curative role of Se towards *Leishmaniasis* disease is also well documented in the literature. The peripheral conversion of T4 to T3 in liver and kidneys was also modulated with iodothyronine deiodinase (IDI) and Se. The deficiencies of Se also led to the inadequacy of iodine, which further affects the synthesis, discharge and use of thyroid hormone. The scarcity of Se further leads to the development of bone and growth plates, which is the primary cause of Kashin–Beck disease (KBD). The composites of Se with chondroitin sulphate showed better curative effects towards KBD and osteoarthritis.⁴¹⁵ The iron homeostasis and transferrin gene expression in sheep were modulated by hypoferremia and cell internalization with Se.⁴¹⁸ The anti-inflammatory applications towards lipopolysaccharide (LPS)-stimulated nitric oxide (NO) production by suppressing the expression of TNF- α mRNA and iNOS mRNA were modulated with a water-soluble derivative of *Ganoderma lucidum* polysaccharide (SPS).^{419a} In a separate study, Huang et al.^{419b} developed highly effective antibacterial agents by using the Se nanoparticles. These agents have a direct irreversible effect on the bacterial membrane. Recently, the *in vitro* growth of calcium oxalate (CaC_2O_4) crystals has also been investigated in the presence of BSA-modified Se nanoparticles.⁴²⁰ The resultant particles affect the crystallization of CaC_2O_4 crystals and prevent the accumulation of crystals in the body, which further generates

stones in the body. Therefore, these particles facilitate the bio-mineralization of body stones with low concentrations of nanoparticles.

In summary, the bio-remedial, diagnostic and therapeutic applications of Se nanomaterials opened modern prospects in medical science, as it provides superior and effective diagnostic and remedial approaches. Because of the excellent biological performances at the laboratory level, recently several nano-based drugs have been used in clinical trials such as adenosine triphosphate (ATP)-functionalized Se nanoparticles for *in vitro* diagnostic and tumour targeting.¹⁶⁶ Although considerable diagnostic and therapeutic applications have been documented, further studies are required before using these drugs for real medical applications.

6.2. Antagonistic effect of selenium on minerals

Toxicity of various metal ions such as silver (Ag), arsenic (As), cadmium (Cd), mercury (Hg), fluorine (F) and thallium (Tl) was treated by using Se nanoparticles. The corresponding higher binding efficiencies of Se nanoparticles with heavy transition metal ions (Hg or Cd) change them into a less-toxic form.⁴²¹ The antagonistic effect of selenobacterial strains on wheat plants was very much affected in the presence of nanoparticles.⁴²² Zhao et al.⁴²³ have correlated the Pearson correlation analysis among topsoil-cultivated grains and primary cancer tissue of liver, lung and gastric organs in the Anhui province of Eastern China to compare the antagonistic effect on heavy metal ions. The exogenetic and antioxidative properties of N, P, Zn, polysaccharide, catechins, polyphenol, free amino acid and tea caffeine are also affected by nano-Se.⁴²⁴ The productivity and yield of tea leaves were enhanced by fertilizing with Se nanoparticles. Detoxification of Hg was also achieved by preparing non-reactive mercury–selenium complexes.^{425–428} The metal uptake, absorption and redistribution properties of As, Zn and Ni from the soil were affected by nano-Se.⁴²⁹ The oxidative damage and genotypic variation of Fe,

Zn, Cu, Mn Hg, Pb and Ar were also modified by antagonistic interactions with Se in Broccoli.^{430,431} The presence of particles only influenced the antioxidative properties of the respective system without affecting the uptake of essential micronutrients from soil. Bertoldi et al.⁴³² studied the combined effects of elemental accumulation and distribution pattern in *Vitis vinifera L.* cv. Chardonnay berries. The comparative results demonstrated that several elements such as Hg, Ge, Li, K, Na, Mg, Se, Sb, Rb, Tl, U, Th and Zr mainly accumulated in the flesh of the berries. Some elements such as Ca, Eu, Ba, Mn, P, Fe, Zn and Sr are present mostly in the seeds. Moreover, elements such as Sn, Ga, B, Al and some rare earth elements (except Eu) accumulated generally in the skin (**Fig. 53**).

-----Figure 53-----

The corresponding cadmium-induced hepatotoxicity, reduction in malondialdehyde (MDA) levels and enhancement in antioxidant activities of enzymes were also influenced with nano-Se.⁴³³ The retaining power of lipids and cholesterol esters in triglycerides, total phospholipids and mono- and polyunsaturated fatty acids showed a significant increase in the presence of nano-Se. The corresponding decrease in the activities of GSH-Px and TR in the livers of Se-treated rats showed the antagonistic effect of scutellarin on Se.⁴³⁴ Copper-induced DNA damage in the blue mussel *Mytilus edulis* was also controlled in the presence of Se.⁴³⁵

Recently, Jain et al.⁴³⁶ have shown that biogenic elemental Se nanoparticles have a higher tendency to absorb divalent cationic heavy metals from paper mill waste water,^{422a} and Jain and co-workers^{422b} have analysed the adsorptive removal efficiency of Se nanoparticles towards metal ions. It was found that approximately 78% of the added Cu was removed by using these nanoparticles at pH 5.2. The results showed the prospects of Se nanoparticles to treat industrial

waste from electroplating and acid mine drainage, as they work very well in acidic and near-neutral media.

6.3. Electronic applications of selenium nanomaterials

The high surface area, photoconductive, thermoelectric, piezoelectric and nonlinear responses of nano-Se make it useful to prepare light-weight electronic devices. Catalysis, photographic exposure metres, solar cells, electrical rectifiers, pressure and chemical sensors and xerography and fuel cells were also prepared with these particles.^{437–439} Se-based thin-film metal chalcogenide solar cells represent an efficient and low-cost alternative to common silicon-based photovoltaic devices.^{440,441} In 1899, Charles Fritts fabricated Se-coated ultra-thin junctions of Au-based solar cells for the first time.⁴⁴² During the 1930s, both Se- and copper oxide-based cells were used to fabricate light-sensitive photometers in cameras.⁴⁷ The rate of diffusion, electron transportation and spectral response were easily controlled in solar cells with surface-modified Se particles and their nanocomposites.^{443–445} The electrical J – V properties of copper- and indium-based solar cells were easily amended with Se.⁴⁴⁶ An open-circuit voltage of 371 mV and current density of 29.6 mA/cm² were easily achieved with such materials. The lower value of photocurrent for the respective system was due to the existence of large-scale defects on the free surface (**Fig. 54**).

----- Figure 54 -----

Se@CuSe core@shell nanoparticles were also used to prepare mechanical sensors and electrical rectifiers and in tumour therapy or xerographic agents. The first laboratory-scale solar cell with up to 3% conversion efficiency was achieved with these modified core-shell particles of Se (**Fig. 55**).⁴⁴⁷ In a separate study, Dun and co-workers⁴⁴⁸ developed a simple and efficient ligand-exchange scheme to amend the surface properties of CZTSe NPs by using Na₂S as a non-

toxic solvent. The generated cells exhibit a higher carrier mobility of approximately $8.9\text{ cm}^2/\text{Vs}$. On the contrary, Zhang et al.^{449a} used the solution-based approach to fabricate $\text{Cu}_2\text{ZnSn}(\text{S},\text{Se})_4$ thin films, which were further used in solar cells. The as-generated cells exhibited a 7.86% conversion efficiency, which was approximately 60% higher than available cells. Laramona et al.^{449b} developed a fast, eco-friendly and scalable approach to prepare CZTSSe films with cell efficiencies of approximately 9%. The use of water as solvent makes this process more useful for practical applications. The effect of hot solution injection method on the preparation of CuFeSe_2 nanocrystals was studied by Wang et al.⁴⁵⁰ in metallic acetylacetones with diphenyl diselenide (Ph_2Se_2) in oleylamine solution. The as-generated particles directly influenced the magnetic and optoelectronic properties of Se nanoparticles and opened a new prospect in photovoltaic devices.

---- Figure 55----

The use of Se also eliminates the limitation of conventional methods for preparing thin films under high temperature and inert atmosphere.⁴⁵¹ At present, the binary nanocomposites of copper, zinc, tin, sulphur and selenium have been easily generated with cost-effective process. The probability of contamination during hot injection method was also zero. The presence of ethanolic media during synthesis has also made the extraction process more convenient than the commercially available ones. The amendable morphologies and band gap energies for CuInSe_2 (CIS) were also achieved by simple solution process in the presence of oleic acid as solvent.⁴⁵² The pure chalcopyrite-based long spectral ranged thin-film solar cells of Se were also prepared by a rapid one-pot synthesis.⁴⁵³ In a separate study, Liu et al.⁴⁵⁴ examined the formation of different morphologies of copper–indium–gallium–diselenide thin films by adjusting the mole ratio of Cu:In:Ga:Se (0.95:0.69:0.38:1.99) and corresponding ratios of Ga/(In + Ga) and Cu/(In +

Ga) to 0.35 and 0.89, respectively, in organic polymer matrix. The ultra-sensitive reversible redox fluorescent switch of Se was fabricated by doping the nano-Se with graphene QDs.^{456a} The as-fabricated switch has a higher sensitivity towards the detection of oxidative hydroxyl radical ($\cdot\text{OH}$) and reductive GSH in both aqueous solutions and living HeLa cells. This new detection device provided a better understanding for redox events associated with the cellular systems. The cation exchangeability of $\text{Cu}_{2-x}\text{Se}/\text{Cu}_{2-x}\text{S}$ core/shell nanocrystals resulted in high diffusivity of electronic devices. Such changing aptitude has a direct effect on the selective transformation of cores and shells in the core/shell copper chalcogenide NCs.^{456b}

6.4. Selenium nanoparticle-based DMFCs

The rapidly increasing demand for energy, shrinking of fossil resources and serious global warming effects have enhanced the search for environmentally sustainable energy sources. Se-based DMFCs is one of the newly introduced renewable energy technologies, as they assist in fuel efficiency and low functioning temperatures without affecting the environment from poisonous matters such as SO_x and NO_x .⁴⁵⁷⁻⁴⁶¹ Cathode poisoning and lower rate of oxygen reduction in the presence of methanol can be easily rectified by using Se.⁴⁶² The customized catalyst improves reactivity and durability against the electrochemical oxidation in DMFCs.⁴⁶³⁻⁴⁶⁸ The corresponding methanol tolerance limit is also enhanced with Se modification in DMFCs. Bron et al.⁴⁶⁴ studied the effect of Se nanoparticles on ruthenium-based cluster catalysts for oxygen reduction by using rotating-disc electrode measurements. Four to five times higher current densities were achieved by using Se than Ru alone. Whipple et al.⁴⁶⁹ studied the applications of Se-functionalized Ru particles for methanol-tolerant light-weight tiny cathode catalysts for fuel cells with laminar flow. CNT-modified Se-supported Ru catalysts open new prospects for non-platinum-based oxygen reduction in DMFCs.⁴⁷⁰ Cell efficiency was easily

controlled by varying the size, shape and composition of the materials. Higher catalytic activities of ORR in acidic media were also achieved by fabricating RuSeMo- and RuSnMo-based fuel cells.⁴⁷¹ The presence of Se has a significant inhibitory effect for dormant oxide layer over Ru. Moreover, Se particles acted as a barrier for oxide formation over ruthenium surface and maintained high oxygen reduction activity of the cells. Inukai et al.⁴⁷² found that there was a significant effect of surface coverage with Se nanoparticles in DMFC fabrication. Se-modified Ru electrodes are smoother and exhibit spontaneous reactivity towards oxygen reduction. The effects of Se concentrations on the ORRs in DMFCs of Ru were also studied by Zehl et al.⁴⁷³

These Se-based fabricated fuel cells highly affect the overall system configuration, which results in the production of more compact and highly specific energy power source with simple working operation.

6.5. Selenium nanomaterials for chemical sensor applications

Biosensing of H₂O₂ was easily achieved by using biogenic Se nanoparticles.⁴⁷⁴ The biosensor fabricated on glassy carbon electrodes exhibited better analytical performance with a lower detection limit of 8×10^{-8} M. Being conductive in nature, the as-synthesized Se nanoparticles offered an excellent micro-environment for electron transport in HRP. The higher electrocatalytic activities of Se towards H₂O₂ were identified from the comparative role of different concentrations on reduction current values. Iranifam and co-workers⁴⁷⁵ investigated the presence of dinitrobutylphenol (DNBP) in waste water by using nano-Se. It was observed that direct reaction of environmental contaminants in the acidic medium was significantly improved in the presence of Se. The changes were explained based on the higher electron transport ability of Se for redox reactions of KMnO₄-DNBP. Se-functionalized silica nanopores also provided better heterojunctions for preparing optical filters for sensing applications.⁴⁷⁶ Zapp et al.^{477a} also

fabricated an electrochemical sensor for the detection H_2O_2 by using amino derivative of Se nanoparticles, and GPx, an amino selenide, was immobilized on CHI–GN nanoplatelets using glyoxal. In the presence of hydrogen peroxide, GPx catalyses the oxidation of reduced GSH and used a cofactor of GPx. The best analytical responses were obtained by using GPx (7.4 μg per electrode), CHI–GN (0.10:0.05%, w/v) and 0.1 M Britton–Robinson buffer solution (pH 7.0) containing 99.0 μM of GSH. Similarly, Qiao et al.^{477b} performed the colorimetric detection of H_2O_2 and xanthine compounds by using selenium-doped graphitic carbon nitride nanosheets.

In summary, it is clear that Se nanomaterials exhibit excellent conductivity and electrochemical properties, and hence they can be used as an efficient electrode material for fabricating highly sensitive and selective chemical sensors.

7. Summary and future prospects

The major technical and scientific concerns in the growth, properties and applications of semiconducting nanomaterials have motivated researchers to explore new methods to prepare and design technologically important materials. Interesting properties and potential applications of Se make it the most important functional material for generating smart devices. The lower intrinsic toxicity, high surface area and amendable surface chemistry make Se an extremely important material in the fields of medicine, diagnostics and therapeutics, and for clinical applications. The distinctive morphological variations and physical attributes make Se one of the potential elements for preparing efficient optical devices. In summary, this study updated recent information on the synthesis, properties and various applications of Se nanomaterials. The major developments were also outlined with respect to characterization, properties and applications of Se nanomaterials. A detailed in-depth knowledge on the nucleation and growth phenomena for

different morphologies of Se has opened new prospects for technologically important smart materials. The rapidly developing chemo-preventive and chemotherapeutic applications of Se nanomaterials have revolutionized the fields of biotechnology and medical science. The formation of non-toxic and highly pure Se nanomaterials has opened new pathways for their use in various high-technological applications in electronic devices, catalysis, fuel cells and bio-remedial and environmental remediation, including antagonistic effects on various metal ions. Although Se nanomaterials are studied in detail, their applications pose many crucial drawbacks, which require proper handling and comprehension. In particular, these fundamental points include:

1. (i) Development of new and improved low-cost and facile synthetic methodologies to control the shapes, sizes and properties of Se nanomaterials.
2. (ii) Better understanding of physical and chemical properties related with specific application of Se nanomaterials.
3. (iii) Exploration of new physical and chemical properties of doped and nanocomposites of Se.
4. (iv) Understanding the relationship between Se-based nanocomposites and their efficient applications in diagnostics and therapy, catalysis, electronics, fuel cells, bio-remedial applications and environmental remediation.

This study provides a brief overview of interdisciplinary applications of Se nanomaterials by including chemistry, physics, materials science and biotechnology. It is aimed to provide an outline of the remarkable potentials of Se nanomaterials with novel and improved properties. The future prospects of Se nanomaterials contain a combination of both hopes and confronts. Se nanomaterials with controlled shapes and sizes are expected to exhibit unique properties, not

only for optical devices but also in various areas of science and technology. It may also present new hopes for the development of functionalized Se structural elements with the aspiration of characteristics and desired applications. Most importantly, because of their less toxicity towards normal cells, it is expected that Se nanomaterial-based drugs can be commercialized in the near future. In summary, Se nanoparticles have shown significant improvements and the multi-branched activities of Se can offer a valuable means for enhancing the properties of these nanomaterials for various high-technological applications.

Acknowledgements

Savita Chaudhary is grateful to DST Inspire Faculty Award [IFA-CH-17] and DST Purse grant for financial assistance. Ahmad Umar would like to acknowledge the support of the Ministry of Higher Education, the Kingdom of Saudi Arabia, under the Promising Centre for Sensors and Electronic Devices (PCSED) project (PCSED-002-11) at Najran University, the Kingdom of Saudi Arabia.

References

- [1] Flohe L. Glutathione peroxidise. Basic Life Sci 1988;49:663-8.
- [2] Arteel GE, Mostert V, Oubrahim H, Briviba K, Abel J, Sies H. Protection by selenoprotein P in human plasma against peroxynitrite-mediated oxidation and nitration. Biol Chem 1998;379:1201-5.
- [3] Burke RF, Hill KE, Awad JA, Morrow JD, Kato T, Cockell KA, Lyons PR. Pathogenesis of diquat-induced liver necrosis in selenium-deficient rats: assessment of the roles of lipid peroxidation and selenoprotein P. Hepatology 1995;21:561-69.
- [4] Saito Y, Hayashi T, Tanaka A, Watanabe Y, Suzuki M, Saito E, Takahashi K. Selenoprotein P in human plasma as an extracellular phospholipid hydroperoxide glutathione peroxidase.

Isolation and enzymatic characterization of human selenoprotein p. J Biol Chem 1999;274:2866-71.

- [5] Löwig CJ. Constitution of the Organic compoundsand comparision with the inorganics. Poggendorff's Ann Phys 1836;37:552-61.
- [6] Waitkins GR, Clark CW. Selenium Dioxide: Preparation, Properties, and Use as Oxidizing Agent. Chem. Rev 1945;36:235–289.
- [7] Banks CK, Hamilton CS. Organoselenium Compounds. I. Diphenylselenium Dihydroxides and Diphenylselenides. J Am Chem Soc 1939;61:2306-8.
- [8] White RN, Smith JV, Spears DA, Rivers ML, Sutton SR. Analysis of iron sulphides from UK coal by synchrotron radiation X-ray fluorescence. Fuel 1989;68:1480-86.
- [9] Mastalerz M, Hower JC, Mardon S, Drobnik A, Lis G. From in-situ coal to fly ash: a study of coal mines and power plants from Indiana. Int J Coal Geol 2004;59:171-92.
- [10] Waitkins GR, Bearse AE, Shutt R. Industrial Utilization of Selenium and Tellurium. Ind Eng Chem 1942;34:899-910.
- [11] Greenwood NN, Earnshaw A. Selenium, tellurium, and polonium, of Chemistry of the elements (2nd ed.): Oxford, England, Butterworth-Heinemann, 1998,Chap.16,p. 747.
- [12] Boggs CR, Blake JT. Deprotonized Rubber. Ind Eng Chem 1936;28:1198-1202.
- [13] Zhang J, Zhang SY, Xu JJ, Chen HY. A new method for the synthesis of selenium nanoparticles and the application to construction of H₂O₂ biosensor. Chin Chem Lett 2004;15:1345-54.
- [14] Mann RS, Yao KC. Oxidation of Isobutene over Selenium Dioxide-Modified Copper Oxide Catalysts. I&EC Product Research and Development 1967;6:263-66.
- [15] Luce WA. Stainless Steels and Other Ferrous Alloys. Ind Eng Chem 1951;43:2258-71.

- [16] Kolomiets BT, Rukhlyadev YV, Shilo VP. The effect of copper and silver on the conductivity and photoelectric properties of glassy arsenic selenide. *J Non-Cryst Solids* 1971; 5:402.
- [17] Smith W. Selenium. *Nature* 1873;7:303-13.
- [18] Wang H, Wei W, Zhang SY, Shen YX, Yue L, Wang NP, Xu SY. Melatonin-selenium nanoparticles inhibit oxidative stress and protect against hepatic injury induced by *Bacillus Calmette–Guérin/lipopolysaccharide* in mice. *J. Pineal Res.* 2005;39:156-63.
- [19] Remitz KE, Neuroth N, Spert B. Semiconductor doped glass as a nonlinear material. *Mater Sci Eng* 1991;139:413-16.
- [20] Horan P, Blau W. Linear and nonlinear optical properties of semiconductor particles. *Phase Transit* 1990;24:605-39.
- [21] Shalaev VM. Transforming Light. *Science* 2008;322:384-86.
- [22] Wolf E, Kollonitsch V, Kline CH. Selenium supplementation, survey of selenium treatment in livestock production. *J Agric Food Chem* 1963;11:355-61.
- [23] Cherin P, Ungar P. Refinement of the crystal structure of α -monoclinic Se. *Acta Crystallogr B* 1972;28:313-17.
- [24] Foster LH, Sumar S. Selenium in health and disease: A review. *Crit Rev Food Sci Nutr* 1997;37:211-28.
- [25] Reyes LH, Marchante-Gayón JM, García Alonso JI, Sanz-Medel A. Application of isotope dilution analysis for the evaluation of extraction conditions in the determination of total selenium and selenomethionine in yeast-based nutritional supplements. *J Agric Food Chem* 2006;54:1557-63.

- [26] Huang Y, Xu J, Hu Q. Effect of selenium on preservation quality of green tea during autumn tea-processing season. *J Agric Food Chem* 2005;53:7444-47.
- [27] Sharp DE. Chemical Composition of Commercial Glasses. *Ind Eng Chem* 1933;25:755-64.
- [28] Kolb D, Kolb KE. The chemistry of glass. *J Chem Educ* 1979;56:604-08.
- [29] Holubova J, Cernosek Z, Cernoskova E, Cerna A. Crystallization of supercooled liquid of selenium: The comparison of kinetic analysis of both isothermal and non-isothermal DSC data. *Material Lett* 2006;60:2429-32.
- [30] Bureau B, Troles J, LeFloch M, Smektala F, Silly G, Lucas S. Solid state ^{77}Se NMR investigations on arsenic-selenium glasses and crystals. *J Solid States Sci* 2003;5:219-24.
- [31] Brus LE. Chemical Approaches to Semiconductor Nanocrystals. *J Phys Chem Solids* 1998;59:459-65.
- [32] Wang Y, Herron N. Nanometer-Sized Semiconductor Clusters: Materials Synthesis, Quantum Size Effects, and Photophysical Properties. *J Phys Chem* 1991;95:525-32.
- [33] Yanagida S, Kawakami H, Midori Y, Kizumoto H, Pac CJ, Wada Y. Semiconductor Photocatalysis. ZnS-Nanocrystallite-Catalyzed Photooxidation of Organic Compounds. *Bull Chem Soc Jpn* 1995;68:1811-23.
- [34] Zhang B, Ye X, Dai W, Hou W, Zuo F, Xie Y. Biomolecule-assisted synthesis of single-crystalline selenium nanowires and nanoribbons via a novel flake-cracking mechanism. *Nanotechnology* 2006;17:385-90.
- [35] Chakraborty I, Moulik SP. Preparation and characterization of PbS nanoparticles in AOT micellar medium. *J Nanopart Res* 2004;6:233-40.
- [36] Banyai L, Koch SW. Semiconductor Quantum Dots: Singapore: World Scientific 1993.

- [37] Pandey P, Singh SP, Arya SK, Gupta V, Dutta M, Singh S, Malhotra BD. Application of thiolated gold nanoparticles for the enhancement of glucose oxidase activity. *Langmuir* 2007; 23:3333-37.
- [38] Byron G, Yin YD, Xia YN. A Solution-Phase Approach to the Synthesis of Uniform Nanowires of Crystalline Selenium with Lateral Dimensions in the range of 10-30 nm. *J Am Chem Soc* 2000;122:12582-83.
- [39] Kerker M. The optics of colloidal silver: something old and something new. *J Colloid Interface Sci* 1985;105:297-314.
- [40] Alarcon MN, Vique CC. Selenium in food and the human body: A review. *Sci Total Environment* 2008;400:115-41.
- [41] Qin D, Zhou J, Luo C, Liu Y, Han L, Cao Y. Surfactant-assisted synthesis of size-controlled trigonal Se/Te alloy nanowires. *Nanotechnology* 2006;17:674-79.
- [42] Rong J, Oberbeck F, Wang X, Li X, Oxsher J, Niu Z, et al. Tobacco mosaic virus templated synthesis of one dimensional inorganic–polymer hybrid fibres. *J Mater Chem* 2009;19:2841-45.
- [43] Bradstreet RB. A Review of the Kjeldahl Determination of Organic Nitrogen. *Chem Rev* 1940;27:331-42.
- [44] Hatfield DL, Berry MJ, Gladyshev VN. Selenium: Its Molecular Biology and Role in Human health, (3rd Ed), Springer New York Dordrecht Heidelberg London 2011.
- [45] Kotkata MF, Nouh SA, Farkas L, Radwan MM. Structural studies of glassy and crystalline selenium-sulphur compounds. *J Mater Sci* 1992;27:1785-94.
- [46] Lenher V. Action of selenic acid on gold. *J Am Chem Soc* 1902;24:354-55.
- [47] Wen HJ, Qiu YZ. Geology and Geochemistry of Se-Bearing Formations in Central China. *Int Geol Rev* 2002;44:164-78.

- [48] Wu L. Review of 15 years of research on ecotoxicology and remediation of land contaminated by agricultural drainage sediment rich in selenium. *Ecotoxicol Environ Saf* 2004;57:257-69.
- [49] Bajaj M, Eiche E, Neumann T, Winter J, Gallert C. Hazardous concentrations of selenium in soil and groundwater in North-West India. *J Hazard Mater* 2011;189:640-46.
- [50] Manceau A, Charlet L. The Mechanism of Selenate Adsorption on Goethite and Hydrous Ferric Oxide. *J Colloid Interface Sci* 1994;168:87-93.
- [51] Smith GBL. Selenium oxychloride as a solvent. *Chem Rev* 1938;23:165-85.
- [52] Krief A. Comprehensive Org Synthesis Pergamon Press, Oxford, 1991;1:629-45.
- [53] Spallholz JE. On the nature of selenium toxicity and carcinostatic activity. *Free Radical Bio Medicine* 1994;17:45-65.
- [54] Lucia Marcocci L, Flohe L, Packer L. Evidence for a functional relevance of the selenocysteine residue in mammalian thioredoxin reductase. *Biofactors* 1997;6:351-58.
- [55] Flohe L. The labour pains of biochemical selenology: The history of selenoprotein biosynthesis. *Biochim Biophys Acta* 2009;1790:1389-1403.
- [56] Flohe L, Harris JR. History of peroxiredoxins and topical perspectives, 44, 1, Springer, New York 2007.
- [57] Lakin HW. Trace Elements in the Environment 1973;123:Ch 6, 96.
- [58] Spallholz JE, Hoffman DJ. Selenium toxicity: cause and effects in aquatic birds. *Aquatic Toxicology* 2002;57:27-37.
- [59] Alvarez GS, Muhammed M, Zagorodni AA. Novel flow injection synthesis of iron oxide nanoparticles with narrow size distribution. *Chem Eng Sci* 2006;61:4625-33.

- [60] Basak S, Chen DR, Biswas P. Electrospray of ionic precursor solutions to synthesize iron oxide nanoparticles: Modified scaling law. *Chem Eng Sci* 2007;62:1263-68.
- [61] Sjogren CE, Johansson C, Naevestad A, Sontum PC, Briley-Saebo K, Fahlvik AK. Crystal size and properties of superparamagnetic iron oxide (SPIO) particles. *Magn Reson Imaging* 1997;15:55-67.
- [62] Triantis T, Troupis A, Gkika E, Alexakos G, Boukos N, Papaconstantinou E, Hiskia A. Photocatalytic synthesis of Se nanoparticles using polyoxometalates. *Catalysis Today* 2009;144:2-6.
- [63] Pope MT. *Heteropoly and Isopoly Oxometalates*, Springer-Verlag, Berlin, 1983, p. 1.
- [64] Pope MT, Muller A. Polyoxometalate Chemistry: An Old Field with New Dimensions in Several Disciplines. *Angew Chem Int Ed* 1991;30:34-38.
- [65] Day VW, Klemperer WG. Metal Oxide Chemistry in Solution: The Early Transition Metal Polyoxoanions. *Science* 1985;228:533-41.
- [66] Papaconstantinou E. Photochemistry of polyoxometallates of molybdenum and tungsten and/or vanadium. *Chem Soc Rev* 1989;18:1-31.
- [67] Hiskia A, Mylonas A, Papaconstantinou E. Comparison of the photoredox properties of polyoxometallates and semiconducting particles. *Chem Soc Rev* 2001;30:62-69.
- [68] Hiskia A, Papaconstantinou E. Photocatalytic oxidation of organic compounds by polyoxometalates of molybdenum and tungsten, Catalyst regeneration by dioxygen. *Inorg Chem* 1992;31:163-67.
- [69] Gkika E, Troupis A, Hiskia A, Papaconstantinou E. Photocatalytic Reduction and Recovery of Mercury by Polyoxometalates. *Environ Sci Technol* 2005;39:4242-48.

- [70] Nguyen VN, Amal R, Beydoun D. Photocatalytic reduction of selenium ions using different TiO₂ photocatalysts. *Chem Eng Sci* 2005;60:5759-69.
- [71] Serpone N, Borgarello E, Pelizzetti E. *Photocatalysis and Environment, Trends and Applications*. Kluwer Academic Publishers, Dordrecht, Boston, London, 1988, pp. 527.
- [72] Chen D, Ray AK. Removal of toxic metal ions from wastewater by semiconductor photocatalysis. *Chem Eng Sci* 2001;56:1561-70.
- [73] Yang LB, Shen YH, Xie AJ, Liang JJ, Zhang BC. Synthesis of Se nanoparticles by using TSA ion and its photocatalytic application for decolorization of cango red under UV irradiation. *Materila Research Bulletin* 2008;43:572-82.
- [74] Smith HM, Turner AF. Vacuum deposited thin films using a ruby laser. *Appl Opt* 1965; 4:147-48.
- [75] Dijkkamp D, Venkatesan T, Wu XD, Shareen SA, Jiswari N, Min- Lee YH, McLean W L, Croft M. Preparation of Y- Ba- Cu oxide superconductor thin films using pulsed laser evaporation from high T_c bulk material. *Appl Phys Lett* 1987;51:619-21.
- [76] Maldotti A, Photochemical and photocatalytic properties of transition-metal compounds, *Photochemistry*: 2010;38:275-306.
- [77] Shi W, Hughes RW, Denholme SJ, Gregory DH, Synthesis design strategies to anisotropic chalcogenide nanostructures, *Cryst Eng Comm*, 2010;12:641–659.
- [78] Fujishima M, Tanaka K, Sakami N, Wada M, Morii K, Hattori T, Sumida Y, Tada H, Photocatalytic Current Doubling-Induced Generation of Uniform Selenium and Cadmium Selenide Quantum Dots on Titanium(IV) Oxide, *J. Phys. Chem. C* 2014;118:8917–8924.

- [79] O'Connor T, Panov MS, Mereshchenko A, Tarnovsky AN, Lorek R, Perera D, Diederich G, Lambright S, Moroz P, Zamkov M, The Effect of the Charge-Separating Interface on Exciton Dynamics in Photocatalytic Colloidal Heteronanocrystals, *ACS Nano* 2012;6: 8156–8165.
- [80] Youn HC, Jegal JP, Park SH, Kim HK, Park HS, Roh KC, Kim KB, Phase Transition Method to form Group 6A Nanoparticles on Carbonaceous Templates, *ACS Nano* 2014;8: 2279–2289.
- [81] Quintana M, Poniatowski EH, Morales J, Batina N. Synthesis of selenium nanoparticles by pulsed laser ablation. *Applied Surf Sci* 2002;195:175-86.
- [82] Jiang ZY, Xie ZX, Xie SY, Zhang XH, Huang RB, Zheng LS. High purity trigonal selenium nanorods growth via laser ablation under controlled temperature. *Chem Phys Lett* 2003;368:425-29.
- [83] Duan X, Lieber CM. General Synthesis of Compound Semiconductor Nanowires. *Adv Mater* 2000;12:298-302.
- [84] Duan X, Lieber CM. Laser-Assisted Catalytic Growth of Single Crystal GaN Nanowires. *J Am Chem Soc.* 2000;122:188-89.
- [85] Trentler TJ, Hickman KM, Goel SC, Viano AM, Gibbons PC, Buhro WE. Solution-Liquid-Solid Growth of Crystalline III-V Semiconductors: An Analogy to Vapor-Liquid-Solid Growth. *Science* 1995;270:1791-94.
- [86] Trentler TJ, Goel SC, Hickman KM, Viano AM, Chiang MY, Beatty AM, Gibbons PC, Buhro WE. Solution-liquid-solid growth of indium phosphide fibres from organometallic precursors: Elucidation of molecular and nonmolecular components of the pathway. *J Am Chem Soc* 1997;119:2172-81.

- [87] Haber JA, Gibbons PC, Buhro WE. Morphological control of nanocrystalline Aluminum Nitride; Aluminum-Chloride-Assisted nanowhisker growth. *J Am Chem Soc* 1997;119:5455-56.
- [88] Haber JA, Gibbons PC, Buhro WE. Morphologically selective synthesis of nanocrystalline Aluminum Nitride. *Chem Mater* 1998;10:4062-71.
- [89] Yu L, Chen J, Fu ZW. Influence of sulphate-reducing bacteria on environmental parameters and marine corrosion behaviour of Q235 steel in aerobic conditions. *Electrochimica Acta* 2010;55:1258-34.
- [90] a. Morales AM, Lieber CM. A Laser Ablation Method for the Synthesis of Crystalline Semiconductor Nanowires. *Science* 1998;279:208-11.
b. Mendliv MI, García LV, Krishnan B, Avellaneda D, Martinez JA, Shaji S, CuInGaSe₂ nanoparticles by pulsed laser ablation in liquid medium, *Mat. Res. Bull.* 2015;72:106–15.
- [91] Singh SC, Mishra SK, Srivastava RK, Gopal R. Optical Properties of Selenium Quantum Dots Produced by Laser Irradiation of Water Suspended Se Nanoparticles. *J Phys Chem C* 2010;114:17374-84.
- [92] Grigorieva SN, Fominski VY, Romanov RI, Gnedovets AG, Volosova MA, Shadow masked pulsed laser deposition of WSe_x films: Experiment and modelling, *Appl Surf Sci* 2013;282:607–614.
- [93] Jeonga AR, Joa W, Ko C, Han M, Kang SJ, Kim M, Park DY, Cheong H, Yun HJ, Growth and structural properties of pulsed laser-ablated CuInSe₂ nanoparticles by pulsed-laser ablation and selenization process. *J Alloys Comp* 2011;509:8073–8076.
- [94] Fominski VY, Grigoriev SN, Celis JP, Romanov RI, Oshurko VB, Structure and mechanical properties of W–Se–C/diamond-like carbon and W–Se/diamond-like carbon bi-layer coatings prepared by pulsed laser deposition. *Thin Solid Films* 2012;520:6476–6483.

- [95] Grigoriev SN, Fominski VY, Romanov RI, Gnedovets AG. Tribological properties of gradient Mo–Se–Ni–C thin films obtained by pulsed laser deposition in standard and shadow mask configurations. *Thin Solid Films* 2014;556:35–43.
- [96] Wu ZH, Sun M, Mei XY, Ruda HE. Growth and photoluminescence characteristics of AlGaAs nanowires. *Appl Phys Lett* 2004;85:657–59.
- [97] Engelko V, Georg Mueller G. Formation of plasma and ion flux on a target, irradiated by an intense electron beam. *J Appl Phys Lett* 2005;98:013301–08.
- [98] Stroyuk AL, Raevskaya AE, Kuchmiy SY, Dzhagan VM, Zahn DRT, Schulze S. Structural and optical characterization of colloidal Se nanoparticles prepared via the acidic decomposition of sodium selenosulfate. *Colloids Surf A* 2008;320:169–74.
- [99] Muth OH, Oldfield JE, Weswig PH. Symposium: Selenium in Biomedicine, 7–26.
- [100] Cooper WC. The physics of selenium and tellurium. 3–20.
- [101] Franklin TC, Adeniyi WK, NnodimeleR. The Electro-oxidation of some insoluble inorganic sulfides, selenides, and tellurides in cationic surfactant-aqueous sodium hydroxide systems. *J Electrochem Soc* 1990;137:480–84.
- [102] Ibragimov NI, Abutalibova ZM, Agaev VG. Electrophotographic layers of trigonal Se in the binder obtained by reduction of SeO_2 by hydrazine. *Thin Solid Films* 2000;359:125–26.
- [103] Badr Y; Mahmoud MA. Effect of PVA surrounding medium on ZnSe nanoparticles: Size, optical, and electrical properties. *Spectrochim Acta Part A* 2006;65:584–90.
- [104] Yu DP, Lee CS, Bello I, Sun XS, Zhou GW, Bai ZG, Zhang Z, Feng SQ. Synthesis of nano-scale silicon wires by excimer laser ablation at high temperature. *Solid State Commun* 1998;105:403–07.

[105] Mayers B, Gates B, Yin YD, Xia YN. Large-Scale Synthesis of Monodisperse Nanorods of Se/Te Alloys through a Homogeneous Nucleation and Solution Growth Process. *Adv Mater* 2001;13:1380-84.

[106] Yu DP, Bai ZG, Wang JJ, Zou YH, Qian W, Zhang HZ, Ding Y, Xiong GC, Feng SQ. Direct evidence of quantum confinement from the size dependence of the photoluminescence of silicon quantum wires. *Phys Rev. B* 1999;59:R2498-R2501.

[107] Yu DP, Bai ZG, Ding Y, Hang QL, Zhang HZ. Nanoscale silicon wires synthesized using simple physical evaporation. *Appl Phys Lett* 1998;72:3458-60.

[108] Prokes SM, Wang KL. Novel methods of nanoscale wire formation. *MRS Bull* 1999;24: 13-19.

[109] Ren L, Zhang H, Tan P, Chen Y, Zhang Z, Chang Y, Xu J, Yang F, Yu D. Hexagonal selenium nanowires synthesized via vapor-phase growth. *J Phys Chem B* 2004;108:4627-30.

[110] Cao X, Xie Y, Zhang S, Li F. Ultra- Thin Trigonal Selenium Nanoribbons Developed from Series- Wound Beads. *Adv Mater* 2004;16:649-53.

[111] Ara Cho A, Ahn SJ, Yun JH, Gwak J, Ahn SK, Shin K, Song H, Yoon KH, Non-vacuum processed CuInSe₂ thin films fabricated with a hybrid ink. *Solar Energy Mat Solar Cells* 2013;109:17–25.

[112] a. Uhl AR, Koller M, Wallerand AS, Fella CM, Kranz L, Hagendorfer H, Romanyuk YE, Tiwari AN, Yoon S, Weidenkaff A, Friedlmeier TM, Ahlsweide E, VanGenechten D, Stassin F, Cu(In,Ga)Se₂ absorbers from stacked nanoparticle precursor layers. *Thin Solid Films* 2013;535:138–142.

b. Chiera NM, Eichler R, Vögele A, Türler A, Vapor deposition coating of fused silica tubes with amorphous selenium, *Thin Solid Films* 2015;592: 8–13.

- [113] Golan Y, Margulis L, Rubinstein I, Hodes G. Epitaxial electrodeposition of cadmium selenide nanocrystals on gold. *Langmuir* 1992;8:749-52.
- [114] Golan Y, Hodes G, Rubinstein I. Electrodeposited quantum dots. 3. Interfacial factors controlling the morphology, size, and epitaxy. *J Phys Chem* 1996;100:2220-28.
- [115] Zhang Y, Hodes G, Rubinstein I, Grunbaum E, Nayak RR, Hutchison JL. Electrodeposited quantum dots: Metastable rocksalt CdSe nanocrystals on {111} gold alloys. *Adv Mater* 1999;11:1437-41.
- [116] Ruach-Nir I, Zhang Y, Popovitz-Biro R, Rubinstein I, Hodes G. Shape control in electrodeposited, epitaxial CdSe nanocrystals on (111) gold. *J Phys Chem B* 2003;107:2174-79.
- [117] Mastai Y, Polksy R, Koltypin Y, Gedanken A, Hodes G. Pulsed sonoelectrochemical synthesis of cadmium selenide nanoparticles. *J Am Chem Soc* 1999;121:10047-52.
- [118] Zhu JJ, Aruna ST, Koltypin Y, Gedanken A. A novel method for the preparation of lead selenide: Pulse sonoelectrochemical synthesis of lead selenide nanoparticles. *Chem Mater* 2000;12:143-47.
- [119] Yang YJ. A novel electrochemical preparation of PbS nanoparticles. *Mater Sci Eng B* 2006;131:200-02.
- [120] Wang CL, Sun L, Yun H, Li J, Lai YK, Lin CJ. Sonoelectrochemical synthesis of highly photoelectrochemically active TiO₂ nanotubes by incorporating CdS nanoparticles. *Nanotechnology* 2009;20:295601-07.
- [121] Ham S, Choi B, Paeng KJ, Myung N, Rajeshwar K. Photoinduced cathodic deposition of CdTe nanoparticles on polycrystalline gold substrate. *Electrochim Commun* 2007;9:1293-97.

- [122] Ivanou DK, Streltsov EA, Fedotov AK, Mazanik AV, Fink D, Petrov A. Electrochemical deposition of PbSe and CdTe nanoparticles onto p-Si (100) wafers and into nanopores in SiO₂/Si (100) structure. *Thin Solid Films* 2005;490:154-60.
- [123] Rabchynski SM, Ivanou DK, Streltsov EA. Photoelectrochemical formation of indium and cadmium selenide nanoparticles through Se electrode precursor. *Electrochim Commun* 2004;6:1051-56.
- [124] Somasundaram S, Chenthamarakshan CR, de Tacconi NR, Ming Y, Rajeshwar K. Photoassisted deposition of chalcogenide semiconductors on the titanium dioxide surface: mechanistic and other aspects. *Chem Mater* 2004;16:3846-52.
- [125] Zhang SY, Zhang J, Liua Y, Xiang Mac X, Chena HY. Electrochemical synthesis of selenium nanotubes by using CTAB soft-template. *Electrochimica Acta* 2005;50:4365-70.
- [126] Devers T, Kante I, Allam L, Fleury V. Preparation of dendritic tin nanoaggregates by electrodeposition. *J Non-Cryst Solids* 2003;321:73-80.
- [127] Barabasi AL, Stanley HE. *Fractal Concepts in Surface Growth*, Cambridge University Press, Cambridge, 1995.
- [128] Cabral MF, Coelho D, Machado SAS. Analyzing Cd underpotential deposition behavior on Se thin-films: Atomic force microscopy, cyclic voltammetry and electrochemical quartz crystal nanobalance studies. *Electrochimica Acta* 2013;91:361–66.
- [129] Zhao D, Zhang S, Yin G, Dua C, Wang Z, Wei J. Tungsten doped Co–Se nanocomposites as an efficient non precious metal catalyst for oxygen reduction. *Electrochimica Acta* 2013;91:179–84.
- [130] Saji VS, Lee CW, Selenium electrochemistry, **RSC Adv** 2013;3:10058-10077.

- [131] Mahmoodi SR, Bayati M, Hosseinirad S, Foroumadi A, Gilani K, Rezayat SM, AC electrokinetic manipulation of selenium nanoparticles for potential nanosensor applications, Mater Res Bulletin 2013;48:1262–1267.
- [132] Kershaw SV, Susha AS, Rogach AL, Narrow bandgap colloidal metal chalcogenide quantum dots: synthetic methods, heterostructures, assemblies, electronic and infrared optical properties, Chem Soc Rev 2013;42:3033-3087.
- [133] Dembinska B, Kiliszek M, Elzanowska H, Pisarek M, Kulesza PJ, Enhancement of activity of RuSe_x electrocatalyst by modification with nanostructured iridium towards more efficient reduction of oxygen. J Power Sources 2013;243:225-232.
- [134] Gao MR, Xu YF, Jiang J, Yu SH, Nanostructured metal chalcogenides: synthesis, modification, and applications in energy conversion and storage devices, Chem Soc Rev 2013;42:2986-3017.
- [135] Liu J, Yang W, Li Y, Fana L, Li Y, Electrochemical studies of the effects of the size, ligand and composition on the band structures of CdSe, CdTe and their alloy nanocrystals, Phys Chem Chem Phys 2014;16:4778-4788.
- [136] Thakkar KN, Mhatre SS, Parikh RY. Biological synthesis of metallic nanoparticles. Nanomedicine NBM 2010;6:257-62.
- [137] Narasingarao P, Haggblom MM. Identification of anaerobic selenate-respiring bacteria from aquatic sediments. Appl Environ Microbiol 2007;73:3519-27.
- [138] Lortie L, Gould WD, Rajan S, Meeready RGL, Cheng KJ. Reduction of Selenate and Selenite to Elemental Selenium by a *Pseudomonas stutzeri* Isolate. Appl Environ Microbiol 1992;58:4042-44.

- [139] Oremland RS, Blum JS, Culbertson CW, Visscher PT, Miller LG, Dowdle P, Strohmaier FE. Isolation, growth, and metabolism of an obligately anaerobic, selenate-respiring bacterium, strain SES-3. *Appl Environ Microbiol* 1994;60:3011-19.
- [140] Sabaty M, Avazeri C, Pignol D, Vermeglio A. Characterization of the reduction of selenate and tellurite by nitrate reductases. *Appl Environ Microbiol* 2001;67:5122-26.
- [141] Oremland RS, Herbel MJ, Blum JS, Langley S, Beveridge TJ, Ajayan PM, Sutto T, Ellis AV, Curran S. Structural and spectral features of selenium nanospheres produced by Se-respiring bacteria. *Appl Environ Microbiol* 2004;70:52-60.
- [142] Wang T, Yang L, Zhang B, Liu J. Extracellular biosynthesis and transformation of selenium nanoparticles and application in H₂O₂ biosensor. *Colloids and Surfaces B: Biointerfaces* 2010;80:94-102.
- [143] Yadav V, Sharma N, Prakash R, Raina KK, Bharadwaj LM, TejoPrakash N. Generation of Selenium Containing Nano-Structures By Soil Bacterium, *Pseudomonas aeruginosa*. *Biotechnology* 2008;7:299.
- [144] Dungan RS, Yates SR, Frankenberger Jr. WT. Transformations of selenate and selenite by *Stenotrophomonas maltophilia* isolated from a seleniferous agricultural drainage pond sediment. *Environ Microbiol* 2003;5:287-95.
- [145] Zahir AZ, Zhang Y, Frankenberger Jr. WT. Fate of selenate metabolized by *Enterobacter taylorae* isolated from rice straw. *Agri Food Chem* 2003;51:3609-13.
- [146] Losi M; Frankenberger Jr. WT. Reduction of selenium oxyanions by *Enterobacter cloacae* SLD1a-1: isolation and growth of the bacterium and its expulsion of selenium particles. *Appl Environ Microbiol* 1997;63:3079-84.

- [147] Kessi JM, Ramuz E, Wejrli M, Bachofen R. Reduction of selenite and detoxification of elemental selenium by the phototrophic bacterium *Rhodospirillum rubrum*. *Appl Environ Microbiol* 1999;65:4734-40.
- [148] Switzer-Blum J, Bindi BA, Buzzelli J, Stoltz JF, Oremland RS. *Bacillus arsenicoselenatis*, sp. nov., and *Bacillus selenitireducens*, sp. nov.: two haloalkaliphiles from Mono Lake, California that respire oxyanions of selenium and arsenic. *Arch Microbiol* 1998; 171:19-30.
- [149] Dhanjal S, Cameotra SS. Aerobic biogenesis of selenium nanospheres by *Bacillus cereus* isolated from coalmine soil. *Microbial Cell Factories* 2010;9:52-3.
- [150] Tam K, Ho CT, Lee JH, Lai M, Chang CH, Rheem Y, Chen W, Hur HG, Myung NV. Growth mechanism of amorphous selenium nanoparticles synthesized by *Shewanella* sp. HN-41. *Biosci Biotechnol Biochem* 2010;74:696-700.
- [151] Bajaj M, Schmidt S, Winter Formation of Se (O) nanoparticles by *Dugenella* sp. and *Agrobacterium* sp. isolated from Se-laden soil of north-east Punjab, India. *J Microbial Cell Factories* 2012;11:64-78.
- [152] Hunter WJ, Manter DK. Bio-reduction of selenite to elemental red selenium by *Tetrathiobacter kashmirensis*. *Curr Microbiol* 2008,57:83-88.
- [153] Zhang L, Li D, Gao P. Expulsion of selenium/protein nanoparticles through vesicle-like structures by *Saccharomyces cerevisiae* under microaerophilic environment. *World J Microbiol Biotechnol*. 2012,28;3381-86.
- [154] Gregorio SD, Lampis S, Vallini G. Plant Selenium Metabolism—Genetic Manipulation, Phytotechnological Applications, and Ecological Implications. *Environment Inter* 2005;31:233-41.

- [155] Mishra RR, Prajapati S, Das J, Dangar TK, Das N, Thatoi H. Reduction of selenite to red elemental selenium by moderately halotolerant *Bacillus megaterium* strains isolated from Bhitarkanika mangrove soil and characterization of reduced product. *Chemosphere* 2011;84:1231-37.
- [156] Zhang W, Chena Z, Liu H, Zhang L, Gao P, Li D. Biosynthesis and structural characteristics of selenium nanoparticles by *Pseudomonas alcaliphila*. *Colloids and Surfaces B: Biointerfaces* 2011;88:196-201.
- [157] Dobias J, Suvorova EI, Bernier-Latmani R. Role of proteins in controlling selenium nanoparticle size. *Nanotechnology* 2011;22:195605-14.
- [158] a. Kaur G, Iqbal M, Bakshi MS. Biominerization of fine selenium crystalline rods and amorphous spheres. *J Phys Chem C* 2009;113:13670-76.
b. Kalishwaralal K, Jeyabharathi SCB, Sundar K, Muthukumaran A, Sodium selenite/selenium nanoparticles (SeNPs) protect cardiomyoblasts and zebrafish embryos against ethanol induced oxidative stress, *J. Trace Elements in Med. Bio.* 2015;32:135–44.
- [159] Chen Z, Shen Y, Xie A, Zhu J, Wu Z, Huang F. L-cysteine-assisted controlled synthesis of selenium nanospheres and nanorods. *Crystal Growth & Design* 2009;9:1327-33.
- [160] Li Q, Chen T, Yang F, Liu J, Zheng W. Facile and controllable one-step fabrication of selenium nanoparticles assisted by l-cysteine. *Materials Lett* 2010;64:614-17.
- [161] Ingole AR, Thakare SR, Khati NT, Wankhade AV, Burghate DK. Green synthesis of selenium nanoparticles under ambient condition. *Chalcogenide Lett* 2010;7:485-89.
- [162] Chen T, Wong YS, Zheng W, Bai Y, Huang L. Selenium nanoparticles fabricated in *Undaria pinnatifida* polysaccharide solutions induce mitochondria-mediated apoptosis in A375 human melanoma cells. *Colloids and Surfaces B: Biointerfaces* 2008;67:26-31.

- [163] Bai Y, Wang Y, ZhouY, Li W, Zheng W. Modification and modulation of saccharides on elemental selenium nanoparticles in liquid phase. Materials Lett 2008;62:2311-14.
- [164] a. Abdelouas A, Gong WL, Lutze W, Shelnutt JA, Franco R, Moura I. Using cytochrome c 3 to make selenium nanowires. Chem Mater 2000;12:1510-12.
b. Peng X, Wang L, Zhang X, Gao B, Fu J, Xiao S, Huo K, Chu PK, Reduced graphene oxide encapsulated selenium nanoparticles for high-power lithiumeselenium battery cathode, J. Power Sources 2015;288:214-220.
- [165] Zhang Y, Wang J, Zhang L. Creation of highly stable selenium nanoparticles capped with hyperbranched polysaccharide in water. Langmuir 2010;26:17617-23.
- [166] Schröfel A, Kratošová G, Šafařík I, Šafaříková M, Raška I, Shor LM, Applications of biosynthesized metallic nanoparticles – a review, Acta Biomaterialia 2014; doi: <http://dx.doi.org/10.1016/j.actbio.2014.05.022>.
- [167] Bansal V, Bharde A, Ramanathan R, Bhargava SK, Inorganic materials using ‘unusual’ microorganisms. Adv Colloid Interface Sci 2012;179–182:150–168.
- [168] Prasada SK, Patel H, Patel T, Patel K, Selvaraj K, Biosynthesis of Se nanoparticles and its effect on UV-induced DNA damage, Colloids Surf B 2013;103:261–266.
- [169] Mendoza-Reséndez R, Núñez NO, Barriga-Castro ED, Carlos Luna C, Synthesis of metallic silver nanoparticles and silver organometallic nanodisks mediated by extracts of Capsicum annuum var. aviculare(piquin) fruits. RSC Adv 2013;3:20765-20771.
- [170] Shinchi H, Wakao M, Nagata N, Sakamoto M, Mochizuki E, Uematsu T, Kuwabata S, Suda Y, Cadmium-Free Sugar-Chain-Immobilized Fluorescent Nanoparticles Containing Low-Toxicity ZnS-AgInS₂ Cores for Probing Lectin and Cells. Bioconjugate Chem 2014; 25:286–295.

- [171] Leo VD, Catucci L, Falqui A, Marotta R, Striccoli M, Agostiano A, Comparelli R, Milano F, Hybrid Assemblies of Fluorescent Nanocrystals and Membrane Proteins in Liposomes, *Langmuir* 2014;30:1599–1608.
- [172] Rabeneau A. The Role of Hydrothermal Synthesis in Preparative Chemistry. *Angew Chem Int Ed Engl* 1985;24:1026-40
- [173] Zhang L, Ni Y, Hong J. t-Se microspheres with holes: Hydrothermal synthesis and growth mechanism. *J Phys and Chem of Solids* 2009;70:1408–12.
- [174] Firestone MA, Williams DE, Seifert S, Csencsits R. Nanoparticle arrays formed by spatial compartmentalization in a complex fluid. *Nano Lett* 2001;1:129-35.
- [175] Mann S. Dalton perspectives. Biomineralization: the hard part of bioinorganic chemistry. *J Chem Soc Dalton Trans* 1993;1-9.
- [176] Lee TAT, Cooper A, Apkarian RP, Conticello VP. Thermo- reversible self- assembly of nanoparticles derived from elastin- mimetic polypeptides. *Adv Mater* 2000;12:1105-10.
- [177] Wang X, Li Y. Selected-control hydrothermal synthesis of α -and β -MnO₂ single crystal nanowires. *J Am Chem Soc* 2002;124:2880-81.
- [178] Jiang Y, Wu Y, Zhang S, Xu C, Yu W, Xie Y, Qian Y. A Catalytic-Assembly Solvothermal Route to Multiwall Carbon Nanotubes at a Moderate Temperature. *J Am Chem Soc* 2000;122:12383-84.
- [179] Lu Q, Gao F, Komarneni S. Cellulose-directed growth of selenium nanobelts in solution. *Chem Mater* 2006;18:159-63.
- [180] Liu XY, Mo MS, Zeng JH, Qian YT. Large-scale synthesis of ultra-long wire-like single-crystal selenium arrays. *J Cryst Growth* 2003;259:144-48.

- [181] Ding Y, Li Q, Jia Y, Chen L, Xing J, Qian Y. Growth of single crystal selenium with different morphologies via a solvothermal method. *J Cryst Growth* 2002;241:489-97.
- [182] Lu J, Xie Y, Xu F, Zhu L. Study of the dissolution behaviour of selenium and tellurium in different solvents—a novel route to Se, Te tubular bulk single crystals. *J Mater Chem* 2002;12:2755-61.
- [183] Zhang H, Yang D, Ji Y, Ma X, Xu J, Que D. Selenium nanotubes synthesized by a novel solution phase approach. *J Phys Chem B* 2004;108:1179-82.
- [184] Xia Q, Dai Z, Huang W, Zhang W, Ma D, Hu X, Qian Y. Large-scale synthesis and growth mechanism of single-crystal Se nanobelts. *Crystal Growth & Design* 2006;6: 1514-17.
- [185] Gautam UK, Natha M, Rao CNR. New strategies for the synthesis of t-selenium nanorods and nanowires. *J Mater Chem* 2003;13:2845-47.
- [186] Xie SY, Wang CF, Zhang XH, Ziang ZY, Xie ZX, Tian ZQ, Huang RB, Zheng LS. Spontaneous transformation of selenium from monoclinic micro-balls to trigonal nano-rods in ethanol solution. *J Mater Chem* 2003;13:1447-50.
- [187] Klayman DL, Griffin TS. Reaction of selenium with sodium borohydride in protic solvents. A Facile Method for the introduction of selenium into organic molecules. *J Am Chem Soc* 1973;95:197-99.
- [188] Henshaw G, Parkin IP, Shaw GA. Convenient, room-temperature liquid ammonia routes to metal chalcogenides. *J Chem Soc Dalton Trans* 1997;2:231-36.
- [189] Ostapenko GT, Kvasnitsa VN, Timoshkova LP, Semenenko NP, Dorogovin BA. Synthetic andalusite crystals: morphology and growth features. *J Cryst Growth* 1998;186:420-26.

- [190] Byrappa K, Yoshimura M, Hydrothermal Technology for Nanotechnology—A Technology for Processing of Advanced Materials. Handbook of Hydrothermal Technology, 2nd Edition 2013;615-762.
- [191] Chen YT, Zhang W, Fan YQ, Xu XQ, Zhang ZX. Hydrothermal preparation of selenium nanorods. *Mater Chem Phys* 2006;98:191-94.
- [192] Hu JQ, Deng B, Zhnag WX, Qian YT. Synthesis and characterization of CdIn₂S₄ nanorods by converting CdS nanorods via the hydrothermal route. *Inorg Chem* 2001;40:3130-33.
- [193] Zeng K, Chen S, Song Y, Li H, Li F, Liu P. Solvothermal synthesis of trigonal selenium with butterfly-like microstructure. *Particuology* 2013; 11: 614-617
- [194] Ray C, Dutta S, Sarkar S, Sahoo R, Roy A, Pal T, A facile synthesis of 1D nano structured selenium and Au decorated nano selenium: catalysts for the clock reaction. *RSC Adv* 2013;3:24313-24320.
- [195] Zhang H, Miao G, Ma X, Wang B, Zheng H, Facile synthesis and enhanced photocatalytic activity of ZnSe/TiO_{2-x}N_x composite nanoparticles. *Mater Lett* 2014;121: 188–190.
- [196] Sobhani A, Salavati-Niasari M, Synthesis and characterization of CdSe nanostructures by using a new selenium source: Effect of hydrothermal preparation conditions. *Mater Res Bulletin* 2014;53:7–14.
- [197] Sobhani A, Salavati-Niasari M, Synthesis and characterization of a nickel selenide series via a hydrothermal process. *Superlattices and Microstructures* 2014;65:79–90.
- [198] Shi W, Zhang X, Che G, Hydrothermal synthesis and electrochemical hydrogen storage performance of porous hollow NiSe nanospheres. *Int J Hydrogen Energy* 2013;38:7037-7045.

- [199] Shi W, Zhang X, Che G, Fan W, Liu C. Controlled hydrothermal synthesis and magnetic properties of three-dimensional FeSe₂ rod clusters and microspheres. *Chem Eng J* 2013;215–216:508–516.
- [200] Chen LJ, Chuang YJ. Diethylenetriamine assisted synthesis and characterization of stannite quaternary semiconductor Cu₂ZnSnSe₄ nanorods by self-assembly. *J Crystal Growth* 2013;376:11–16.
- [201] Mehta SK, Chaudhary S, Kumar S, Bhasin KK, Torigoe K, Sakai H, Abe M. Surfactant assisted synthesis and spectroscopic characterization of selenium nanoparticles in ambient conditions. *Nanotechnology* 2008;19:295601-12.
- [202] Mehta SK, Chaudhary S, Bhasin KK. Understanding the role of hexadecyltrimethylammonium bromide in the preparation of selenium nanoparticles: a spectroscopic approach. *J Nanoparticle Res* 2009;10:1759-66.
- [203] Mehta SK, Kumar S, Chaudhary S, Bhasin KK, Gradzielski M. Evolution of ZnS nanoparticles via facile CTAB aqueous micellar solution route: a study on controlling parameters. *Nanoscale Res Lett* 2009;4:17-28.
- [204] Mehta SK, Kumar S, Chaudhary S, Bhasin KK. Nucleation and growth of surfactant-passivated CdS and HgS nanoparticles: Time-dependent absorption and luminescence profiles. *Nanoscale* 2010;2:145-52.
- [205] Mehta SK, Chaudhary S, Gradzielski M. Time dependence of nucleation and growth of silver nanoparticles generated by sugar reduction in micellar media. *J Colloid Interface Sci* 2010;343:447-53.

- [206] Mehta SK, Chaudhary S, Bharti B, Bhasin KK, Gradzielski M. Correspondence via electron and charge carrier dynamics of silver nanoparticles with organic dyes. *Science of Advanced Materials* 2012;4:1-11.
- [207] Bockstaller MR, Mickiewicz RA, Thomas EL. Block copolymer nanocomposites: perspectives for tailored functional materials. *Adv Mater* 2005;17:1331-49.
- [208] Grubbs RB. Hybrid metal–polymer composites from functional block copolymers. *J Polym Sci Part A Polym Chem* 2005;43:4323-36.
- [209] Vaia RA, Maguire JF. Polymer nanocomposites with prescribed morphology: going beyond nanoparticle-filled polymers. *Chem Mater* 2007;19:2736-51.
- [210] Pozzo DC, Walker LM. Macroscopic alignment of nanoparticle arrays in soft crystals of cubic and cylindrical polymer micelles. *Eur Phys JE Soft Matter Biol Phys* 2008;26:183-89.
- [211] Kumar SK, Krishnamoorti R. Nanocomposites: structure, phase behavior, and properties. *Ann Rev Chem Biomol Eng* 2010;1:37-58.
- [212] Alexandridis P, Hatton TA. Poly(ethylene oxide)-poly(propylene oxide)-poly(ethylene oxide) block copolymer surfactants in aqueous solutions and at interfaces: thermodynamics, structure, dynamics, and modelling. *Colloids Surf. A* 1995;96:1-46.
- [213] Alexandridis P. Poly(ethylene oxide)/poly(propylene oxide) block copolymer surfactants. *Curr Opin Colloid Interface Sci* 1997;2:478-89.
- [214] Zhao D, Feng J, Huo Q, Melosh N, Fredrickson GH, Chmelka BF, Stucky GD. Triblock copolymer syntheses of mesoporous silica with periodic 50 to 300 angstrom pores. *Science* 1998;279:548-32.
- [215] Soler-Illia GJ, Crepaldi EL, Grosso D, Sanchez C. Block copolymer-templated mesoporous oxides. *Curr Opin Colloid Interface Sci* 2003;8:109-26.

- [216] Karanikolos GN, Alexandridis P, Itskos G, Petrou A, Mountziaris TJ. Synthesis and size control of luminescent ZnSe nanocrystals by a microemulsion-gas contacting technique. *Langmuir* 2004;20:550-53.
- [217] Karanikolos GN, Alexandridis P, Mallory R, Petrou A, Mountziaris TJ. Templated synthesis of ZnSe nanostructures using lyotropic liquid crystals. *Nanotechnology* 2005;16: 2372-80.
- [218] Karanikolos GN, Law NL, Mallory R, Petrou A, Alexandridis P, Mountziaris TJ. Water-based synthesis of ZnSe nanostructures using amphiphilic block copolymer stabilized lyotropic liquid crystals as templates. *Nanotechnology* 2006;17:3121-28.
- [219] Karanikolos GN, Alexandridis P, Mountziaris TJ. Growth of ZnSe and CdSe nanostructures in self-assembled block copolymer-stabilized templates. *Mater Sci Eng B* 2008;152:66-71.
- [220] Alexandridis P, Karanikolos GN, Mountziaris TJ. Synthesis of nanostructured materials Using liquid crystalline templates. US Patent 2009,237:7608.
- [221] Alexandridis P, Holzwarth JF, Hatton TA. Micellization of Poly(ethylene oxide)-Poly(propylene oxide)-Poly(ethylene oxide) Triblock Copolymers in Aqueous Solutions: Thermodynamics of Copolymer Association. *Macromolecules* 1994;27:2414-25.
- [222] Lin YN, Alexandridis P. Temperature-dependent adsorption of pluronic F127 block copolymers onto carbon black particles dispersed in aqueous media. *J Phys Chem B* 2002; 106:10834-44.
- [223] Alexandridis P, Spontak RJ. Advances in self-ordering macromolecules and nanostructure design. *Curr Opin Colloid Interface Sci* 1999;4:130-39.

- [224] Pomogailo AD. Nanochastitsy metallov v polimerakh (Metal Nanoparticles in Polymers), Moscow: Nauka, 1999.
- [225] Litmanovich AA, Papisov IM. Formation of selenium sols via reduction of selenium ions in solutions of cationic and anionic polyelectrolytes. Vysokomol Soedin Ser B 1997;39:313-26.
- [226] Kopeikin VV, Panarin EF. Formation of Se^0 Nanoparticles in an Aqueous Cationic Polyelectrolyte. Dokl Ross Akad Nauk 2001;243:497-500.
- [227] Balogh L, Swanson DR, Tomalia DA. Dendrimer-silver complexes and nanocomposites as antimicrobial agents. Nano Lett, 2001;1:18-21.
- [228] Connelly S, Fitzmaurice D. Biologically programmed nanoparticle assembly. Adv Mater 2000;12:147-50.
- [229] Borovikova LN, Matveeva NA, Baklagina YG, Khripunov AK, Tkachenko AA. Formation of a composite based on selenium nanoparticles stabilized with poly-N,N,N,N-trimethylmethacryloyloxyethylammonium methyl sulfate and on Acetobacter xylinum cellulose gel films. Russian J of Appl Chem 2009;82:2006-10.
- [230] Shah CP, Singh KK, Kumar M, Bajaj PN. Vinyl monomers-induced synthesis of polyvinyl alcohol-stabilized selenium nanoparticles. Mater Res Bull 2010;45:56-62.
- [231] Shah CP, Kumar M, Bajaj PN. Acid-induced synthesis of polyvinyl alcohol-stabilized selenium nanoparticles. Nanotechnology 2007;18:385607-613.
- [232] Shah CP, Dwivedi C, Singh KK, Kumar M, Bajaj PN. Riley oxidation: A forgotten name reaction for synthesis of selenium nanoparticles. Mater Res Bull 2010;45:1213-17.
- [233] Langi B, Shah CP, Singh KK, Chaskar A, Kumar M, Bajaj PN. Ionic liquid-induced synthesis of selenium nanoparticles. Mater Res Bull 2010;45:668-71.
- [234] Mainfray G, Manus C. Multiphoton ionization of atoms. Rep Prog Phys 1991;54:1333-72.

- [235] Durkop TG, Cobas S, Fuhrer MS. Extraordinary mobility in semiconducting carbon nanotubes. *Nano Lett* 2004;4:35-39.
- [236] Zhang L, Li Y, Shena Y, Xie A. One-step synthesis of poly(2-hexadecyloxyaniline)/selenium nanocomposite Langmuir–Blogett film by in situ redox reaction. *Mater Chem Phys* 2011;125:522-27.
- [237] Valueva SV, Borovikova LN, Matveeva NA. Influence of the nature of the stabilizing polymeric matrix on the self-organization of selenium nanoclusters. *Russ J Appl Chem* 2011; 84:266-71.
- [238] Stroyuk AL, Raevskaya AE, Ya S, Kuchmii N, Dzhagan VM, Zahn DRT, Schulze S. Structure and spectral-optical characteristics of Se, Se/CdS, and Se/Cd_{0.5}Zn_{0.5}S nanoparticles, stabilized in polymer-containing media. *Theoret Exp Chem* 2007;43:28-34.
- [239] Song JM, Zhu JH, Yu SH. Crystallization and shape evolution of single crystalline selenium nanorods at liquid-liquid interface: From monodisperse amorphous Se nanospheres toward Se nanorods. *J Phys Chem B* 2006;110:23790-95.
- [240] Liu Y, Goebel J, Yin Y. Templated synthesis of nanostructured materials, *Chem Soc Rev* 2013;42:2610-2653.
- [241] Song CC, Du FS, Li ZC, Oxidation-responsive polymers for biomedical applications, *J. Mater. Chem. B*, 2014;2:3413-3426.
- [242] Matthew G. Moffitt, Self-Assembly of Polymer Brush-Functionalized Inorganic Nanoparticles: From Hairy Balls to Smart Molecular Mimics. *J Phys Chem Lett* 2013;4:3654–3666.
- [243] Boutonnet M, Kitzling J, Stenius P. The preparation of monodisperse colloidal metal particles from microemulsions. *Colloids Surf* 1982;5:209-25.

- [244] Eastoe J, Hollamby MJ, Hudson L. Recent advances in nanoparticle synthesis with reversed micelles. *Adv Colloid Interface Sci* 2006;128:5-15.
- [245] Takami A, Kurita H, Koda S. Laser-induced size reduction of noble metal particles. *J Phys Chem B* 1999;103:1226-32.
- [246] Johnson JA, Saboungi ML, Thiagarajan P, Csencsits R, Meisel D. Selenium nanoparticles: a small-angle neutron scattering study. *J Phys Chem B* 1999;103:59-63.
- [247] Liu MZ, Zhang SY, Shen YH, Zhang ML. Selenium nanoparticles prepared from reverse microemulsion process. *Chinese Chem Lett* 2004;15:1249-52.
- [248] Zhang B, Dai W, Ye X, Hou W, Xie Y. Solution-phase synthesis and electrochemical hydrogen storage of ultra-long single-crystal selenium submicrotubes. *J Phys Chem B* 2005; 109:22830-35.
- [249] Nath S, Ghosh SK, Panigrahi S, Thundat T, Pal T. Synthesis of selenium nanoparticle and its photocatalytic application for decolorization of methylene blue under UV irradiation. *Langmuir* 2004;20:7880-83.
- [250] Ma Y, Qi L, Shen W, Ma J. Selective synthesis of single-crystalline selenium nanobelts and nanowires in micellar solutions of nonionic surfactants. *Langmuir* 2005;21:6161-64.
- [251] Lin ZH, Wang CRC. Evidence on the size-dependent absorption spectral evolution of selenium nanoparticles. *Mater Chem Phys* 2005;92:591-94.
- [252] Zhang SY, Liu Y, Ma X, Chen HY. Rapid, large-scale synthesis and electrochemical behavior of faceted single-crystalline selenium nanotubes. *J Phys Chem B* 2006;110:9041-47.
- [253] Tornblom M, Henriksson U. Effect of solubilization of aliphatic hydrocarbons on size and shape of rodlike C₁₆TABr micelles studied by ²H NMR relaxation. *J Phys Chem B* 1997;101:6028-35.

- [254] Mayers B, Liu K, Sunderland D, Xia YN. Sonochemical synthesis of trigonal selenium nanowires. *Chem Mater* 2003;15:3852-58.
- [255] Jolivet JP, Henry M, Livage J. Metal Oxide chemistry and synthesis from solution to solid state; Bescher, E., Translator; John Wiley and Sons: Chichester, U.K., 2000.
- [256] Ma YR, Qi LM, Ma JM, Cheng HM. Micelle-mediated synthesis of single-crystalline sselenium nanotubes. *Adv Mater* 2004;16:1023-26.
- [257] An C, Tang K, Liu X, Qian Y. Large- scale synthesis of high quality trigonal selenium nanowires. *Eur J Inorg Chem* 2003;3250-55.
- [258] Ladj R, Bitar A, Eissa M, Mugnier Y, Le Dantec R, Fessi H, Elaissari A, Individual inorganic nanoparticles: preparation, functionalization and in vitro biomedical diagnostic applications. *J. Mater. Chem. B*, 2013;1:1381-1396.
- [259] Lu Z, Yin Y, Colloidal nanoparticle clusters: functional materials by design, *Chem Soc Rev* 2012;41:6874-6887.
- [260] Yang L, Zhu J, Xiao D, Microemulsion-mediated hydrothermal synthesis of ZnSe and Fe-doped ZnSe quantum dots with different luminescence characteristics. *RSC Adv* 2012;2: 8179-8188 .
- [261] Xu H, Cao W, Zhang X, Selenium-Containing Polymers: Promising Biomaterials for Controlled Release and Enzyme Mimics, *Acc Chem Res* 2013;46:1647–1658.
- [262] Ehlert S, Taheri SM, Pirner D, Drechsler M, Schmidt HW, Förster S, Polymer Ligand Exchange to Control Stabilization and Compatibilization of Nanocrystals, *ACS Nano* 2014; DOI: 10.1021/nn5014512.

- [263] Kortschot RJ, Rijssel JV, Dijk-Moes RJA, Erné BH, Equilibrium Structures of PbSe and CdSe Colloidal Quantum Dots Detected by Dielectric Spectroscopy. *J. Phys. Chem. C*, 2014;118:7185–7194.
- [264] Olivas RM, Donard OFX. Microwave assisted reduction of Se^{VI} to Se^{IV} and determination by HG/FI-ICP/MS for inorganic selenium speciation. *Talanta* 1998;45:1023-29.
- [265] Zhu YJ, Hu XL. Preparation of powders of selenium nanorods and nanowires by microwave-polyol method. *Mater Lett* 2004;58:1234-36.
- [266] Kolachi NF, Kazi TG, Afridi HI, Khan S, Wadhwa SK, Shah AQ, Shah F, Baig JA, Sirajuddin A. Determination of selenium content in aqueous extract of medicinal plants used as herbal supplement for cancer patients. *Food and Chemical Toxi* 2010;48:3327-32.
- [267] Yan X, Michael E, Komarneni S, Brownson JR, Yan ZF, Microwave- and conventional-hydrothermal synthesis of CuS, SnS and ZnS: Optical properties. *Ceramics Int* 2013;39:4757-63.
- [268] Pei J, Chen G, Jia D, Jin R, Xua H, Chen D, Rapid synthesis of Ag₂Se dendrites with enhanced electrical performance by microwave-assisted solution method. *New J Chem* 2013; 37:323-328.
- [269] Ayela DW, Su WN, Wu CC, Shiaua CY, Hwang BJ, Amorphous precursor compounds for CuInSe₂ particles prepared by a microwave-enhanced aqueous synthesis and its electrophoretic deposition. *Cryst Eng Comm* 2014;16:3121–3127.
- [270] Pan L, Liu X, Suna Z, Sunb CQ, Nanophotocatalysts via microwave-assisted solution-phase synthesis for efficient photocatalysis. *J Mater Chem A* 2013;1:8299–8326.
- [271] Zhu YJ, Chen F, Microwave-Assisted Preparation of Inorganic Nanostructures in Liquid Phase, *Chem Rev*, 2014 DOI: 10.1021/cr400366s.

- [272] Gao X, Gao T, Zhang L. Solution-solid growth of α -monoclinic selenium nanowires at room temperature. *J Mater Chem* 2003;13:6-8.
- [273] Zhang H, Zuo M, Tan S, Li G, Zhang S, Hou J. Carbothermal chemical vapor deposition route to Se one-dimensional nanostructures and their optical properties. *J Phys Chem B* 2005;109:10653-57.
- [274] Xia YY. Synthesis of selenium nanoparticles in the presence of silk fibroin. *Mater Lett* 2007;61:4321-24.
- [275] Zhang B, Ye X, Wang C, Xie Y. A facile solution-phase deposition approach to porous selenium material. *J Mater Chem* 2007;17:2706-12.
- [276] Jiang X, Kemal L, Yu A. Silver-induced growth of selenium nanowires in aqueous solution. *Mater Lett* 2007;61:2584-88.
- [277] Redman DW, Murugesan S, Stevenson KJ, Cathodic Electrodeposition of Amorphous Elemental Selenium from an Air- and Water-Stable Ionic Liquid, *Langmuir* 2014;30: 418–425.
- [278] Shah CP, Kumar M, Pushpa KK, Bajaj PN. Acrylonitrile-induced synthesis of polyvinyl alcohol-stabilized selenium nanoparticles. *Crystal Growth & Design* 2008;8:4159-64.
- [279] Xi G, Xiong K, Zhao Q, Zhang R, Zhang H, Qian Y. Nucleation-dissolution-recrystallization: a new growth mechanism for t-selenium nanotubes. *Crystal Growth & Design* 2006;6:577-82.
- [280] Nirmal M, Brus L. Luminescence photophysics in semiconductor nanocrystals. *Acc Chem Res* 1999;32:407-14.
- [281] Alivisatos AP. Semiconductor Clusters, Nanocrystals, and Quantum Dots. *Science* 1996;271:933-37.

- [282] Chan WCW, Nie S. Quantum dot bioconjugates for ultrasensitive nonisotopic detection. *Science* 1998;281:2016-18.
- [283] Dujardin E, Mann S. Bio-inspired materials chemistry. *Adv Mater* 2002;11:775-88.
- [284] Brus LE. Chemical approaches to semiconductor nanocrystals. *J Phys Chem Solids* 1998;59:459-65.
- [285] Wang Y, Herron N. Nanometer-sized semiconductor clusters: materials synthesis, quantum size effects, and photophysical properties. *J Phys Chem* 1991;95:525-32.
- [286] Ipe BI, Thomas KG, Barazzouk S, Hotchandani S, Kamat PV. Photoinduced charge separation in a fluorophore-gold nanoassembly. *J Phys. Chem B* 106;1:18-21.
- [287] Zhang B, Ye X, Dai W, Hou W, Zuo F, Xie Y. Biomolecule-assisted synthesis of single-crystalline selenium nanowires and nanoribbons via a novel flake-cracking mechanism. *Nanotechnology* 2006;17:385-90.
- [288] Hecht D, Hu LB, Gruner G. Conductivity scaling with bundle length and diameter in single walled carbon nanotube networks. *Appl Phys Lett* 2006;89;133112 -3 .
- [289] Banyai L, Koch SW. *Semiconductor Quantum Dots*: Singapore: World Scientific 1993.
- [290] Wyckoff RWG. *Crystal Structure*. 1964;1:39.
- [291] Zhang X, Chan KY. Water-in-oil microemulsion synthesis of platinum-ruthenium nanoparticles, their characterization and electrocatalytic properties. *Chem Mater* 2003;15:451-59.
- [292] Tang H, Chen JH, Huang ZP, Wang DZ, Ren ZF, Nie LH, Kuang YF, Yao SZ. High dispersion and electrocatalytic properties of platinum on well-aligned carbon nanotube arrays. *Carbon* 2004;42:191-97.

- [293] Bensebaa F, Patrito N, Le Page Y, Lecuyer P, Wang D. Tunable platinum–ruthenium nanoparticle properties using microwave synthesis. *J Mater Chem* 2004;14:3378–84.
- [294] Solla-Gullon J, Vidal-Iglesias FJ, Montiel V, Alda A. Electrochemical characterization of platinum–ruthenium nanoparticles prepared by water-in-oil microemulsion. *Electrochim Acta* 2004;49:5079–88.
- [295] Rodrigues OED, Saraiva GD, Nascimento RO, Barros EB, Filho JM, Kim YA, Muramatsu H, Endo M, Terrones M, Dresselhaus MS, Souza Filho AG. Synthesis and Characterization of Selenium– Carbon Nanocables. *Nano Lett* 2008;8:3651–55.
- [296] Song JM, Zhan YJ, Xu AW, Yu SH. Cellulose acetate-directed growth of bamboo-raft-like single-crystalline selenium superstructures: High-yield synthesis, characterization, and formation mechanism. *Langmuir* 2007;23:7321–27.
- [297] Dong H, Quintilla A, Cemernjak M, Popescu R, Gerthsen D, Ahlswede E, Feldmann C, Colloidally stable selenium@copper selenide core@shell nanoparticles as selenium source for manufacturing of copper–indium–selenide solar cells. *J Colloid Interface Sci* 2014;415: 103–110.
- [298] Xiao G, Wang Y, Ning J, Wei Y, Liu B, Yu WW, Zou G, Bo Zou B, Recent advances in IV–VI semiconductor nanocrystals: synthesis, mechanism, and applications. *RSC Adv* 2013;3:8104–8130.
- [299] Lesnyak V, Gaponik N, Eychmuller A, Colloidal semiconductor nanocrystals: the aqueous approach, *Chem Soc Rev* 2013;42:2905–2929.
- [300] Kim WD, Baum F, Kim D, Lee K, Moon JH, Lee DC, Photocorrosion-Assisted Transformation of Metal Selenide Nanocrystals into Crystalline Selenium Nanowires. *Cryst Growth Des* 2014;14:1258–1263.

- [301] Kumar A, Sevonkaev I, Goia DV. Synthesis of selenium particles with various morphologies, *J Colloid Interface Sci* 2014;416:119–123.
- [302] Alonso-Vante N, Tributsch H, Solorza-Feria O. Kinetics studies of oxygen reduction in acid medium on novel semiconducting transition metal chalcogenides. *Electrochim Acta* 1995;40:567-76.
- [303] Inukai J, Cao D, Wieckowski A, Chang KC, Menzel A, Komanicky V, You H. In situ synchrotron X-ray spectroscopy of ruthenium nanoparticles modified with selenium for an oxygen reduction reaction. *J Phys Chem C* 2007;111:16889-94.
- [304] Gilleo MA. Optical absorption and photoconductivity of amorphous and hexagonal selenium. *J Chem Phys* 1951;19:1291-98.
- [305] Le Rhun V, Alonso-Vante N. Tailoring of nanodivided electrocatalyst materials based on transition metal. *J New Mater Electrochem Syst* 2000;3:331-38.
- [306] Yang LB, Shen YH, Xie AJ, Liang JJ, Zhang BC. Synthesis of Se nanoparticles by using TSA ion and its photocatalytic application for decolorization of cango red under UV irradiation. *Mater Res Bull* 2008;43:572-82.
- [307] Espinosa AM, Tascon ML, Vazquez MD, Batanero PS. Electroanalytical study of selenium (+IV) at a carbon paste electrode with electrolytic binder and electroactive compound incorporated. *Electrochim Acta* 1992;37:1165-72.
- [308] Chiou YD, Hsu Y. Room-temperature synthesis of single-crystalline Se nanorods with remarkable photocatalytic properties. *J Appl Catalysis B Environ* 2011;105:211-19.
- [309] Liu P, Ma YR, Cai WW, Wang ZZ, Wang J, Qi LM, Chen DM. Photoconductivity of single-crystalline selenium nanotubes. *Nanotechnology* 2007;18:205704-08.

- [310] Qin A, Li Z, Yang R, Gu Y, Liu Y, Wang ZL. Rapid photoresponse of single-crystalline selenium nanobelts. *Solid State Commun* 2008;148:145-47.
- [311] Song L, Chen C, Zhang S. Preparation and photocatalytic activity of visible light sensitive selenium-doped bismuth sulphide. *Powder Tech.* 2011;207:170-74.
- [312] Bhavani P, Nenavathu AVR, Rao K, Goyal A, Kapoor A, Dutta RK. Synthesis, characterization and enhanced photocatalytic degradation efficiency of Se doped ZnO nanoparticles using trypan blue as a model dye. *Appl. Catalysis A: General* 2013;459:106-113.
- [313] Wang L, Zou H, Dong Z, Zhou L, Li J, Luo Q, Zhu J, Xu J, Liu J, Temperature-Driven Switching of the Catalytic Activity of Artificial Glutathione Peroxidase by the Shape Transition between the Nanotubes and Vesicle-like Structures. *Langmuir* 2014;30: 4013–4018.
- [314] Jin ZP, Nie HG, Yang Z, Zhang J, Liu Z, Xu XJ, Huang SM, Metal-free selenium doped carbon nanotube/graphene networks as a synergistically improved cathode catalyst for oxygen reduction reaction. *Nanoscale* 2012, 4, 6455.
- [315] Engel JH, Alivisatos AP, Postsynthetic Doping Control of Nanocrystal Thin Films: Balancing Space Charge to Improve Photovoltaic Efficiency. *Chem. Mater.* 2014;26:153–162.
- [316] Llave E, Scherlis D, Selenium-Based Self-Assembled Monolayers: The Nature of Adsorbate-Surface Interactions. *Langmuir* 2010;26:173–78.
- [317] Colmenares L, Jusys Z, Behm RJ. Electrochemical Surface Characterization and O₂ Reduction Kinetics of Se Surface-Modified Ru Nanoparticle-Based RuSey/C Catalysts. *Langmuir* 2006;22:10437-445.
- [318] Wang R, Da H, Wang H, Ji S, Tian Z, Selenium functionalized carbon for high dispersion of platinum ruthenium nanoparticles and its effect on the electrocatalytic oxidation of methanol. *J Power Sources* 2013;233:326-30.

- [319] Zapp E, Nascimento V, Dambrowski D, Braga AL, Vieira IC. Bio-inspired sensor based on glutathione peroxidase mimetic for hydrogen peroxide detection. *Sens. Actuators B* 2013;176:782-88.
- [320] Shih ZY, Yang Z, Lin ZH, Chang HT. Direct methanol fuel cells using Se/Ru core/shell cathodes provide high catalytic activity and stability. *Int J Hydrogen Energy* 2011; 36:7303-09.
- [321] Jeon MK, Liu JH, Lee KR, Lee JW, McGinn PJ, Woo SI. Combinatorial search for quaternary methanol tolerant oxygen electro- reduction catalyst. *Fuel Cells* 2010;10:93-98.
- [322] Neyerlin KC, Greg B, Rhys F, Zengcai L, Peter S. Combinatorial study of high-surface-area binary and ternary electrocatalysts for the oxygen evolution reaction. *J Electrochem Soc* 2009;156:B363-69.
- [323] Jiang L, Hsu A, Chu D, Chen R. Oxygen reduction on carbon supported Pt and PtRu catalysts in alkaline solutions. *J Electroanal Chem* 2009;629:87-93.
- [324] Zhang J, Zhang S, Zhang H, Zhang Y, Zheng Z, Xiang Y, Activated selenium for promoted formation of metal selenide nanocrystals in solvothermal synthesis. *Mater Lett* 2014;122:306–308.
- [325] Xie R, Su J, Liu Y, Guo L, Optical, structural and photoelectrochemical properties of CdS_{1-x}Se_x semiconductor films produced by chemical bath deposition. *Int J Hydrogen Energy* 2014;39:3517-3527.
- [326] Filippo E, Manno D, Serra A. Characterization and growth mechanism of selenium microtubes synthesized by a vapor phase deposition route. *Cryst Growth* 2010;10:4890-97.
- [327] Kumar S. Synthesis and characterisation of selenium nanowires using template synthesis. *J Exp Nanosci* 2009;4:341-46.

- [328] Tutihasi S, Chen I. Optical properties and band structure of trigonal selenium. *Phys Rev* 1967;158:623-30.
- [329] Bogomolov VN, Kholodkevich SV, Romanov SG, Agroskin LS. The absorption spectra of single selenium and tellurium chains in dielectric matrix channels. *Solid State Commun* 1983;47:181-82.
- [330] Gates B, Mayers B, Grossman A, Xia Y. A sonochemical approach to the synthesis of crystalline selenium nanowires in solutions and on solid supports. *Adv Mater* 2002;14:1749-52.
- [331] Zhang W, Chen Z, Liu H, Zhang L, Gao P, Li D. Biosynthesis and structural characteristics of selenium nanoparticles by *Pseudomonas alcaliphila*. *Colloid Surf B* 2011; 88:196-201.
- [332] Li Q, Chen T, Yang F, Liu J, Zheng W. Facile and controllable one-step fabrication of selenium nanoparticles assisted by L-cysteine. *Mater Lett* 2010;64:614-17.
- [333] Hu B, Su CY, Dieter Fenske D, Fuhr O, Synthesis, characterization and optical properties of a series of binuclear copper chalcogenolato complexes. *Inorganica Chimica Acta* 2014;419:118–123.
- [334] Zatsepin AF, Buntov EA, Pustovarov VA, Fitting HJ, Photoluminescence of Se-related oxygen deficient center in ion-implanted silica films. *J Luminescence* 2013;143:498–502.
- [335] Lee YY, Shon JK, Bae S, Jin X, Choi YJ, Kwon SS, Hane TH, Kim JM, Highly ordered mesoporous $\text{Cd}_x\text{Zn}_{1-x}\text{Se}$ ternary compound semiconductors with controlled band gap energies. *New J Chem* 2014, DOI: 10.1039/c4nj00626g.
- [336] Bai T, Li C, Li F, Zhao L, Wang Z, Huang H, Chen C, Han Y, Shi Z, Feng S, A simple solution-phase approach to synthesize high quality ternary AgInSe_2 and band gap tunable quaternary $\text{AgIn}(\text{S}_{1-x}\text{Se}_x)_2$ nanocrystals. *Nanoscale* 2014;6:6782-6789.

- [337] Rajalakshmi M, Arora AK. Optical properties of selenium nanoparticles dispersed in polymer. Solid State Commun 1999;110:75-80.
- [338] Lin ZH, Wang CRC. Evidence on the size-dependent absorption spectral evolution of selenium nanoparticles. Mater Chem Phys 2005;92:591-94.
- [339] Shin Y, Blackwood JM, Bae IT, Arey BW, Gregory J. Synthesis and stabilization of selenium nanoparticles on cellulose nanocrystal. Mater Lett 2007;61:4297-300.
- [340] Zhang L, Yu H, Cao W, Dong Y, Zou C, Yang Y, Huang S, Dai N, Zhu DM, Antimony doped cadmium selenium nanobelts with enhanced electrical and optoelectrical properties. Appl Surf Sci 2014;307:608–614.
- [341] Chang J, Waclawik ER, Colloidal semiconductor nanocrystals: controlled synthesis and surface chemistry in organic media. RSC Adv., 2014;4:23505-23527.
- [342] Seo YH, Jo Y, Choi Y, Yoon KH, Ryu BH, Ahn SJ, Jeong S, Thermally-derived liquid phase involving multiphase Cu(In,Ga)Se₂nanoparticles for solution-processed inorganic photovoltaic devices. RSC Adv 2014;4:18453-18459.
- [343] Ng CHB, Fan WY, Colloidal Beading: Sonication-Induced Stringing of Selenium Particles, Langmuir, 2014;30:7313-7318.
- [344] El-Bayoumy K, Sinha R. Mechanisms of mammary cancer chemoprevention by organoselenium compounds. Mutat Res 2004;551:181-97.
- [345] Abdulah R, Miyazaki K, Nakazawa M, Koyama H. Chemical forms of selenium for cancer prevention. J Trace Elem Med Biol 2005;19:141-50.
- [346] Koller LD, Exon JH. The two faces of selenium-deficiency and toxicity-are similar in animals and man. Can J Vet Res 1986;50:297-302.

- [347] McAdam PA, Levander OA. Chronic toxicity and retention of dietary selenium fed to rats as D-or L-selenomethionine, selenite, or selenate. *Nutrition Res* 1987;7:601-10.
- [348] Garbisu C, Gonzalez S, Yang WH. Physiological mechanisms regulating the conversion of selenite to elemental selenium by *Bacillus subtilis*. *Biofactors* 1995;5:29-37.
- [349] Tomei FA, Barton LL, Semanski CL. Transformation of selenate and selenite to elemental selenium by *Desulfovibrio desulfuricans*. *J Ind Microbiol* 1995;14:329-36.
- [350] Zhang JS, Gao XY, Zhang LD, Bao YP. Biological effects of a nano red elemental selenium. *Biofactors* 2001;15:27-38.
- [351] Huang B, Zhang J, Hou J, Chen C. Free radical scavenging efficiency of Nano-Se in vitro. *Free Radic Biol Med* 2003;35:805-13.
- [352] Sieber F, Daziano JP, Gunther WH, Krieg M, Miyagi K, Sampson RW, Ostrowski MD, Anderson GS, Tsujino I, Bula RJ. Elemental selenium generated by the photobleaching of selenomerocyanine photosensitizers forms conjugated with serum macromolecules that are toxic to tumor cells. *Phosphorus Sulfur Silicon Relat Elem* 2005;180:647-57.
- [353] Mishra B, Hassan PA, Priyadarsini KI, Mohan H. Reactions of biological oxidants with selenourea: formation of redox active nanoselenium. *J Phys Chem B* 2005;109:12718-23.
- [354] Zhang J, Wang H, Yan X, Zhang L. Comparison of short-term toxicity between Nano-Se and selenite in mice. *Life Sci* 2005;76:1099-109.
- [355] Jia X, Li N, Chen JA. A subchronic toxicity study of elemental Nano-Se in Sprague-Dawley rats. *Life Sci* 2005;76:1989-2003.
- [356] Vekariya KK, Kaur J, Tikoo K, Alleviating anastrozole induced bone toxicity by selenium nanoparticles in SD rats, *Toxicol Appl Pharmacol* 2013;268:212–220.

- [357] Kong L, Yuan Q, Zhu H, Li Y, Guo Q, Wang Q, Bi X, Gao X. The suppression of prostate LNCaP cancer cells growth by selenium nanoparticles through Akt/Mdm2/AR controlled apoptosis. *Biomaterials* 2011;32:6515-22.
- [358] Chen T, Wong YS, Zheng W, Bai Y, Huang L. Selenium nanoparticles fabricated in Undaria pinnatifida polysaccharide solutions induce mitochondria-mediated apoptosis in A375 human melanoma cells. *Colloids and Surfaces B Biointerfaces* 2008;67:26-31.
- [359] Mahmoudvand H, Harandi MF, Shakibaie M, Aflatoonian MR, Ali NZ, Makki MS, Jahanbakhsh S, Scolicidal effects of biogenic selenium nanoparticles against protoscolices of hydatid cysts. *Int. J. Surg.* 2014;12:399-403.
- [360] Wang H, Zhang J, Yu H. Elemental selenium at nano size possesses lower toxicity without compromising the fundamental effect on selenoenzymes: comparison with selenomethionine in mice. *Free Radical Biology & Medicine* 2007;42:1524-33.
- [361] Zhang J, Wang X, Xu T. Elemental selenium at nano size (Nano-Se) as a potential chemopreventive agent with reduced risk of selenium toxicity: comparison with se-methylselenocysteine in mice. *Toxicol Sci* 2008;101:22-31.
- [362] Shakibaie M, Khorramizadeh MR, Faramarzi MA, Sabzevari O, Shahverdi AR. Biosynthesis and recovery of selenium nanoparticles and the effects on matrix metalloproteinase- 2 expression. *Biotechnol Appl Biochem* 2010;56:7-15.
- [363] Soflaei S, Dalimi A, Abdoli A, Kamali M, Nasiri V, Shakibaie M, Tat M. Anti-leishmanial activities of selenium nanoparticles and selenium dioxide on Leishmania infantum. *Comp Clin Pathol DOI 10.1007/s00580-012-1561-z.*

- [364] Li H, Zhang J, Wang T, Luo W, Zhou Q, Jiang G. Elemental selenium particles at nano-size (Nano-Se) are more toxic to Medaka (*Oryzias latipes*) as a consequence of hyper-accumulation of selenium: a comparison with sodium selenite. *Aquatic Toxicol* 2008;89:251-56.
- [365] Hu CH, Li YL, Xiong L, Zhang HM, Song J, Xia MS. Comparative effects of nano-elemental selenium and sodium selenite on selenium retention in broiler chickens. *Animal Feed Sci and Tech* 2012;177:204-10.
- [366] Wang X, Sun K, Tan Y, Wu S, Zhang J, Efficacy and safety of selenium nanoparticles administered intraperitoneally for the prevention of growth of cancer Cells in peritoneal cavity. *Free Radical Bio Med* 2014;72:1-10.
- [367] Sun D, Liu Y, Yu Q, Qin X, Yang L, Zhou Y, Chen L, Liu J, Inhibition of tumor growth and vasculature and fluorescence imaging using functionalized ruthenium-thiol protected selenium nanoparticles. *Biomaterials* 2014;35:1572-1583.
- [368] Wu S, Sun K, Wnag X, Wang D, Wan X, Zhang J, Protonation of Epigallocatechin-3-gallate (EGCG) Results in Massive Aggregation and Reduced Oral Bioavailability of EGCG-Dispersed Selenium Nanoparticles. *J Agric Food Chem* 2013;61:7268–7275.
- [369] Forootanfar H, Adeli-Sardou M, Nikkhoo M, Mehrabani M, Amir-Heidari B, Shahverdi AR, Shakibaie M, Antioxidant and cytotoxic effect of biologically synthesized selenium nanoparticles in comparison to selenium dioxide. *J Trace Elem Med Bio* 2014;28: 75-79.
- [370] Yang L, Chen Q, Liu Y, Zhang J, Sun D, Zhou Y, Liu J, Se/Ru nanoparticles as inhibitors of metal-induced A β aggregation in Alzheimer's disease. *J Mater Chem B* 2014;2:1977-1987.
- [371] Faghfuri E, Yazdi M H, Mahdavi M, Sepehrizadeh Z, Faramarzi M A, Mavandadnejad F, Shahverdi A R, Dose-Response Relationship Study of Selenium Nanoparticles as an Immunostimulatory Agent in Cancer-bearing Mice, *Archives Med Res* 2015;46:31-37

- [372] He Y, Chen S, Liu Z, Cheng C, Li H, Wang M, Toxicity of selenium nanoparticles in male Sprague–Dawley rats at supranutritional and nonlethal levels, *Life Sci* 2014;115:44–51.
- [373] Nagya G, Benko I, Kiralya G, Voros O, Tanczos B, Sztrik A, Takács T, Pocsi I, Prokisch J, Banfalvi G, Cellular and nephrotoxicity of selenium species, *J Trace Elements in Med Bio* 2015;30:160–170.
- [374] Panchapakesan B, Caprara R, Velasco V, Loomis J, King B, Xu P et al. Micro- and nanotechnology approaches for capturing circulating tumor cells. *Cancer Nanotechn* 2010;1:3–13.
- [375] Li Y, Li X, Wong YS, Chen T, Zhang H, Liu C, Zheng W, The reversal of cisplatin-induced nephrotoxicity by selenium nanoparticles functionalized with 11-mercapto-1-undecanol by inhibition of ROS-mediated apoptosis. *Biomaterials* 2011;32:9068–9076.
- [376] Zhang J, Wang H, Bao Y, Zhang L. Nano red elemental selenium has no size effect in the induction of seleno-enzymes in both cultured cells and mice. *Life Sci* 2004;75:237–44.
- [377] Peng D, Zhang J, Liu Q, Taylor EW. Size effect of elemental selenium at nano size (Nano-Se) and supra-nutritional levels on selenium accumulation and glutathione S-transferase activity. *J Inorgc Biochem* 2007;101:1457–63.
- [378] Bartůněk V, Junková J, Šuman J, Kolářová K, Rimpelová S, Ulbrich P, Sofer Z, Preparation of amorphous antimicrobial selenium nanoparticles stabilized by odor suppressing surfactant polysorbate 20, *Mat Lett* DOI: <http://dx.doi.org/10.1016/j.matlet.2015.03.092>.
- [379] Jia X, Liu Q, Zou S, Xu X, Zhang L, Construction of selenium nanoparticles/-glucan composites for enhancement of the antitumor activity, *Carbohydrate Polymers* 2015;117:434–442.

- [380] Zheng S, Li X, Zhang Y, Xie Q, Wong YS, Zheng W, Chen T. PEG-nanolized ultrasmall selenium nanoparticles overcome drug resistance in hepatocellular carcinoma HepG2 cells through induction of mitochondria dysfunction. *Int J Nanomed* 2012;7:3939-49.
- [381] a. Liu W, Li X, Wong YS, Zheng W, Zhang Y, Cao W, Chen T. Selenium nanoparticles as a carrier of 5-fluorouracil to achieve anticancer synergism. *ACS Nano* 2012;6:6578-91.
b. Jain R, Jordan N, Weiss S, Foerstendorf H, Heim K, Kacker R, Hübner R, Kramer H, Hullebusch ED, Farges F, Lens PNL. Extracellular polymeric substances govern the surface charge of biogenic elemental selenium nanoparticles. *Environ. Sci. Technol.* 2015;49: 1713–20.
- [382] Gao F, Yuan Q, Gao L, Cai P, Zhu H, Liu R, Wang Y, Wei Y, Huang G, Liang J, Gao X. Cytotoxicity and therapeutic effect of irinotecan combined with selenium nanoparticles. *Biomaterials* 2014;35:8854-8866.
- [383] Kumar S, Tomar M S, Acharya A. Carboxylic group-induced synthesis and characterization of selenium nanoparticles and its anti-tumor potential on Dalton's lymphoma cells. *Colloids Surf B* 2015;126:546–552.
- [384] Liu T, Zeng L, Jiang W, Fu Y, Zheng W, Chen T. Rational design of cancer-targeted selenium nanoparticles to antagonize multidrug resistance in cancer cells. *Nanomed Nanotech Bio Med*, 2015, <http://dx.doi.org/10.1016/j.nano.2015.01.009>.
- [385] Zheng W, Cao C, Liu Y, Yu Q, Zheng C, Sun D, Ren X, Liu J. Multifunctional polyamidoamine-modified selenium nanoparticles dual-delivering siRNA and cisplatin to A549/DDP cells for reversal multidrug resistance. *Acta Biomaterialia* 2015;11:368–380.
- [386] Baker M. Nanotechnology imaging probes: smaller and more stable. *Nat Methods* 2010;7:957-962.

- [387] Rana S, Yeh YC, Rotello VM, Engineering the Nanoparticle-Protein Interface: Applications and Possibilities. *Curr Opin Chem Biol* 2010;14:828-834.
- [388] Liu YS, Wen CF, Yang YM, Cholesterol Effects on the Vesicular Membrane Rigidity and Drug Encapsulation Efficiency of Ethosome-Like Cationic Vesicles. *Sci Adv Mater* 2014;6:954-962.
- [389] Ferlay J, Parkin DM, Steliarova-Foucher E. Estimates of cancer incidence and mortality in Europe in 2008. *Eur J Cancer* 2008;46:765-781.
- [390] Peer D, Karp JM, Hong S, Farokhzad OC, Margalit R, Langer R. Nanocarriers as an emerging platform for cancer therapy. *Nat Nanotechnol* 2007;2:751-60.
- [391] Bindu MB, Kusum B, David B. Novel strategies for poorly water soluble drugs. *Int J Pharm* 2010;4:8-76.
- [392] Navarro-Alarcon M, Lopez-Martinez MC. Essentiality of selenium in the human body: relationship with different diseases. *Sci Total Environ* 2000;249:347-71.
- [393] Jia X, Li N, Chen J, A subchronic toxicity study of elemental Nano-Se in Sprague-Dawley rats. *Life Sci* 2005;76:1989-2003.
- [394] a. Prasad SK, Patel H, Patel T, Patel K, Selvaraj K, Biosynthesis of Se nanoparticles and its effect on UV-induced DNA damage. *Colloids Surf B* 2013;103:261-266.
b. Yu B, Ting L, Du Y, Luo Z, Zheng W, Chen T, X-ray-responsive selenium nanoparticles for enhanced cancer chemo-radiotherapy. *Colloids Surf B* 2016;139:180-189.
- [395] El-Bayoumy K, Sinha R. Mechanisms of mammary cancer chemoprevention by organoselenium compounds. *Mutat Res* 2004;551:181-97.

- [396] Mohammed ET, Safwat GM, Assessment of the ameliorative role of selenium nanoparticles on the oxidative stress of acetaminophen in some tissues of male albino rats. J Basic Appl Sci 2013;2:80-87.
- [397] Nabholz JM, Buzdar A, Pollak M, Harwin W, Burton G, Mangalik A, Steinberg M, Webster A, Von Euler M, Anastrozole is superior to tamoxifen as first-line therapy for advanced breast cancer in postmenopausal women: results of a North American multicenter randomized trial. J Clin Oncol 2000;18:3758-3767.
- [398] Vekariya KK, Kaur J, Tikoo K, Alleviating anastrozole induced bone toxicity by selenium nanoparticles in SD rats. Toxicol Appl Pharmacol 2013;268:212-220.
- [399] Rezvanfar MA, Shahverdi AR, Ahmadi A, Baeeri M, Mohammadirad A, Abdollahi M, Protection of cisplatin-induced spermatotoxicity, DNA damage and chromatin abnormality by selenium nano-particles. Toxicol Appl Pharmacol. 2013;266:356-365.
- [400] Chen T, Wong YS, Zheng W, Bai Y, Huang L, Selenium nanoparticles fabricated in Undaria pinnatifida polysaccharide solutions induce mitochondria-mediated apoptosis in A375 human melanoma cells. Colloids Surf B 2008;67:26-31.
- [401] Zhang Y, Li X, Huang Z, Zheng W, Fan C, Chen T, Enhancement of cell permeabilization apoptosis-inducing activity of selenium nanoparticles by ATP surface decoration. Nanomed. Nanotech Bio Med 2013;9:74-84.
- [402] Huang Y, He L, Liu W, Fan C, Zheng W, Wong YS, Chen T, Selective cellular uptake and induction of apoptosis of cancer-targeted selenium nanoparticles. Biomaterials 2013;34: 7106-7116.

- [403] Kong L, Yuan Q, Zhu H, Li Y, Guo Q, Wang Q, Bi X, Gao X, The suppression of prostate LNCaP cancer cells growth by Selenium nanoparticles through Akt/Mdm2/AR controlled apoptosis. *Biomaterials* 2011;32: 6515-6522.
- [404] Kumar G S, Kulkarni A, Khurana A, Kaur J, Tikoo K, Selenium nanoparticles involve HSP-70 and SIRT1 in preventing the progression of type 1 diabetic nephropathy, *Chemico-Bio Interactions* 2014;223:125–133.
- [405] a. Shakibaie M, Forootanfar H, Golkari Y, Mohammadi-Khorsand T, Shakibaie M R, Anti-biofilm activity of biogenic selenium nanoparticles and selenium dioxide against clinical isolates of *Staphylococcus aureus*, *Pseudomonas aeruginosa*, and *Proteus mirabilis*, *J Trace Elements Med Bio* 2015;29:235–241.
b. Wang Y, Hao H, Li Y, Zhang S, Selenium-substituted hydroxyapatite nanoparticles and their in vivo antitumor effect on hepatocellular carcinoma. *Colloid Surf. B* 2016;140:297–306.
- [406] Kepp KP, Bioinorganic Chemistry of Alzheimer's Disease, *Chem Rev* 2012;112: 5193-5239.
- [407] Goedert M, Spillantini MG, A century of Alzheimer's disease. *Science* 2006;314:777-781.
- [408] Selkoe DJ, Alzheimer's Disease: Genes, Proteins, and Therapy, *Physiol Rev* 2001;81:741-766.
- [409] Karlawish J, Addressing the ethical, policy, and social challenges of preclinical Alzheimer, *Neurology* 2011;77:1487-1493.
- [410] Reyes M, Egrise R, Nève D, Pasteels J, Schoutens JL, Selenium deficiency induced growth retardation is associated with an impaired bone metabolism and osteopenia. *J Bone Miner Res* 2001;16:1556-1563.

- [411] Ranjan B, Daundkar PS, Rampal S, Ameliorative effect of selenium on carbendazim induced oral sub-chronic testicular toxicity in bucks, *Small Rum Res* xxx (2014) xxx–xxx, <http://dx.doi.org/10.1016/j.smallrumres.2014.03.006>.
- [412] Li J-L, Jiang CY, Li S, Xu SW, Cadmium induced hepatotoxicity in chickens (*Gallus domesticus*) and ameliorative effect by selenium. *Ecotox Environ Safe.* 2013;96:103-109.
- [413] Mossaa ATH, Heikal TM, Omar EAA, Liver damage associated with exposure to aspirin and diazinon in male rats and the ameliorative effect of selenium. *Biomed Aging Patho* xxx (2014) xxx–xxx, <http://dx.doi.org/10.1016/j.biomag.2014.01.004>.
- [414] Reddy KP, Sailaja G, Krishnaiah C, Protective effects of selenium on fluoride induced alterations in certain enzymes in brain of mice. *J Environ Biol* 2009;30:859-864.
- [415] Sarkar C, Pal S, Das N, Dinda B, Ameliorative effects of oleanolic acid on fluoride induced metabolic and oxidative dysfunctions in rat brain: Experimental and biochemical studies. *Food Chem Toxicol* 2014;66:224-236.
- [416] Bao P, Chen Z, Tai R Z, Shen H M, Martin F L, Zhu Y G, Selenite-Induced Toxicity in Cancer Cells Is Mediated by Metabolic Generation of Endogenous Selenium Nanoparticles, *J Proteome Res* 2015;14:1127–1136.
- [417] Han J, Guo X, Lei Y, Dennis BS, Wu S, Wu C, Synthesis and characterization of selenium–chondroitin sulfate nanoparticles, *Carbohydrate Polymers* 2012;90:122-126.
- [418] Kojouri GA, Jahanabadi S, Shakibaie M, Ahadi AM, Shahverdi AR, Effect of selenium supplementation with sodium selenite and selenium nanoparticles on iron homeostasis and transferrin gene expression in sheep: A preliminary study. *Res in Veterinary Sci* 2012;93: 275-278.

- [419] a. Wang J, Zhang Y, Yuan Y, Yue T, Immunomodulatory of selenium nano-particles decorated by sulphated Ganoderma lucidum polysaccharides. *Food Chem Toxicol* 2014;68:183-189.
- b. Huang X, Chen X, Chen Q, Yu Q, Sun D, Liu J, Investigation of functional selenium nanoparticles as potent antimicrobial agents against superbugs, *Acta Biomaterialia* 2016;30: 397–407.
- [420] Zhong C, Deng Z, Wang R, Bai Y, *Cryst Growth Des*. 2015;15:1602–1610.
- [421] Ganther HE, Biochemistry of selenium. Selenium. Zingaro, Copper, Eds. VNR, NY. 1974;546-614.
- [422] a. Durán P, Acuña JJ, Jorquera MA, Azcón R, Borie F, Cornejo P, Mora ML, Enhanced selenium content in wheat grain by co-inoculation of selenobacteria and arbuscular mycorrhizal fungi: A preliminary study as a potential Se biofortification strategy, *J Cereal Sci* 2013;57:275-280.
- b. Jain R, Dominic D, Jorda N, Rene ER, Weiss S, van Hullebusch ER, Hübner R, Lens PNL, Preferential adsorption of Cu in a multi-metal mixture onto biogenic elemental selenium nanoparticles, *Chem. Eng. J.* 2016;284:917–925.
- [423] Zhao Q, Wang Y, Cao Y, Chen A, Ren M, Ge Y, Yu Z, Wan S, Hu A, Bo Q, Ruan L, Chen H, Qin S, Chen W, Hu C, Tao F, Xu D, Xu J, Wen L, Li L, Potential health risks of heavy metals in cultivated topsoil and grain, including correlations with human primary liver, lung and gastric cancer, in Anhui province, Eastern China. *Sci Total Env* 2014;470–471: 340–347.
- [424] Yang T, Li H, Hu X, Li J, Hu J, Liu R, Deng ZY, Effects of Fertilizing with N, P, Se, and Zn on Regulating the Element and Functional Component Contents and Antioxidant Activity of Tea Leaves Planted in Red Soil, *J Agric Food Chem* 2014;62:3823–3830.

- [425] Cabanero AI, Madrid Y, Caamara C, Selenium Long-Term Administration and Its Effect on Mercury Toxicity, *J Agric Food Chem* 2006;54:4461-4468.
- [426] Raymond LJ, Ralston NVC, Observations on the level of total Hg and Se in species common to the fisheries of Seychelles. *Seychelles Med Dent J*. 2004;7:56-60.
- [427] Yang DY, Chen YW, Belzile N, Evidences of non-reactive mercury–selenium compounds generated from cultures of *Pseudomonas fluorescens*. *Sci Total Env* 2011;409:1697–1703.
- [428] Truong HYT, Chen YW, Belzile N, Effect of sulfide, selenite and mercuric mercury on the growth and methylation capacity of the sulfate reducing bacterium *Desulfovibrio desulfuricans*. *Sci Total Env* 2013;449:373–384.
- [429] Williams PN, Islam S, Islam R, Jahiruddin M, Adomako E, Soliaman ARM, Rahman GKMM, Lu Y, Deacon C, Zhu YG, Meharg AA, Arsenic Limits Trace Mineral Nutrition (Selenium, Zinc, and Nickel) in Bangladesh Rice Grain, *Environ. Sci. Technol.*, **2009**; 43:8430–8436.
- [430] Guzmán Mar JL, Reyes LH, Rahman GMM, Skip Kingston HM, Simultaneous Extraction of Arsenic and Selenium Species From Rice Products by Microwave-Assisted Enzymatic Extraction and Analysis by Ion Chromatography-Inductively Coupled Plasma-Mass Spectrometry, *J Agric Food Chem* 2009;57:3005–3013.
- [431] Ramos SJ, Yuan Y, Faquin V, Guilherme LRG, Li L, Evaluation of Genotypic Variation of Broccoli (*Brassica oleracea* var.*italic*) in Response to Selenium Treatment. *J Agric Food Chem* 2011;59:3657–3665.
- [432] Bertoldi D, Larcher R, Bertamini M, Otto S, Concheri G, Nicolini G, Accumulation and Distribution Pattern of Macro- and Microelements and Trace Elements in *Vitis vinifera* L. cv. Chardonnay Berries. *J Agric Food Chem* 2011;59:7224–7236.

- [433] Newairy AA, El-Sharaky AS, Badreldeen MM, Eweda SM, Sheweita SA. The hepatoprotective effects of selenium against cadmium toxicity in rats. *Toxicology* 2007;242:23-30.
- [434] Eltayeb AA, Liu Q, Gan L, Liu H, Xu H, Antagonistic effect of scutellarin on the toxicity of selenium in rat livers. *Biol Trace Elem Res.* 2004;98:253-64.
- [435] Trevisan R, Mello DF, Fisher AS, Schuverack PM, Dafre AL, Moody AJ. Selenium in water enhances antioxidant defenses and protects against copper-induced DNA damage in the blue mussel *Mytilus edulis*. *Aquat Toxicol.* 2011;101:64-71.
- [436] Jain R, Jordan N, Schild D, Hullebusch E D, Weiss S, Franzen C, Farges F, Hübner R, Lens P N L, Adsorption of zinc by biogenic elemental selenium nanoparticles, *Chem Eng J* 2015;260:855–863.
- [437] Banyai L, Koch SW, Semiconductor Quantum Dots: World Scientific, Singapore (1993).
- [438] Pandey P, Singh SP, Arya SK, Gupta V, Dutta M, Singh S, Malhotra BD, Application of thiolated gold nanoparticles for the enhancement of glucose oxidase activity. *Langmuir* 2007;23:3333-3337.
- [439] Gates B, Yin YD, Xia YN, A Solution-Phase Approach to the Synthesis of Uniform Nanowires of Crystalline Selenium with Lateral Dimensions in the Range of 10-30 nm. *J Am Chem Soc* 2000;122:12582-12583.
- [440] Andersson BA, Materials availability for large-scale thin-film photovoltaics. *Prog. Photovoltaics* 2000;8:61-76.
- [441] Becquerel ECR, "Mémoire sur les effets électriques produits sous l'influence des rayons solaires". *Comptes Rendus. Acad. Sci. Paris* 1839;9:56-71.

- [442] Perlin. From Space to Earth–The story of solar Electricity. Ann. Arbor, MI: AATEC Publications; (1999).
- [443] Gur I, Fromer NA, Chen CP, Kanaras AG, Alivisatos AP, Hybrid solar cells with prescribed nanoscale morphologies based on hyperbranched semiconductor nanocrystals. *Nano Lett* 2007;7:409-414.
- [444] Mahmoodi SR, Bayati M, Hosseinirad S, Foroumadi A, Gilani K, Rezayat SM, AC electrokinetic manipulation of selenium nanoparticles for potential nanosensor applications. *Mater. Res. Bull.* 2013;48:1262-1267.
- [445] Guijarro N, Lutz T, Villarreal TL, Mahony FO, Gomez R, Haque SA, Toward antimony selenide sensitized solar cells: efficient charge photogeneration at spiro-OMeTAD/Sb₂Se₃/metal oxide heterojunctions. *J. Phys. Chem. Lett.* 2012;3:1351-1356.
- [446] Zaghi AE, Buffière M, Brammertz G, Batuk M, Lenaers N, Kniknie B, Hadermann J, Meuris M, Poortmans J, Vleugels J, Mechanical synthesis of high purity Cu–In–Se alloy nanopowder as precursor for printed CISe thin film solar cells, *Adv. Powder Tech.* 2014;25:1254-1261.
- [447] Dong H, Quintilla A, Cemernjak M, Popescu R, Gerthsen D, Ahlswede E, Feldmann C, Colloidally stable selenium@copper selenide core@shell nanoparticles as selenium source for manufacturing of copper–indium–selenide solar cells. *J Colloid Interface Sci* 2014;415:103-110.
- [448] Dun C, Huang W, Huang H, Xu J, Zhou N, Zheng Y, Tsai H, Nie W, Onken D R, Li Y, Carroll D L, Hydrazine-Free Surface Modification of CZTSe Nanocrystals with All Inorganic Ligand, *J. Phys. Chem. C* 2014;118:30302–30308.

- [449] a. Zhang R, Szczepaniak S M, Carter N J, Handwerker C A, Agrawal R, A Versatile Solution Route to Efficient Cu₂ZnSn(S,Se)₄ Thin-Film Solar Cells, *Chem Mater* 2015; 27:2114–2120.
- b. Laramona G, Bourdais S, Jacob A, Choné C, Muto T, Cuccaro Y, Delatouche B, Moisan C, Péré D, Dennler G, 8.6% efficient CZTSSe solar cells sprayed from water–ethanol CZTS colloidal solutions, *J. Phys. Chem. Lett.* 2014;5: 3763–67.
- [450] Wang W, Jiang J, Ding T, Wang C, Zuo J, Yang Q, Alternative Synthesis of CuFeSe₂ Nanocrystals with Magnetic and Photoelectric Properties, *ACS Appl Mater Inter* 2015; 7:2235–2241.
- [451] Chen G, Yuan C, Liu J, Deng Y, Jiang G, Liu W, Zhu C, Low cost preparation of Cu₂ZnSnS₄ and Cu₂ZnSn(S_xSe_{1-x})₄ from binary sulfide nanoparticles for solar cell application, *J. Power Sources* 2014;262:201-206.
- [452] Hahn JS, Park G, Lee J, Shim J, Synthesis of CuInSe₂ nanoparticles in an oleic acid solution for application in thin film solar cells. *J. Ind. Eng. Chem.* 2014, <http://dx.doi.org/10.1016/j.jiec.2014.04.008>.
- [453] Han Z, Zhang D, Chen Q, Mei T, Zhuang S, One-pot, rapid synthesis of chalcopyrite CuInSe₂ nanoparticles for low-cost thin film solar cell, *Powder Tech.* 2013;249:119–125.
- [454] Liu CP, Chuang CL, Fabrication of copper–indium–gallium–diselenide absorber layer by quaternary-alloy nanoparticles for solar cell applications, *Solar Energy* 2012;86:2795–2801.
- [456] a. Yang S, Sun J, Peng He P, Deng X, Wang Z, Hu C, Ding G, Xie X, Selenium Doped Graphene Quantum Dots as an Ultrasensitive Redox Fluorescent Switch, *Chem. Mater.* 2015; 27:2004–2011.

b. Miszta K, Gariano G, Brescia R, Marras S, Donato FD, Ghosh S, Trizio LD, Manna L, Selective cation exchange in the core region of $\text{Cu}_{2-x}\text{Se}/\text{Cu}_{2-x}\text{S}$ Core/Shell nanocrystals, *J. Am. Chem. Soc.* 2015;137: 12195–198.

[457] Brandon NP, Thompsett D, *Fuel Cells Compendium*, Elsevier, London, (2005).

[458] a. Vielstich W, Lamm A, Gasteiger H, (Eds.), *Handbook of Fuel Cells: Fundamentals, Technology, Applications*, vols. 3 and 4, John Wiley and Sons, New York, (2003).

b. Marai AB, Belgacem JB, Ayadi ZB , Djessas K, Alaya S, Structural and optical properties of $\text{CuIn}_{1-x}\text{Ga}_x\text{Se}_2$ nanoparticles synthesized by solvothermal route, *J. Alloys Comp.* 2016;658: 961–966.

[459] Laramie J, Dicks A, *Fuel Cell Systems Explained*, second ed., John Wiley and Sons, New York, (2003).

[460] a. Thring R. (Ed.), *Fuel Cells for Automotive Applications*, John Wiley and Sons, New York, (2003).

b. Khanaki A, Abdizadeh H, Golobostanfar MR, *J. Phys. Chem. C* 2015;119:23250–23258.

[461] a. Cheng H, Yuan W, Scott K, The influence of a new fabrication procedure on the catalytic activity of ruthenium–selenium catalysts. *Electrochimica Acta* 2006;52:466-473.

b. Mahdi MA, Hmoodb A., Kadhimb A, Hassana JJ, Kasima SJ, Hassan Z, Solvothermal preparation and characterization of ternary alloy $\text{CdS}_x\text{Se}_{1-x}$ nanowires. *Optik* 2016;127:1962–1966.

[462] Vante NA, Handbook of fuel cells, in: Vielstich W, Gasteiger HA, Lamm A, (Eds.), *Electrocatalysis*, vol. 2, John Wiley & Sons, New York, Chapter 36 (2003).

- [463] Hilgendorff M, Diesner K, Schulenburg H, Bogdanoff P, Bron M, Fiechter S, Preparation Strategies towards Selective Ru-Based Oxygen Reduction Catalysts for Direct Methanol Fuel Cells. *J. New Mater. Electrochem. Syst.* 2001;5:71-81.
- [464] M. Bron, P. Bogdanoff, S. Fiechter, I. Dorbant, M. Hilgendorff, H. Schulenburg, and H. Tributsch, Influence of selenium on the catalytic properties of ruthenium-based cluster catalysts for oxygen reduction. *J. Electroanal. Chem.* 2001;500:510-517.
- [465] Reeve RW, Christensen PA, Dickinson AJ, Hamnett A, Scott K, Methanol-tolerant oxygen reduction catalysts based on transition metal sulfides and their application to the study of methanol permeation. *Electrochim. Acta* 2000;45:4237-4250.
- [466] Vante NA, Tributsch H, Feria OS, Kinetics studies of oxygen reduction in acid medium on novel semiconducting transition metal chalcogenides. *Electrochimica Acta*, 1995;40:567-576.
- [467] Zehl G, Schmithals G, Hoell A, Haas S, Hartnig C, Dorbandt I, Bogdanoff P, Fiechter S, On the structure of carbon-supported selenium-modified ruthenium nanoparticles as electrocatalysts for oxygen reduction in fuel cells. *Angew. Chem. Int. Ed.* 2007;38:7311-7314.
- [468] Gago AS, Arriaga LG, Gochi-Ponce Y, Feng YJ, Alonso-Vante N., Oxygen reduction reaction selectivity of Ru_xSe_y in formic acid solutions. *J. of Electroanalytical Chem.* 2010;648:78-84.
- [469] Whipplea DT, Jayashreea RS, Egasa D, Vante NA, Kenis PJA, Ruthenium cluster-like chalcogenide as a methanol tolerant cathode catalyst in air-breathing laminar flow fuel cells. *Electrochimica Acta* 2009;54:4384-4388.
- [470] Jeng KT, Hsu NY, Chien CC, Synthesis and evaluation of carbon nanotube-supported RuSe catalyst for direct methanol fuel cell cathode. *Int J of Hydrogen Energy* 2011;36:3997-4006.

- [471] Suarez-Alcantara K, Ezeta-Mejia A, Ortega-Aviles M, Haase D, Arce-Estrada E, Gonzalez-Huerta RG, Solorza-Feria O, Canton SE, Synchrotron-based structural and spectroscopic studies of ball milled RuSeMo and RuSnMo particles as oxygen reduction electrocatalyst for PEM fuel cells, Int. J. of Hydrogen Energy 2014
<http://dx.doi.org/10.1016/j.ijhydene.2014.03.220>.
- [472] Inukai J, Cao D, Wieckowski A, Chang KC, Menzel A, Komanicky V, You H, In situ synchrotron X-ray spectroscopy of ruthenium nanoparticles modified with selenium for an oxygen reduction reaction. J. Phys. Chem. C 2007;111:16889-16894.
- [473] Zehl G, Bogdanoff P, Dorbandt I, Fiechter S, Wippermann K, Hartnig C, Carbon supported Ru–Se as methanol tolerant catalysts for DMFC cathodes. Part I: preparation and characterization of catalysts. J Appl Electrochem. 2007;37:1475-1484.
- [474] Wang T, Yang L, Zhang B, Liu J, Extracellular biosynthesis and transformation of selenium nanoparticles and application in H_2O_2 biosensor. Colloids and Surf B 2010;80:94-102.
- [475] Iranifam M, Fathinia M, Rad TS, Hanifehpour Y, Khataee AR, Joo SW, A novel selenium nanoparticles-enhanced chemiluminescence system for determination of dinitrobutylphenol. Talanta 2013;107:263-269.
- [476] Ivanova YA, Ivanou DK, Streltsov EA, Fedotov AK, Electrochemical deposition of Te and electroless deposition of Se nanoparticles in etched tracks of Au^+ ions in SiO_2 layer on n-Si(100) wafers. Mater. Sci. Eng. B 2008;147:271-275.
- [477] a. Zapp E, Nascimento V, Dambrowski D, Braga AL, Vieira IC, Bio-inspired sensor based on glutathione peroxidase mimetic for hydrogen peroxide detection. Sens. Actuators B 2013;176:782-788.

- b. Qiao F, Wang J, Ai S, Li L, As a new peroxidase mimetics: The synthesis of selenium doped graphitic carbon nitride nanosheets and applications on colorimetric detection of H₂O₂ and xanthine, Sens. Actuators B 2015;216: 418–27.

ACCEPTED MANUSCRIPT

Author biographies

Dr Savita Caudhary received her BSc and MSc in chemistry and PhD in physical chemistry from Panjab University (PU), Chandigarh, India, with specialization in the synthesis of metallic and semiconducting nanoparticles. She has authored a book, three book chapters and more than 30 research articles in peer-reviewed international journals. Her scientific journals and books have been referred in many studies. She is the editorial member for **Advanced Science, Engineering and Medicine and International Journal of Chemistry and Chemical Engineering (IJCCE)**. She has been the recipient of many awards such as DST-DAAD fellowship (2008), Research Associateship from **Council of Scientific and Industrial Research (CSIR)** New Delhi, India (2011), Dr D.S. Kothari postdoctoral Fellowship (April 2012). In May, 2012, she was selected as '**INSPIRE faculty**' under DST-INSA INSPIRE faculty programme and joined as an assistant professor in Nanoscience Department, PU. In August, 2014, she joined the Department of Chemistry in PU as an assistant professor.



Professor Ahmad Umar received his BSc in biosciences and MSc in inorganic chemistry from Aligarh Muslim University (AMU), Aligarh, India, and PhD in semiconductor and chemical engineering from Chonbuk National University, South Korea. He worked as a research scientist in Brain Korea 21, Centre for Future Energy Materials and Devices, Chonbuk National University, South Korea, in 2007–2008. In December 2008, he joined the Department of Chemistry in Najran University, Najran, Saudi Arabia. He is a distinguished professor of chemistry and is the current deputy director of the Promising Centre for Sensors and Electronic Devices (PCSED), Najran University, Najran, Saudi Arabia.

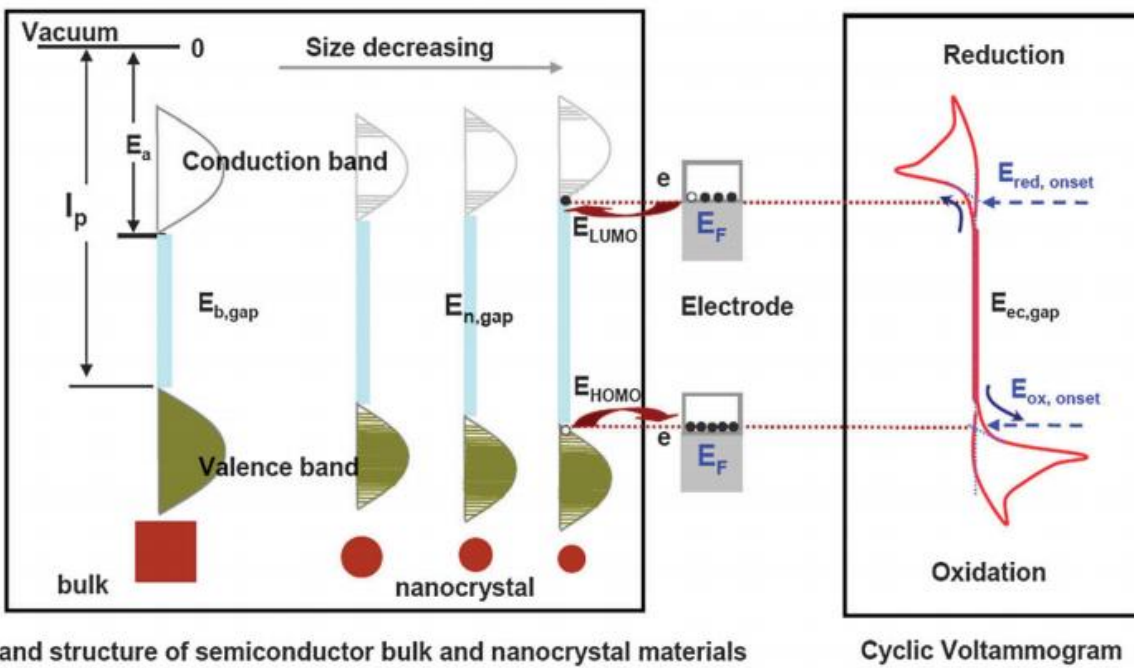
Professor Ahmad Umar is specialized in ‘semiconductor nanotechnology’, which includes growth, properties and applications of semiconductor nanostructures and their various high-technological applications such as semiconductor nanostructure-based gas, chemicals and biosensors, optoelectronic devices, electronic devices, field effect transistors (FETs), nanostructure-based energy-harvesting devices, such as solar cells, Li-ion batteries, supercapacitors, semiconductor nanomaterial-based environmental remediation, that is, catalysis and

photocatalysis. He is also specialized in the modern analytical and spectroscopic techniques used for the characterizations and applications of semiconductor nanomaterials. He has authored 23 book chapters, more than 290 research articles in peer-reviewed international journals, 18 editorial articles, 19 review articles and more than 171 proceedings, abstracts and technical reports. His works have been referred in many scientific journals and foreign expert for PhDs. He has six patents either issued or applied for on metal oxide nanostructures and their based sensors and electronics devices. He demonstrated, for the first time, the fabrication of *hydrazine sensor* using ZnO nanostructures, which has been highlighted on the cover page of *Chemical Communications*.

Professor Umar is the founding editor-in-chief for five reputed internationally recognized scientific journals, namely *Science of Advanced Materials* (www.aspbs.com/sam), *Journal of Nanoengineering and Nanomanufacturing* (www.aspbs.com/jnan), *Reviews in Advanced Sciences and Engineering* (www.aspbs.com/rase), *Energy and Environment Focus* (www.aspbs.com/efocus) and *Materials Focus* (www.aspbs.com/mat). All these journals are published by American Scientific Publishers (ASP; www.aspbs.com). He is also the editor-in-chief for *Sensor Letters* (<http://www.aspbs.com/sensorlett/>) and *Journal of Nanoelectronics and Optoelectronics* (www.aspbs.com/jno). He is the editor for *Journal of Nanoscience and Nanotechnology* (www.aspbs.com/jnn), Asian editor for *Advanced Science Focus* (www.aspbs.com/asfo), editor for *Advanced Science Engineering and Medicine* (www.aspbs.com/ASEM) and editor for *Advanced Science Letters* (www.aspbs.com/science), all published by ASP. He delivered several invited talks in national and international conferences and serves as a session chairs in many national and international conferences. Some of his research works were highlighted in various renowned scientific journals such as *Chemical Communications* and *Journal of Nanoscience and Nanotechnology*. He has received many awards such as *Best Research Award* by *Korean Institute of Chemical Engineers*, South Korea (2004), *Best paper award* by *International Union of Materials Research Societies(IUMRS)*, *International Conference in Asia* (2006), South Korea, *Best researcher award* in Chonbuk National University by *Brain Korea 21*, South Korea, *Highest number of Publication Award* for publishing maximum number of SCI papers in Chonbuk National University, *Highest Impact factor paper award* for publishing research papers in high-impact journals by *Brain Korea 21 Project*, South Korea, *Young scientist award* by European Materials Research Society, France, *Best Researcher Award* by Najran University, Najran, the Kingdom of Saudi Arabia (2009), *Best Scholar Award* (SR, 100,000) by Najran University, Najran, the Kingdom of Saudi Arabia (2010), *Top 100 Scientists award in the arena of Nanoscience and Nanotechnology* by IBC, Cambridge, England (2012) and *Almarai Award* (SR, 100,000) for innovative research by the the Kingdom of Saudi Arabia (2013). He contributed to the world of science by editing world's first handbook series on *Metal Oxide Nanostructures and Their Applications* (5-volume set, 3500 printed pages, www.aspbs.com/mona) and handbook series on *Encyclopedia of Semiconductor Nanotechnology* (7-volume set), both published by ASP. He is also editorial board member of scientific reports, a journal published by Nature Publishing Group (NPG).



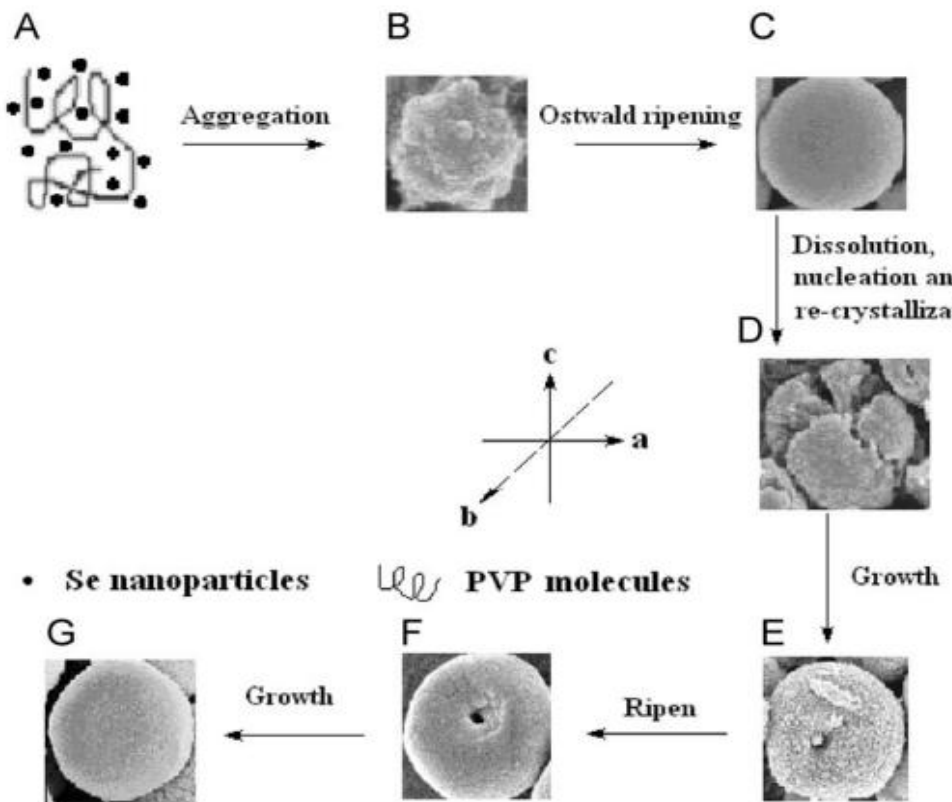
Professor S. K. Mehta is a distinguished professor of chemistry and the current chairman of the Department of Chemistry and Centre of Advanced Studies in Chemistry at Panjab University, Chandigarh, India. He joined Panjab University in 1981. He has educated students in innovative ways by introducing interesting, exciting and entertaining methodologies. Dr Mehta, Honorary DAAD Advisor and recipient of the prestigious German DAAD fellowship, Authors award of Royal Society of Chemistry, U.K. and JSPS invitation fellowship, has made several visits abroad for collaborative research. He has published more than 151 research articles in highly referred scientific journals, three review articles and six book chapters. He has handled two international projects and 12 national research projects. His current fields of interest are nanotechnology, drug delivery and colloidal chemistry.



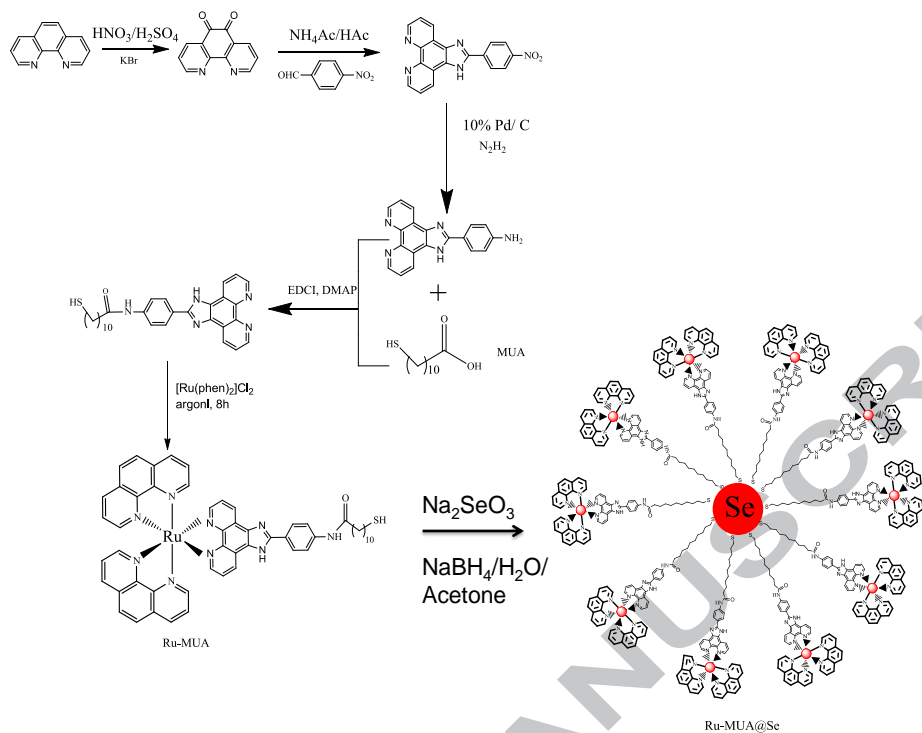
Band structure of semiconductor bulk and nanocrystal materials

Cyclic Voltammogram

Scheme 1. Schematic illustration of the principle of using CV to map the band structure of semiconducting nanoparticles. [Reprinted with permission from ref. (135), Liu J, Yang W, Li Y, Fana L, Li Y, 16, 4778-4788, 2014 @ RSC, 2014].



Scheme 2. Possible formation process of t-Se microspheres with holes. [Reprinted with permission from ref. (173), Zhang L, Ni Y, Hong J. 70:1408–12, 2009; © Elsevier, 2009].



Scheme 3. Schematic illustration of the capping of 11-mercaptoundecanoic acid over the Se nanoparticles [Reprinted with permission from ref. (366), Sun D, Liu Y, Yu Q, Qin X, Yang L, Zhou Y, Chen L, Liu J, 35:1572-1583, 2014; @ Elsevier, 2014].

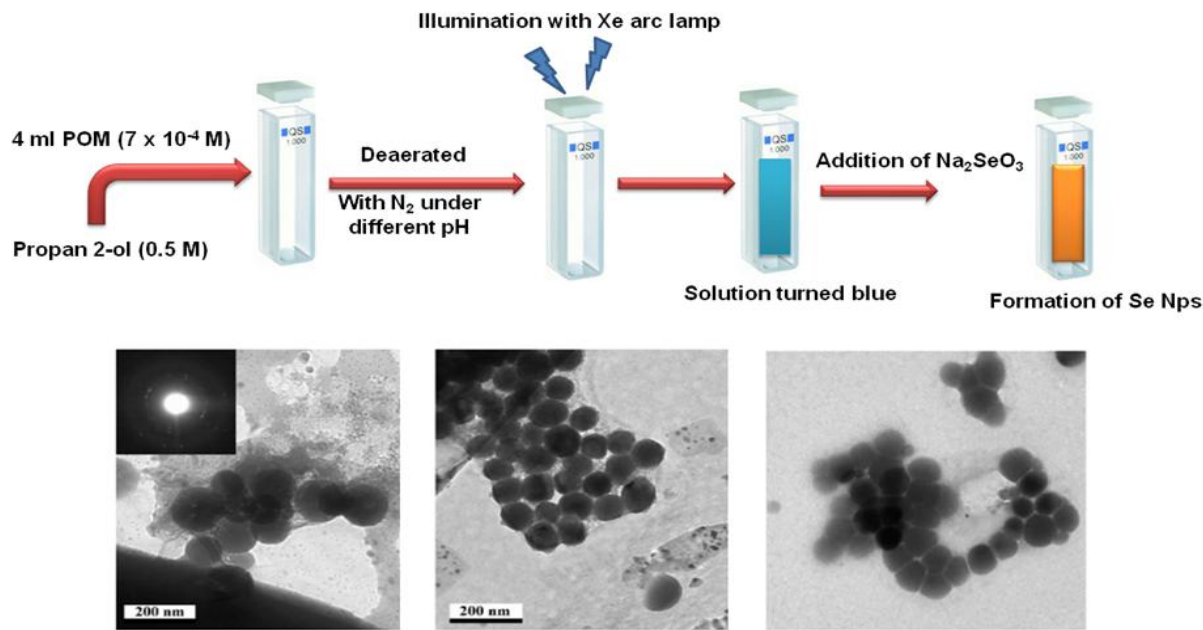
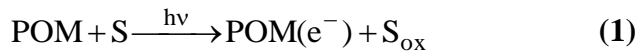


Figure 1. Formation of selenium nanoparticles via photolysis process and their TEM images. [Reprinted with permission from ref. (62), Triantis T, Troupis A, Gkika E, Alexakos G, Boukos N, Papaconstantinou E, Hiskia A, 144. 2-6, 2009 @ Elsevier, 2009].

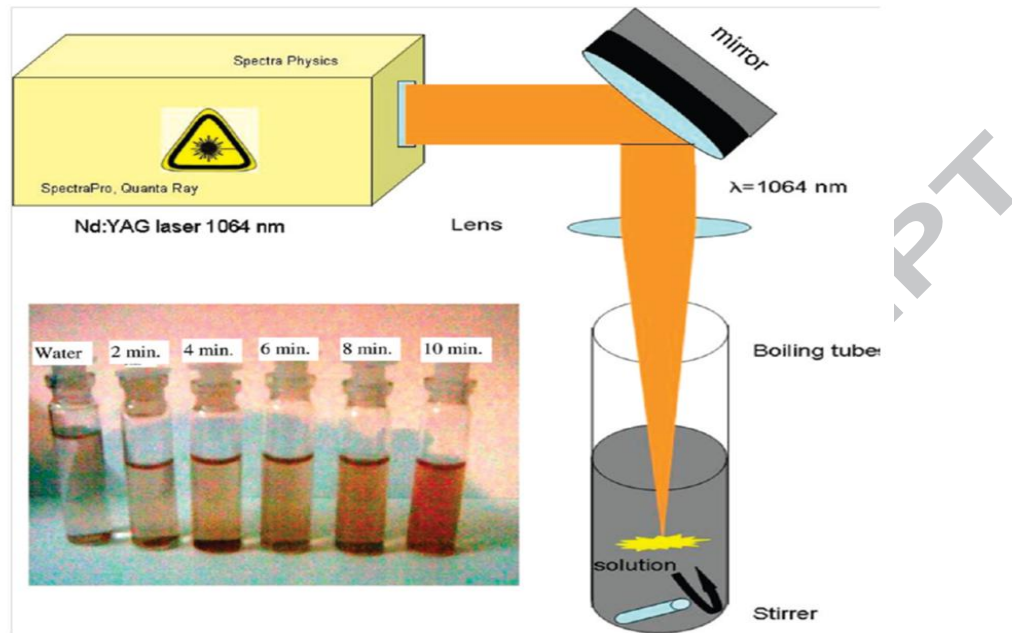


Figure 2. Experimental arrangement and images of colloidal solution of selenium nanoparticles produced after different times of ablation in the inset (from left to right: pure water, 2, 4, 6, 8 and 10 min). [Reprinted with permission from ref. (91), Singh SC, Mishra SK, Srivastava RK, Gopal R. 114, 17374-84, 2010 @ American Chemical Society, 2010].

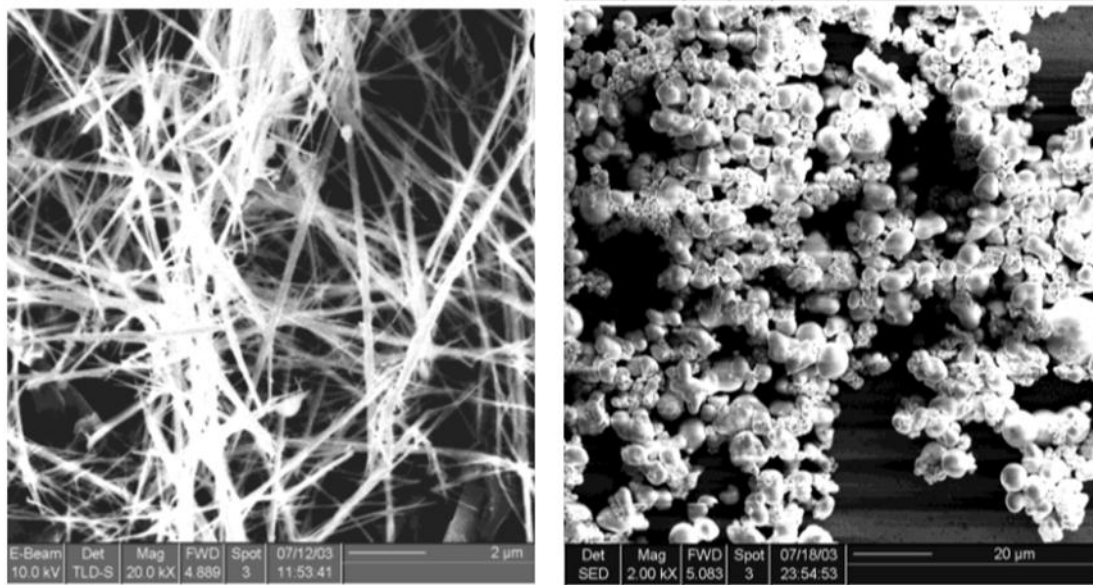


Figure 3. SEM image showing the general morphology of Se nanowires (a) with and (b) without silicon powder. [Reprinted with permission from ref. (109), Ren L, Zhang H, Tan P, Chen Y, Zhang Z, Chang Y, Xu J, Yang F, Yu D, 108, 4627-30, 2004 @ American Chemical Society, 2004]

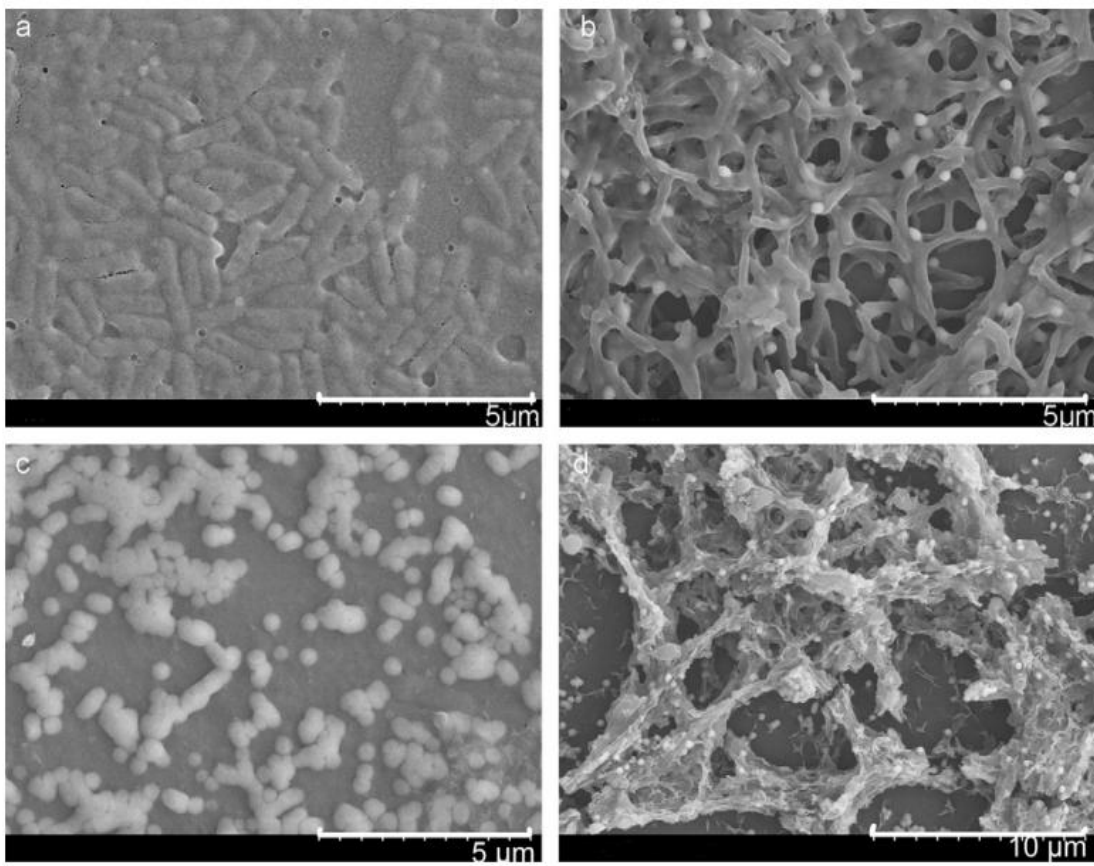


Figure 4. FESEM images of Se nanoparticles at 6 h (a), 12 h (b), 24 h (c) and 48 h (d) after adding selenite pentahydrate into the culture solution of *P. alcaliphila*. [Reprinted with permission from ref. (156), Zhang W, Chen Z, Liua H, Zhangb L, Gao P, Li D. 88: 196-201, 2011, @ Elsevier, 2011].

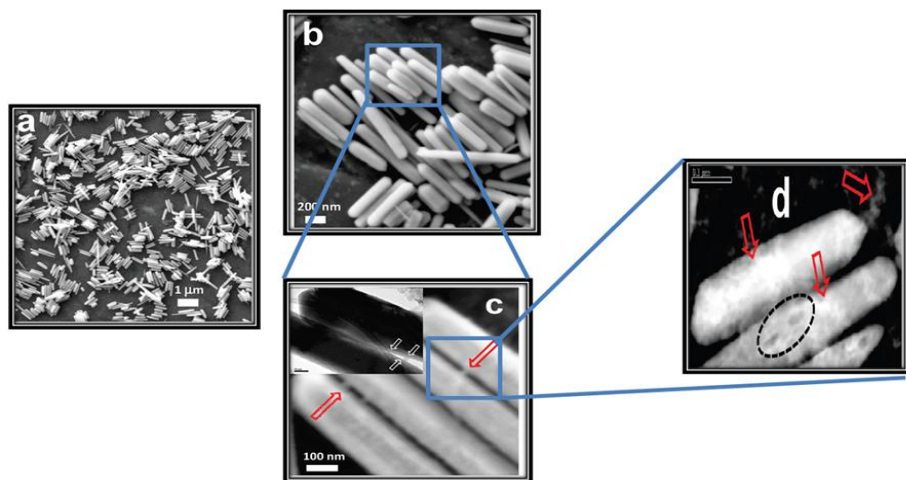


Figure 5. (a) Low-resolution FESEM image of several bundles of NBs. (b) Magnified image of several multifaceted NBs. (c) Zoomed-in image showing surface-adsorbed BSA and the presence of BSA in between the NBs. Inset, dark-field image showing the BSA coating. (d) HAADF image showing bright patches of adsorbed BSA and a few dark patches were created by the exposure to electron beam. [Reprinted with permission from ref. (158a), Kaur G, Iqbal M, Bakshi MS. 113: 13670-76, 2009, @ American Chemical Society, 2009].

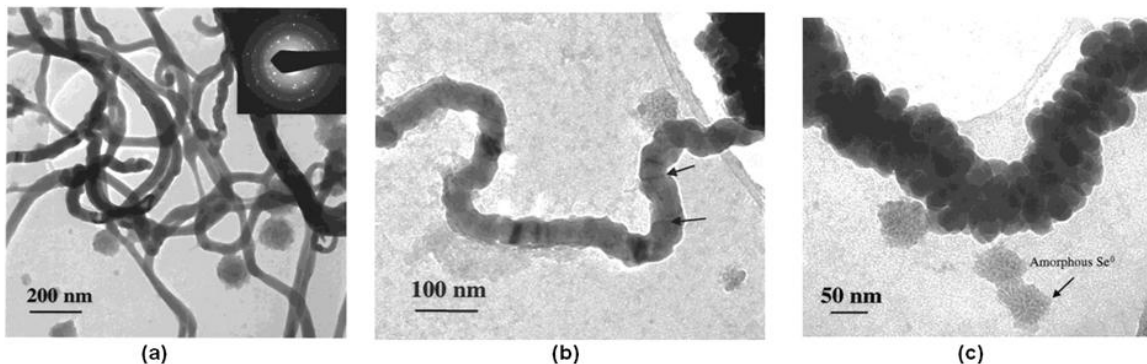


Figure 6. TEM images of monoclinic (red) Se^0 nanowires formed by the reduction of SeO_4^{2-} by cytochrome c_3 . Inset: SAED pattern of Se^0 nanowires. [Reprinted with permission from ref. (164a), Abdelouas A, Gong WL, Lutze W, Shelnutt JA, Franco R, Moura I. 12: 1510-12, 2000; © American Chemical Society, 2000].

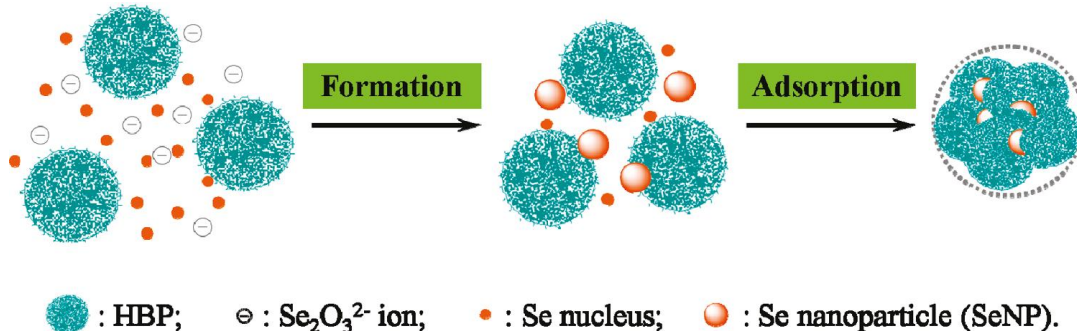


Figure 7. Formation of Se-HBP nanocomposites. [Reprinted with permission from ref. (165), Zhang Y, Wang J, Zhang L. 26:17617-23, 2010; @ American Chemical Society, 2010].

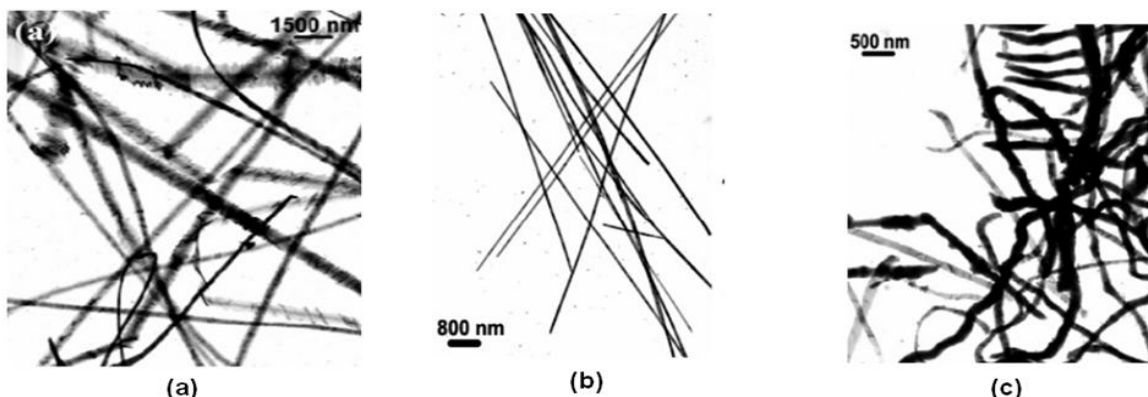


Figure 8. TEM images of the obtained selenium sample prepared using (a) cellulose, (b) sorbitol and (c) polygalacturonic acid as the reducing agent. [Reprinted with permission from ref. (179) Lu Q, Gao F, Komarneni S. 18: 159-63, 2006; @ American Chemical Society, 2006].

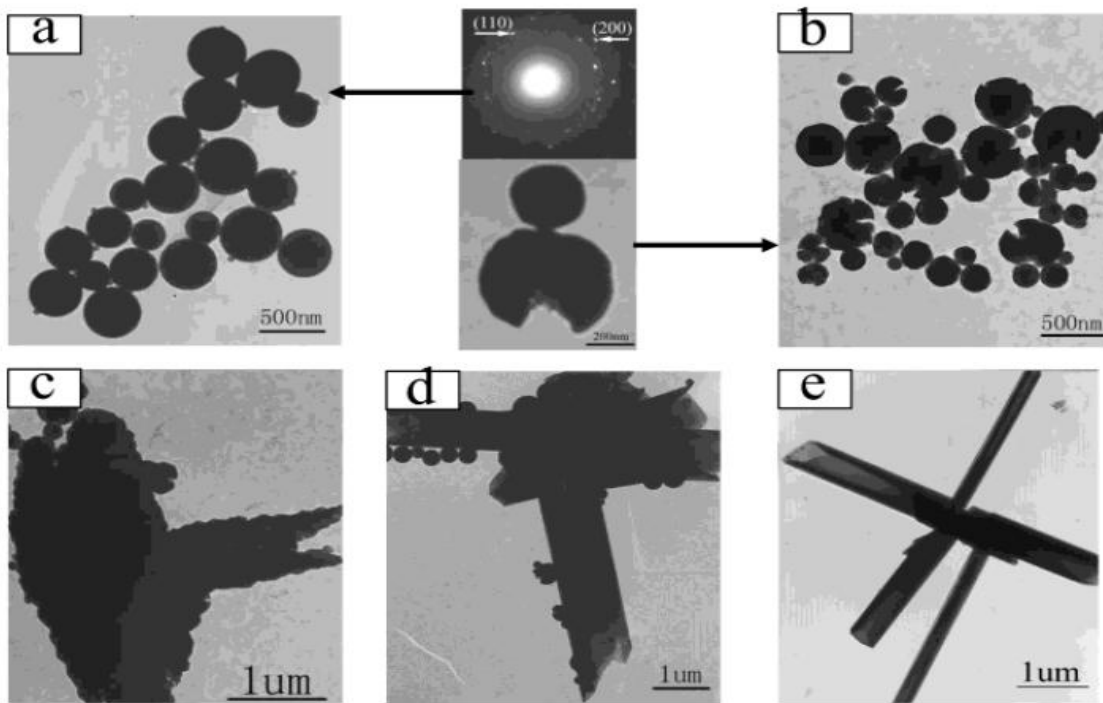


Figure 9. TEM images of Se nanostructures generated by the hydrothermal process for a fixed time of 20 h and the subsequent sonication for different times. [Reprinted with permission from ref. (183) Zhang H, Yang D, Ji Y, Ma X, Xu J, Que D. 108:1179-82, 2004; @ American Chemical Society, 2004].

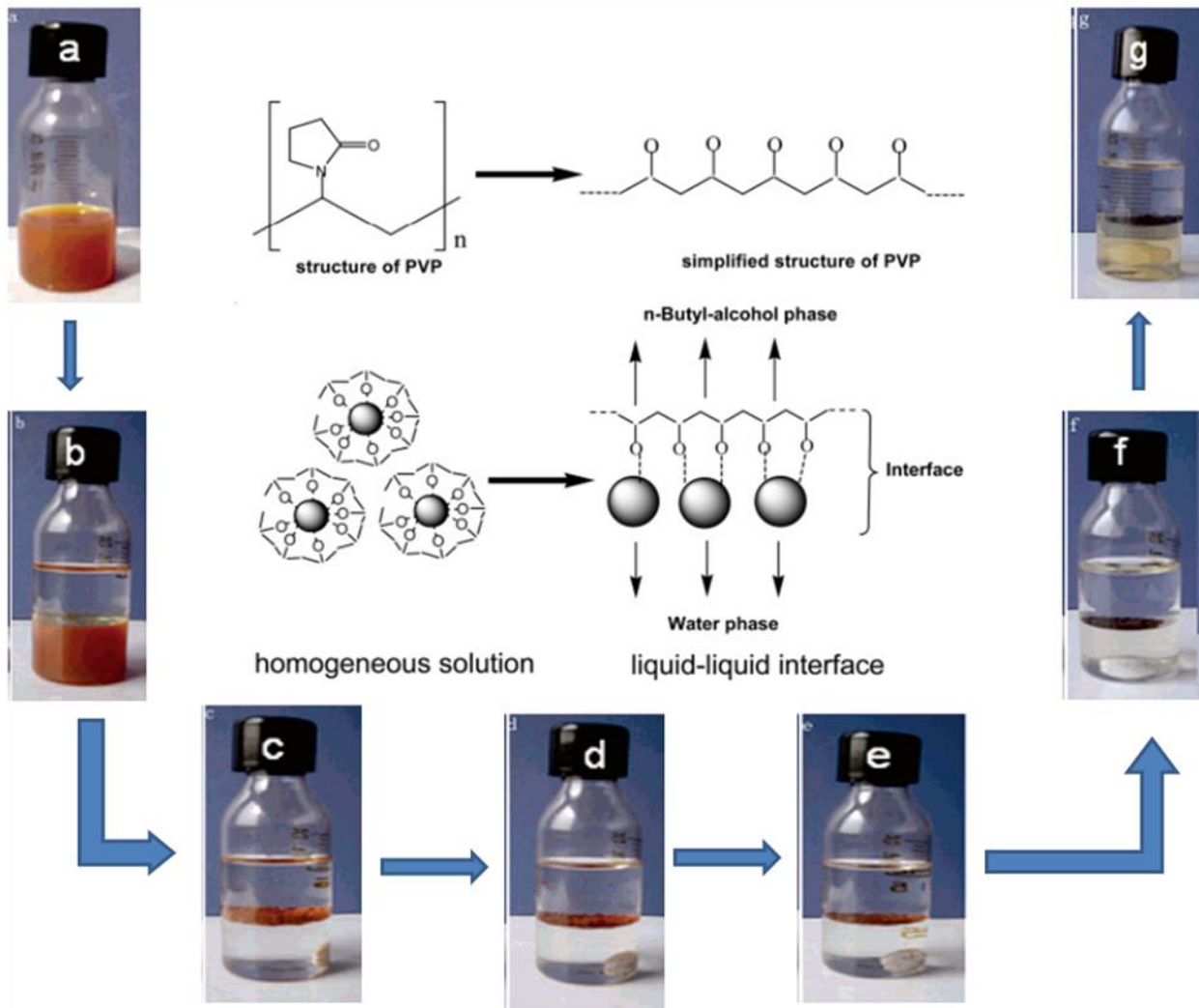


Figure 10. Schematic illustration of the transportation of PVP-stabilized amphiphilic a-Se particles and several typical stages of crystallization of selenium nanorods from a-Se to t-Se on the liquid–liquid interface between water and *n*-butyl alcohol. (a) Initial homogeneous dispersion of amorphous Se solution; (b) adding *n*-butyl alcohol without agitating; (c) after agitating for 10 min and stayed for aging; (d) aging for 30 min; (e) aging for 1 h; (f) aging for 2 h; (g) aging for 12 h. [Reprinted with permission from ref. (239) Song JM, Zhu JH, Yu SH. 110: 23790-95, 2006, @ American Chemical Society, 2006].

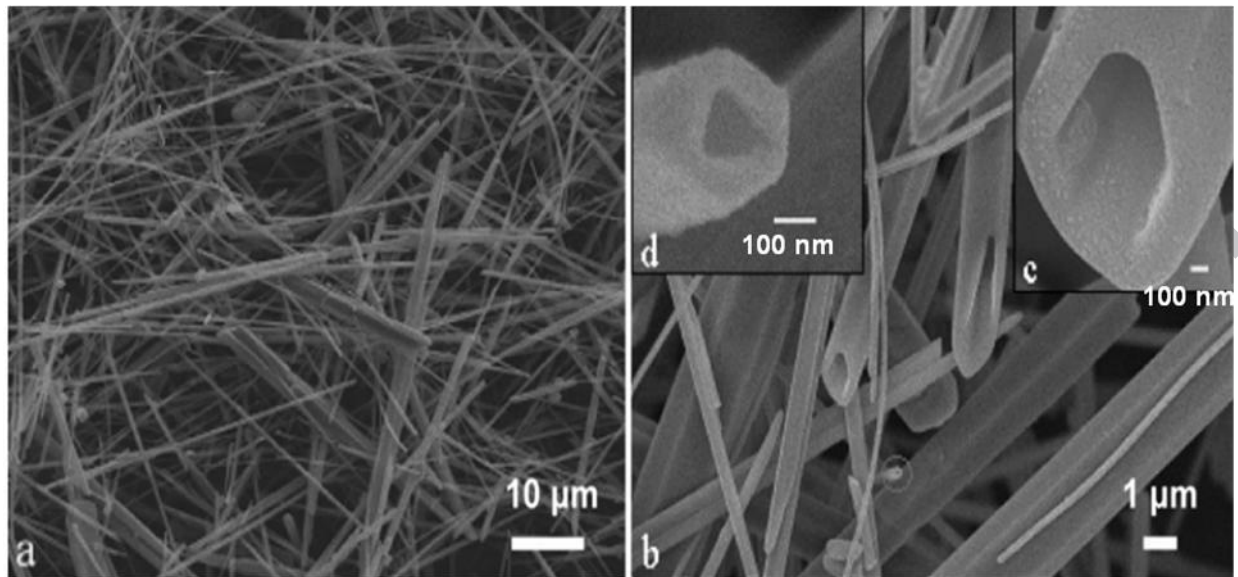


Figure 11. Typical FESEM images of the obtained t-Se sub-microtubes (a) at a low magnification and (b, c, d) high magnification, demonstrating the tubular shape of the Se samples. [Reprinted with permission from ref. (248) Zhang B, Dai W, Ye X, Hou W, Xie Y. 109:22830-35, 2005; @ American Chemical Society, 2005].

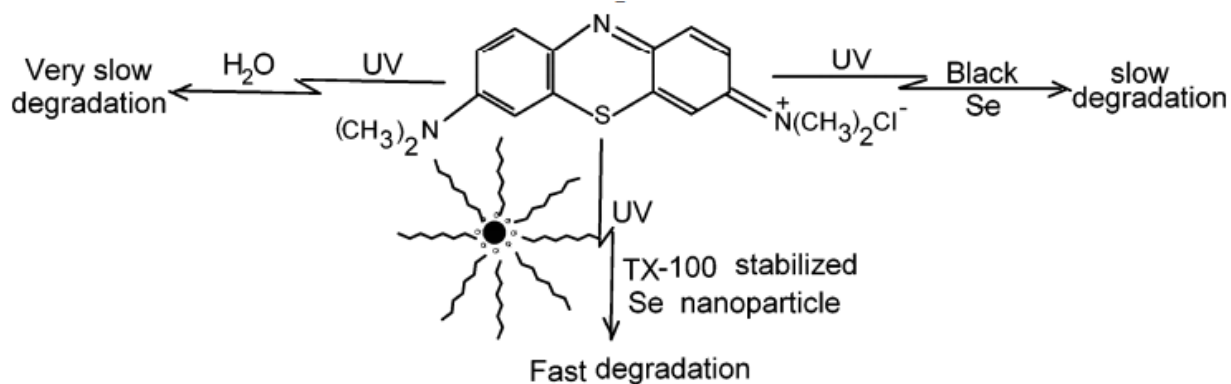


Figure 12. Schematic representation of the degradation of methylene blue in H_2O , Black Se, and TX-100-stabilized Se nanoparticles. [Reprinted with permission from ref. (249) Nath S, Ghosh SK, Panigah S, Thundat T, Pal T. 20:7880-83, 2004; @ American Chemical Society, 2004].

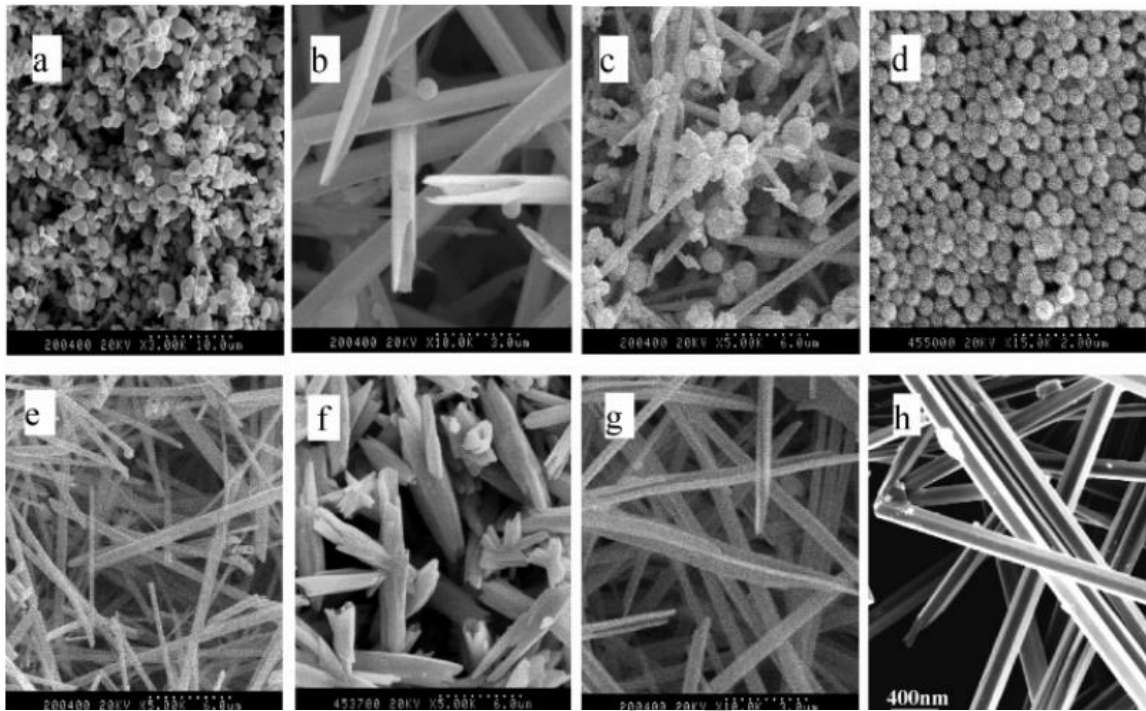


Figure 13. SEM images of the SeNPs obtained under different conditions: (a) without CTAB; (b) in 0.1 M CTAB solution; (c) in solution containing 50% alcohol; (d) in pH 1 solution; (e) in pH 9 solution; (f) the solution aged under ultrasonic irradiation; (g) with a short aging time (1.5 h); (h) Se nanotubes that had been incubated in water for 3 months. [Reprinted with permission from ref. (256) Ma YR, Qi LM, Ma JM, Cheng HM. 16:1023-26,2004; @ WILEY-VCH , 2004].

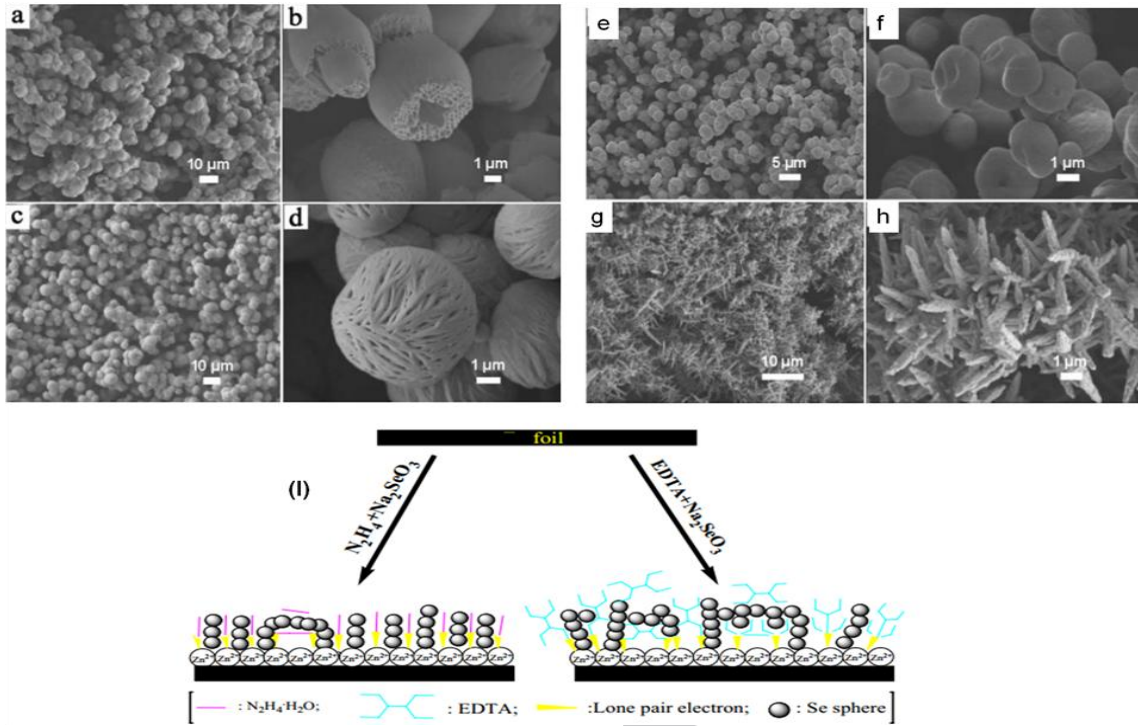


Figure 14. Representative SEM images and schematic growth progression of t-Se samples prepared with (a–d) Zn foil and (e–h) Ni foil. [Reprinted with permission from ref. (275) Zhang B, Ye X, Wang C, Xie Y. 17:2706-12, 2007; @ RSC, 2007].

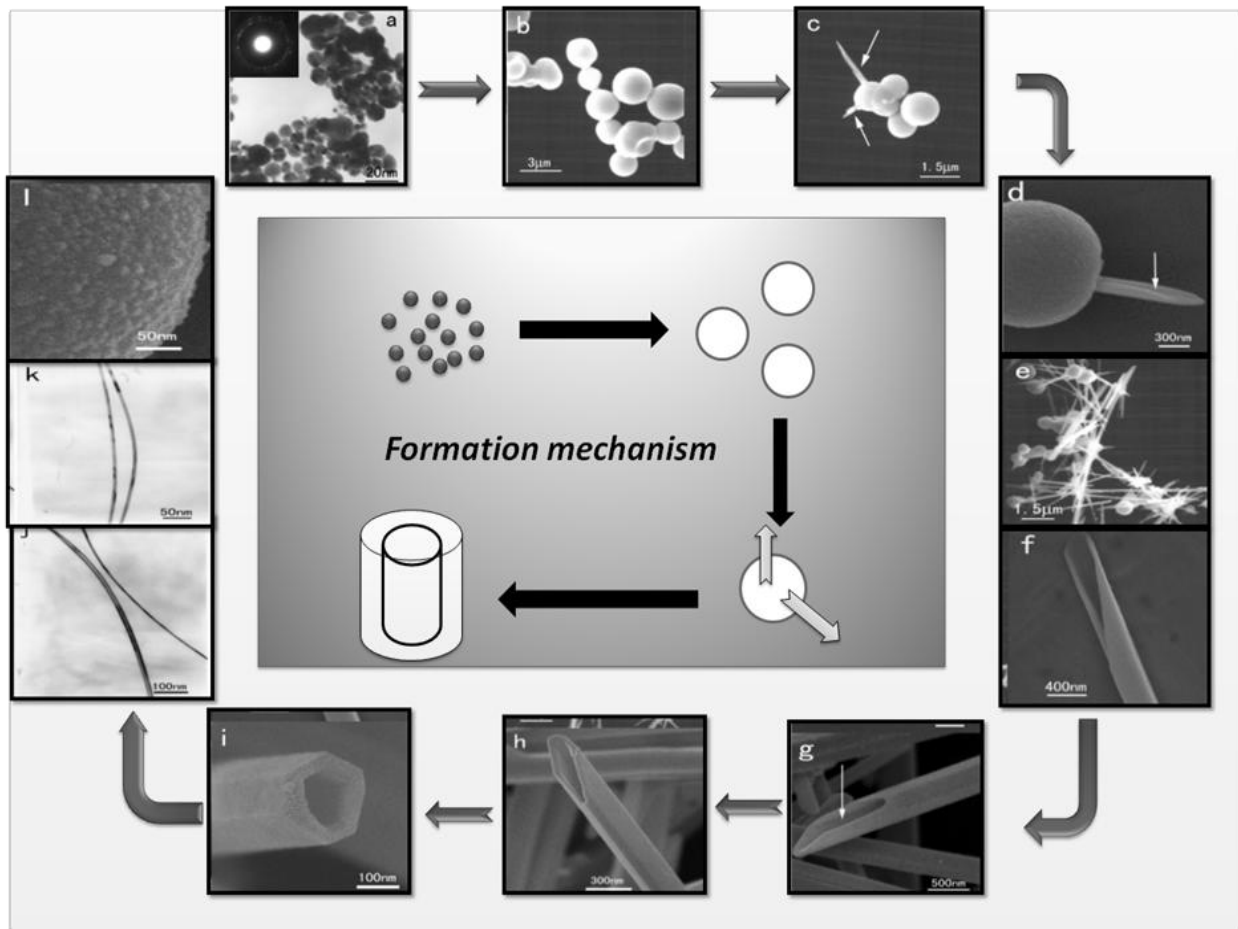


Figure 15. SEM images and formation of t-selenium nanotubes prepared at various time intervals: (a) 2 h, (b) 4 h, (c and d) 8 h, (e and f) 14 h, (g) 17 h, (h) 20 h and (i) 25 h. (j and k) t-selenium nanowires synthesized with PVP as surfactant. (l) Surface morphology of the t-selenium microspheres. [Reprinted with permission from ref. (279) Xi G, Xiong K, Zhao Q, Zhang R, Zhang H, Qian Y. 6: 577-82, 2006; @ American Chemical Society, 2006].

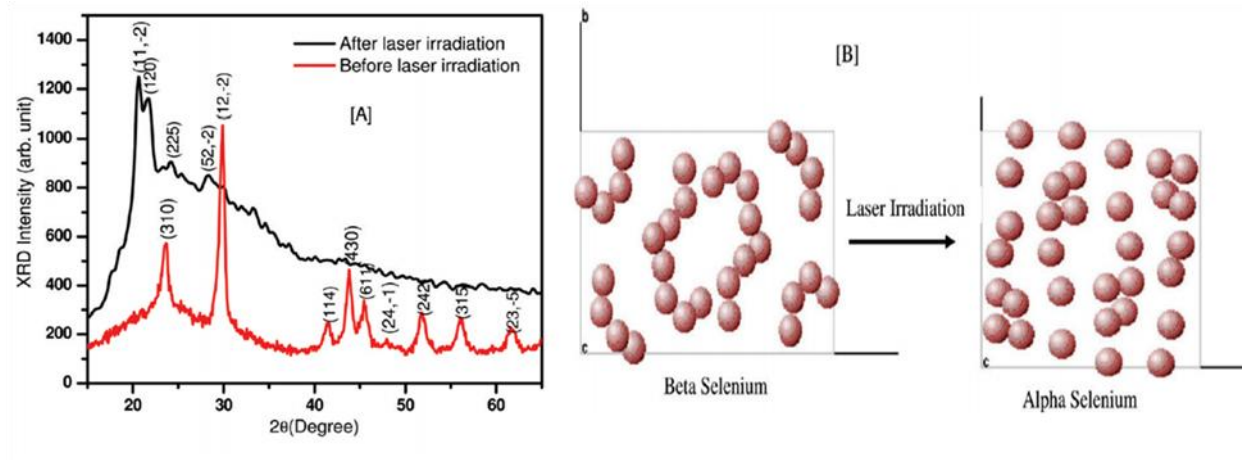


Figure 16. (A) XRD pattern and (B) schematic of the atomic arrangement of selenium nanoparticles before and after laser irradiation. [Reprinted with permission from ref. (91), Singh SC, Mishra SK, Srivastava RK, Gopal R. 114, 17374-84, 2010 @ American Chemical Society, 2010].

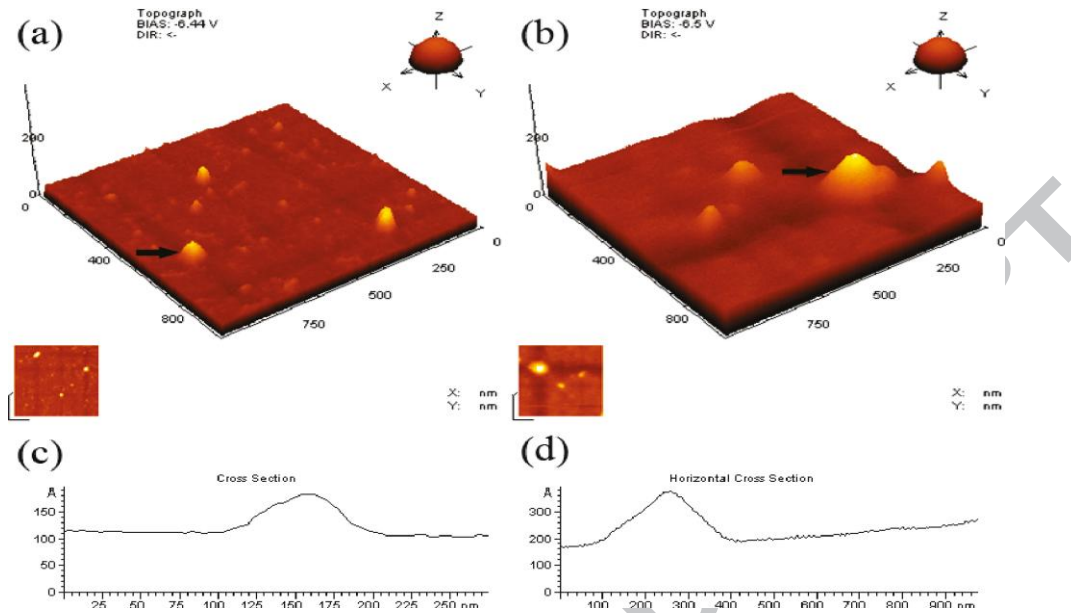


Figure 17. Three-dimensional AFM images of HBP (a) and Se-HBP (b); bird's-eye view is shown in the lower left corner. The corresponding heights of the arrow-marked particle are shown in (c) and (d). [Reprinted with permission from ref. (165) Zhang Y, Wang J, Zhang L. 26:17617-23, 2010; @ American Chemical Society, 2010].

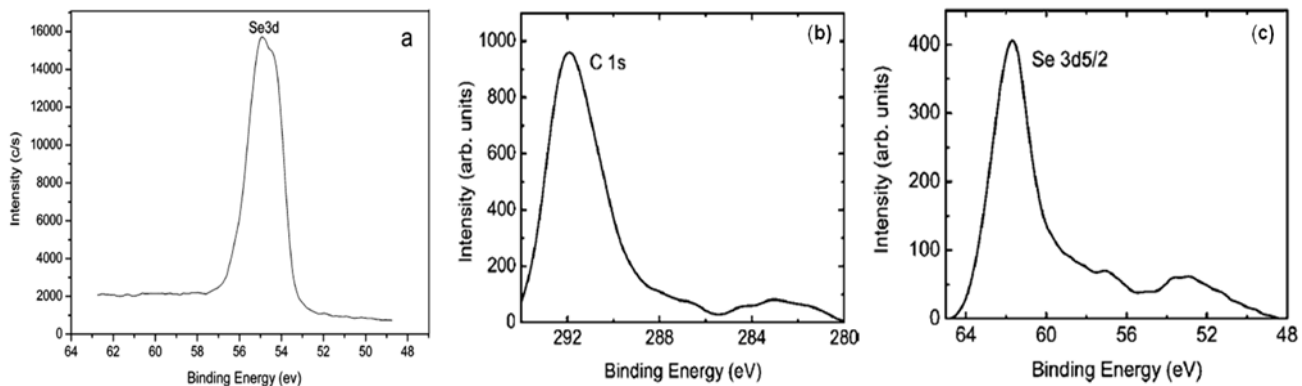


Figure 18. XPS spectra of the Se-CNT samples in (a) C 1s and (b) Se 3d_{5/2} core region. [Reprinted with permission from ref. (295) Rodrigues OED, Saraiva GD, Nascimento RO, Barros EB, Filho JM, Kim YA, Muramatsu H, Endo M, Terrones M, Dresselhaus MS, Souza Filho AG. 8: 3651-55, 2008; @ American Chemical Society, 2008].

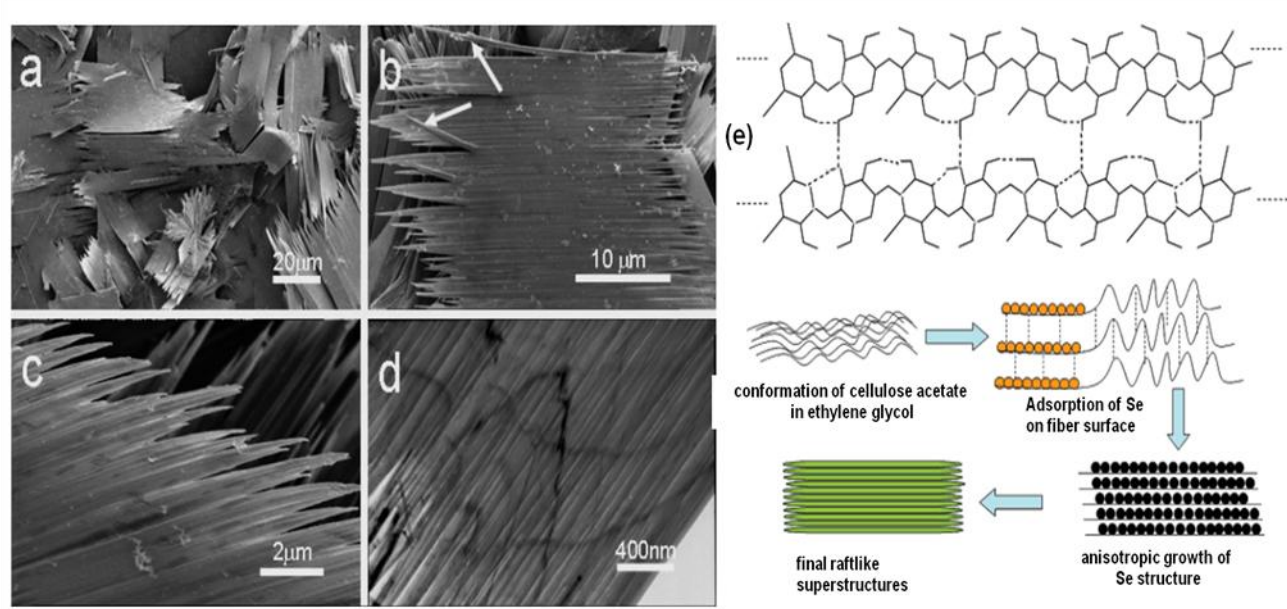


Figure 19. (a–c) FESEM and (d) TEM images and (e) schematic representation of the raft-like t-Se nanoparticle formation. [Reprinted with permission from ref. (296) Song JM, Zhan YJ, Xu AW, Yu SH. 23: 7321-27, 2007; @ American Chemical Society, 2007].

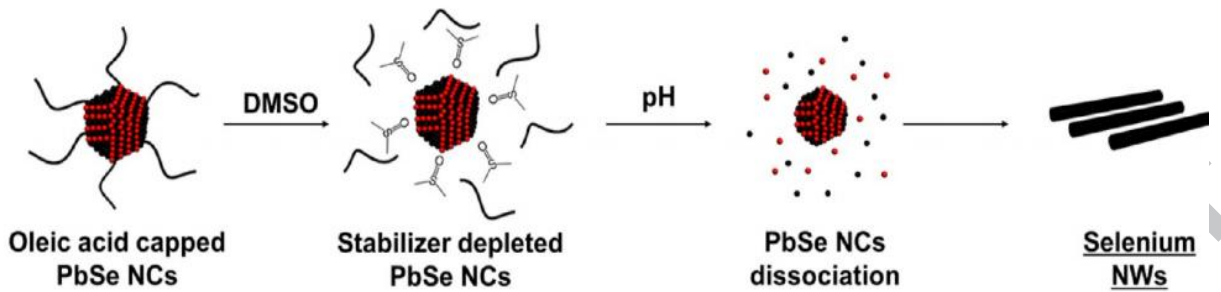


Figure 20. Process of transformation of PbSe NCs into crystalline Se nanowires. [Reprinted with permission from ref. (300) Kim WD, Baum F, Kim D, Lee K, Moon JH, Lee DC, 14:1258–1263, 2014; @ American Chemical Society, 2014].

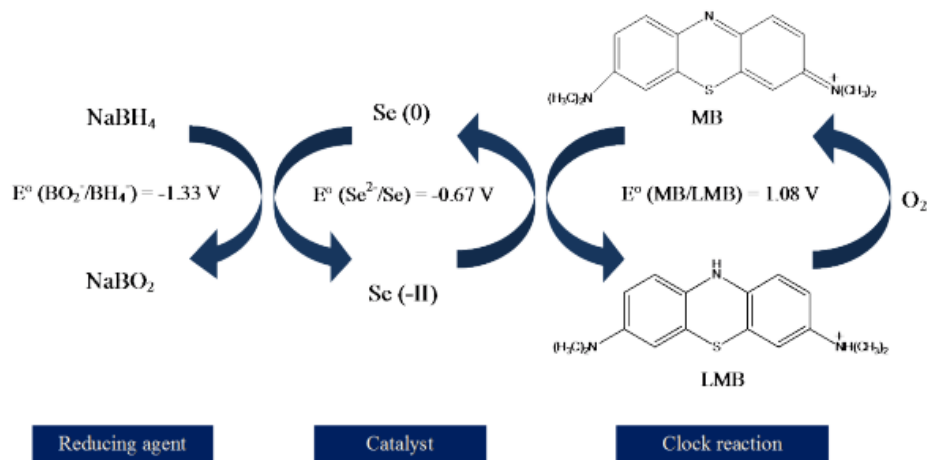
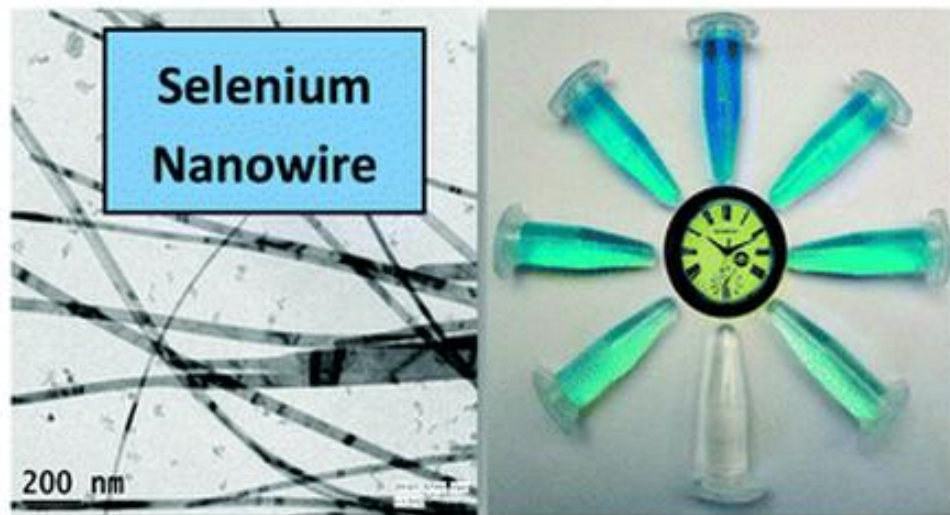


Figure 21. Influence of Se nanowires as a catalyst for clock reaction. [Reprinted with permission from ref. (194) Ray C, Dutta S, Sarkar S, Sahoo R, Roy A, Pal T, 3:24313-24320, 2013; @ RSC, 2013].

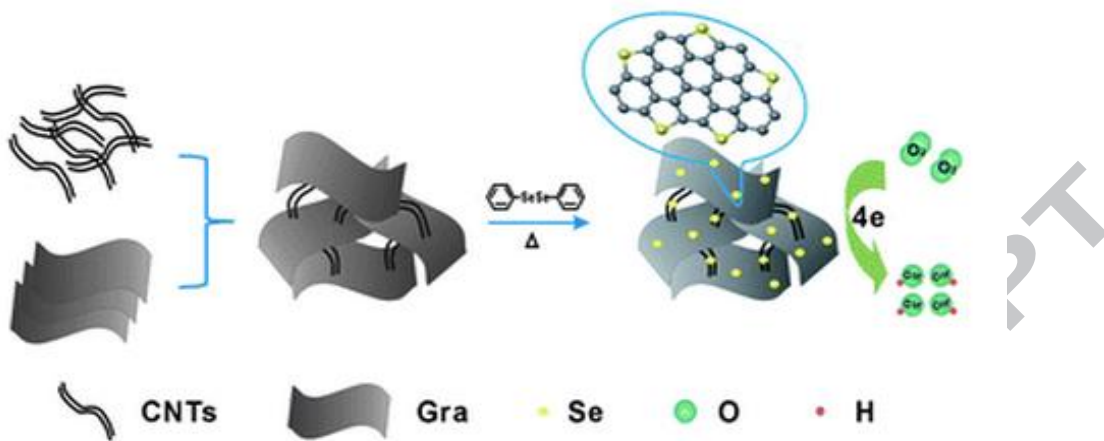


Figure 22. Nanocomposites of Se with CNTs for improving the ORR catalytic activity. [Reprinted with permission from ref. (314) Jin ZP, Nie HG, Yang Z, Zhang J, Liu Z, Xu XJ, Huang SM, 4, 6455, 2012; © RSC, 2012].

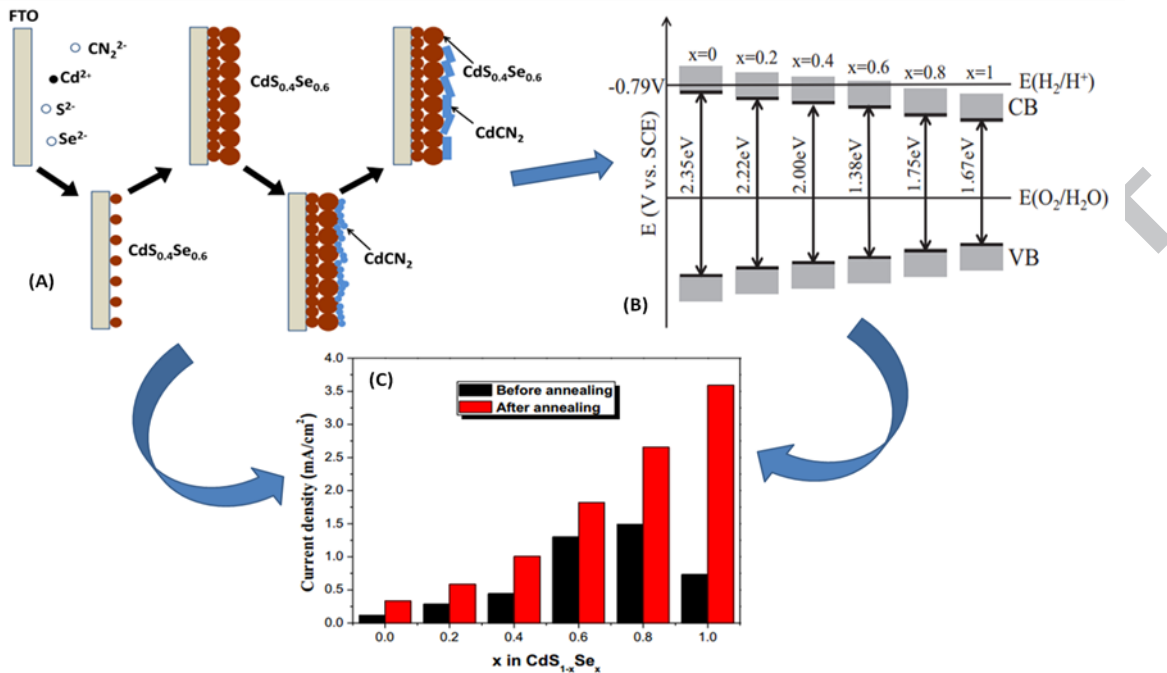


Figure 23. (A) Schematic illustration of the growth, (B) band potential and (c) current density of $\text{CdS}_{0.4}\text{Se}_{0.6}$ thin nanofilms. [Reprinted with permission from ref. (324) Zhang J, Zhang S, Zhang H, Zhang Y, Zheng Z, Xiang Y, 122:306–308, 2014; @ Elsevier, 2014].

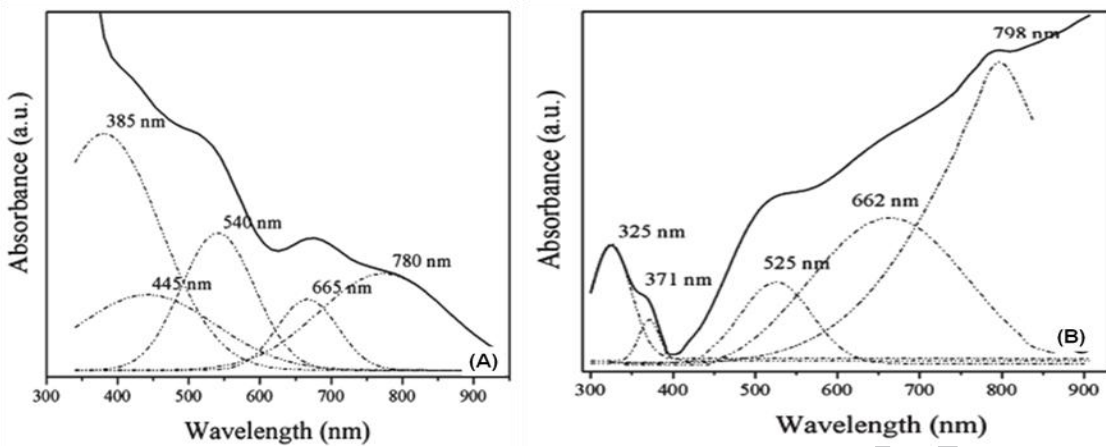


Figure 24. UV and Raman spectra of selenium nanoparticles synthesized by different methods. (A) Nanotubes and (B) bulk selenium source. [Reprinted with permission from ref. (326), E. Filippo, D. Manno, and A. Serra, Cryst. Growth 10, 4890 (2010) @ 2010 American Chemical Society].

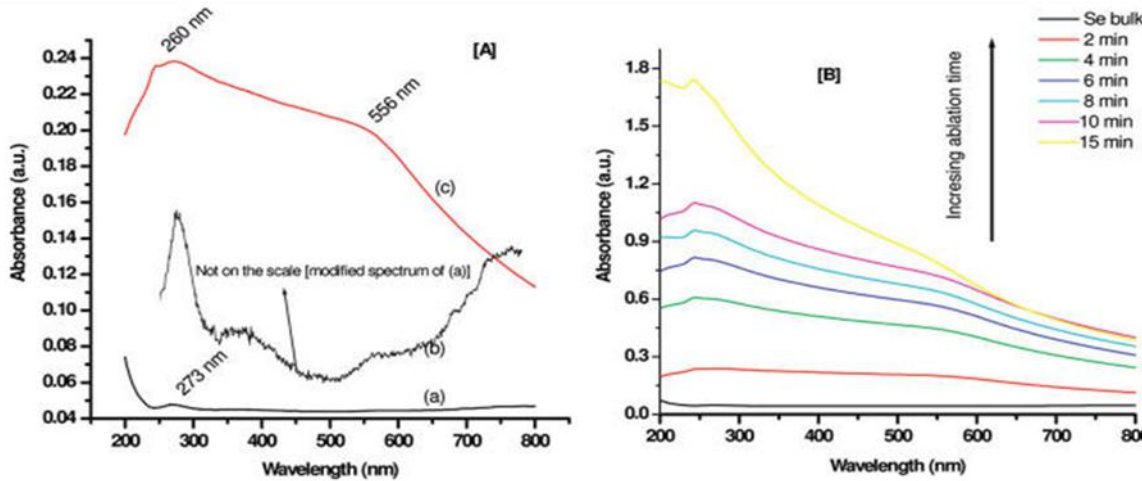


Figure 25. (A and B) UV–Visible spectra of selenium nanospheres synthesized using laser irradiation. [Reprinted with permission from ref. (91), Singh SC, Mishra SK, Srivastava RK, Gopal R. 114, 17374-84, 2010 @ American Chemical Society, 2010].

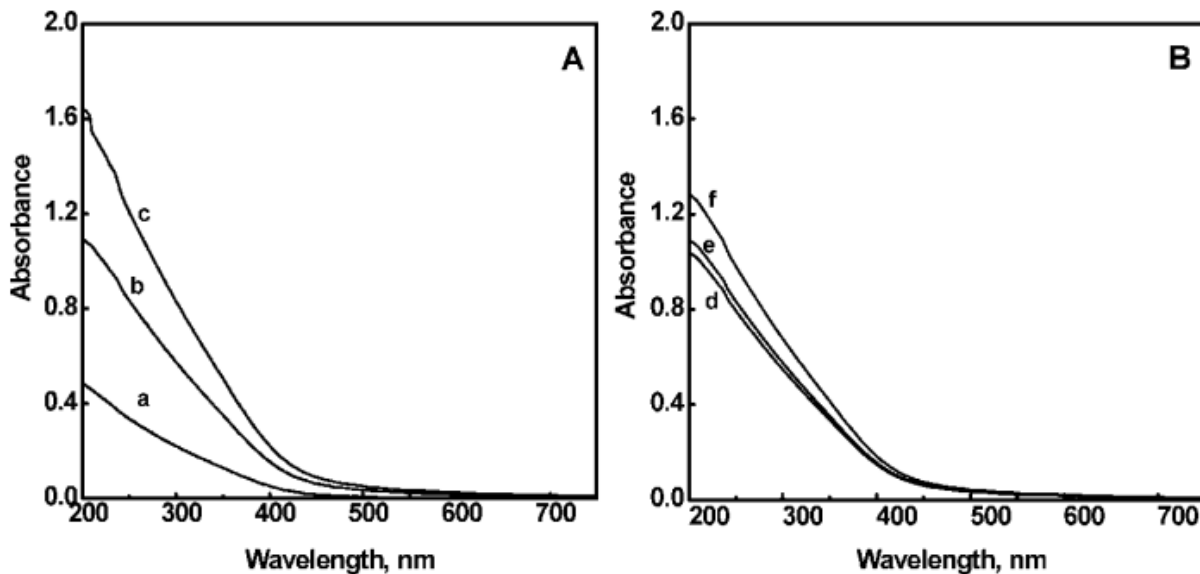


Figure 26. Effect of (A) sodium selenosulphate concentration (a) 5×10^{-4} , (b) 1×10^{-3} and (c) $1.5 \times 10^{-3} \text{ mol dm}^{-3}$, in the presence of 0.05% PVA, and of (B) PVA concentration (d) 0.025%, (e) 0.050% and (f) 0.075%, in the presence of $1.0 \times 10^{-3} \text{ mol dm}^{-3}$ of sodium selenosulphate, on the optical absorption spectrum of selenium nanoparticle sols, prepared in the presence of $9.0 \times 10^{-2} \text{ mol dm}^{-3}$ acrylonitrile. [Reprinted with permission from ref. (278) Shah CP, Kumar M, Pushpa KK, Bajaj PN. 8:4159-64, 2008; @ American Chemical Society, 2008].

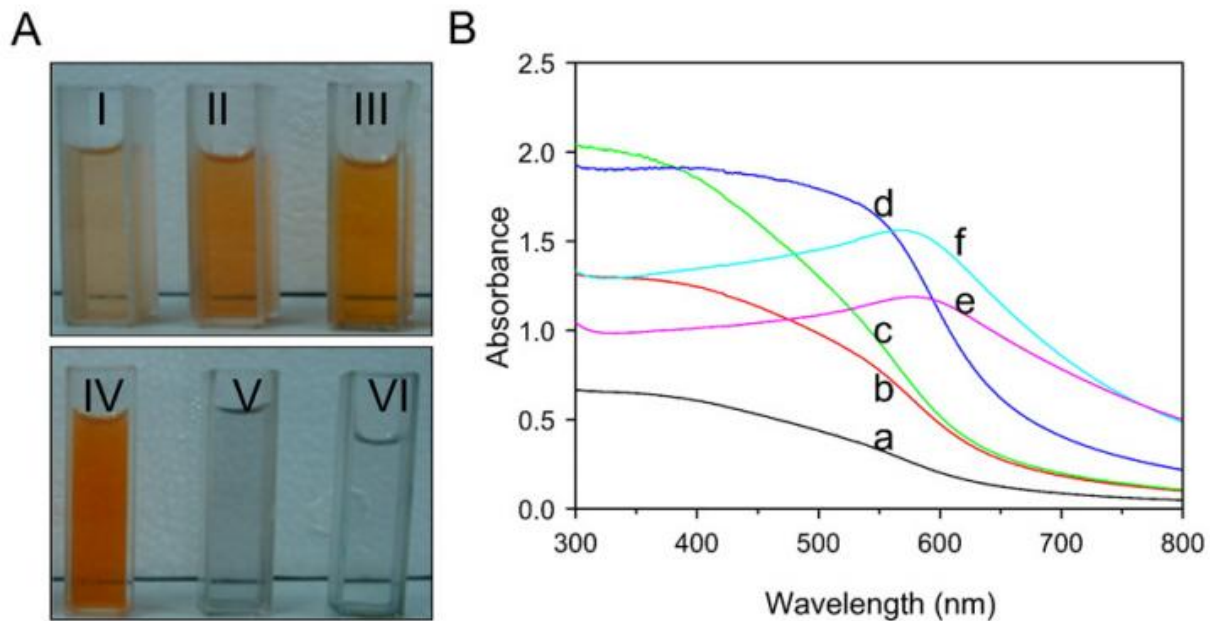


Figure 27. Changes in colours (A) and UV–Visible spectra (B) of nano-Se solutions with different reactant concentration ratios of L-cysteine to Na_2SeO_3 . [Reprinted with permission from ref. (332) Li Q, Chen T, Yang F, Liu J, Zheng W. 64: 614-17, 2010; @ Elsevier, 2010].

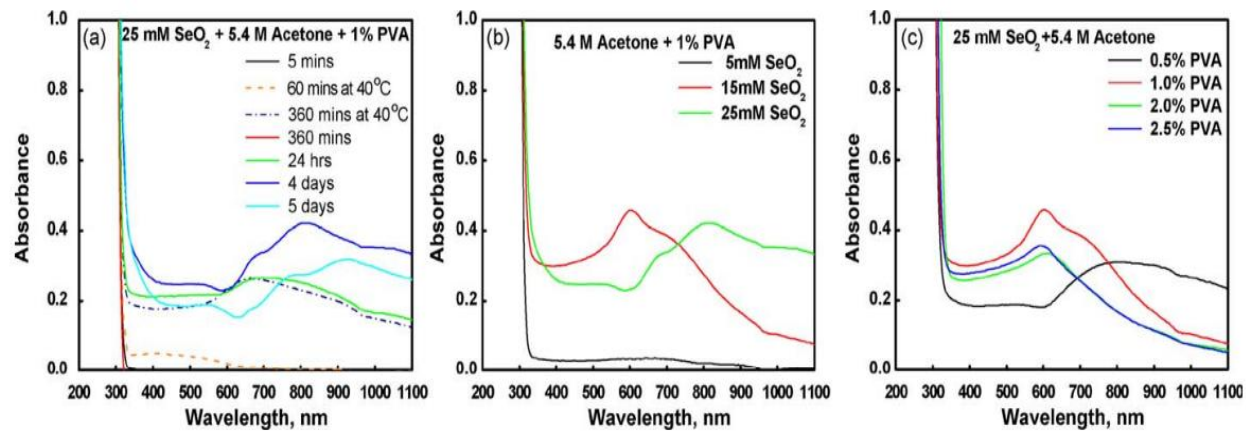


Figure 28. Effect of (a) reaction time, (b) selenium dioxide concentration and (c) PVA concentration on the UV–Visible absorption spectra of the aqueous selenium sols formed by the reaction of selenium dioxide with acetone, in the presence of PVA. [Reprinted with permission from ref. (232) Shah CP, Dwivedi C, Singh KK, Kumar M, Bajaj PN. Mater Res Bull 45: 1213-17. 2010; @ Elsevier, 2010].

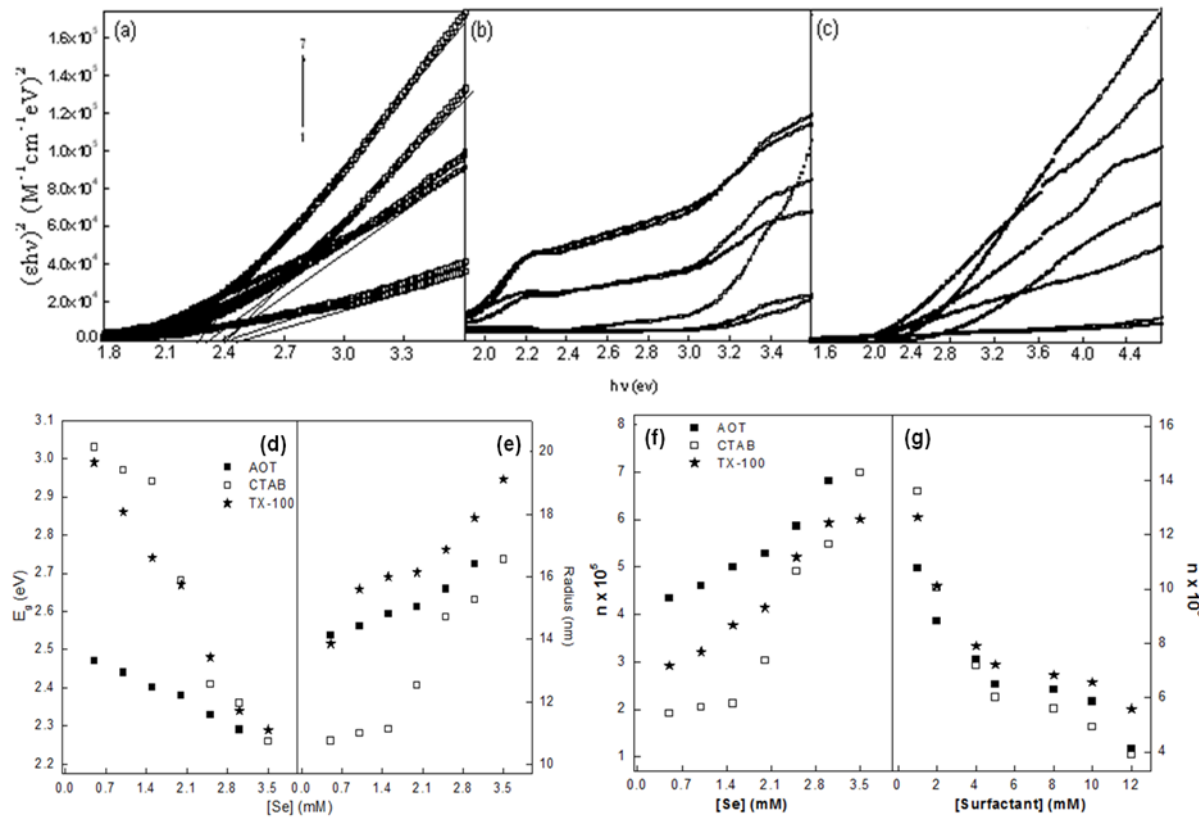


Figure 29. Tauc plot for the determination of band gap of Se (1) 0.5, (2) 1.0, (3) 1.5, (4) 2.0, (5) 2.5, (6) 3.0 and (7) 3.5 mM in 10.0 mM aqueous solution of (a) AOT, (b) CTAB and (c) TX-100. Dependence of (d) optical band gap (E_g) and (e) radius of nanoparticles on [Se] in AOT, CTAB and TX-100 micellar media. The variation of agglomeration number, n as a function of (f) [selenium] and (g) [surfactant] in AOT, CTAB and TX-100 micellar media. [Reprinted with permission from ref. (201) Mehta SK, Chaudhary S, Kumar S, Bhasin KK, Torigoe K, Sakai H, Abe M. 19: 295601-12, 2008; @ IOPscience, 2008].

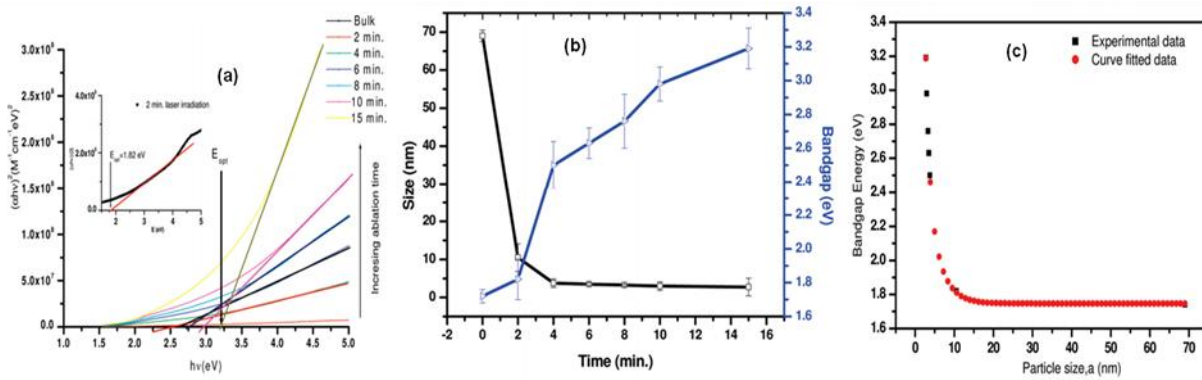


Figure 30. (a) Tauc plots of UV–Visible spectra for different times of ablation from 0 to 15 min for the calculation of band gap energy. The inset shows the Tauc plot corresponding to 2 min of laser irradiation for clarity. (b) Variation of band gap energy and size of the Se particles with ablation time. (c) Experimental and curve-fitted data points of band gap energy of Se QDs with size. [Reprinted with permission from ref. (91), Singh SC, Mishra SK, Srivastava RK, Gopal R. 114, 17374-84, 2010 @ American Chemical Society, 2010].

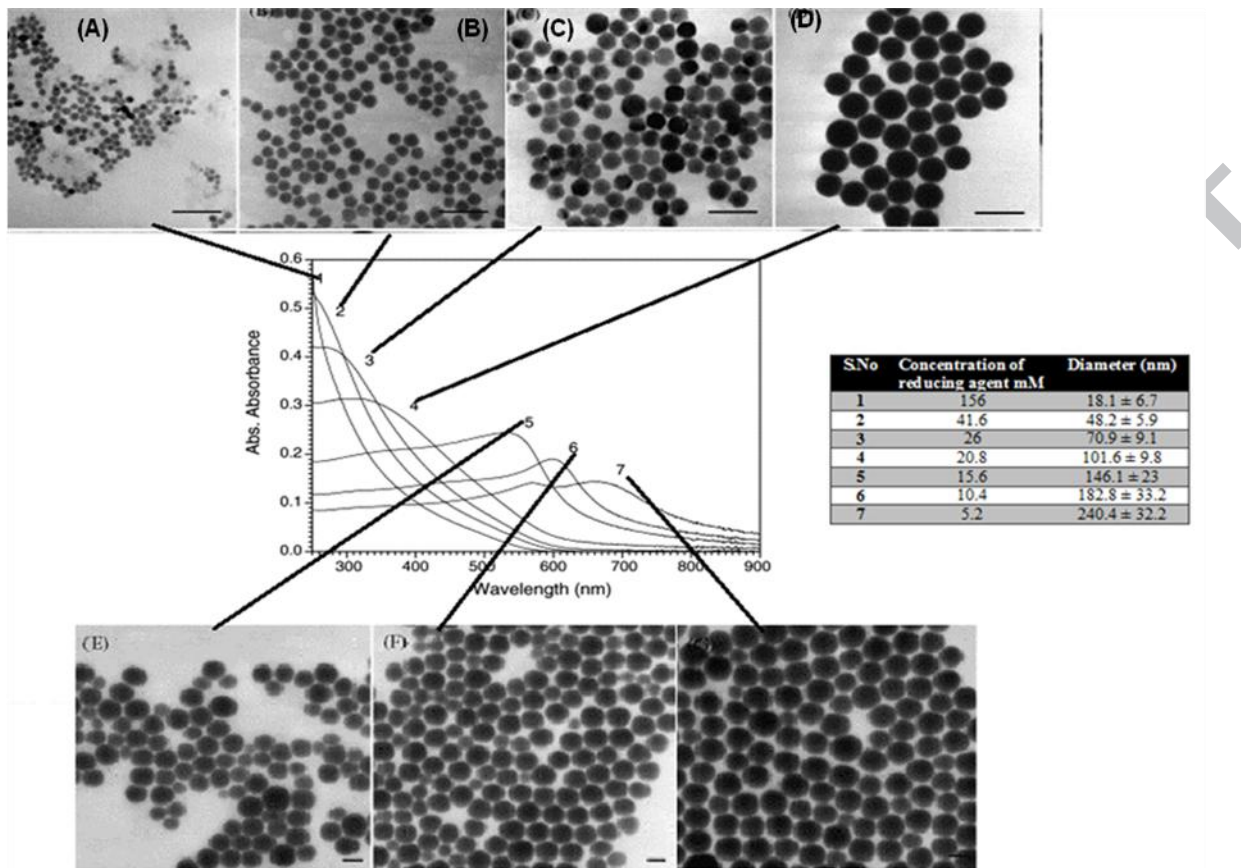


Figure 31. TEM images and the corresponding UV–Vis spectra of selenium nanoparticles in different concentrations of sodium thiosulphate. The inset table shows the concentration of reducing agents and the corresponding diameter of the obtained particles. [Reprinted with permission from ref. (338), Lin ZH, Wang CRC. 92: 591-94, 2005; @ Elsevier, 2005].

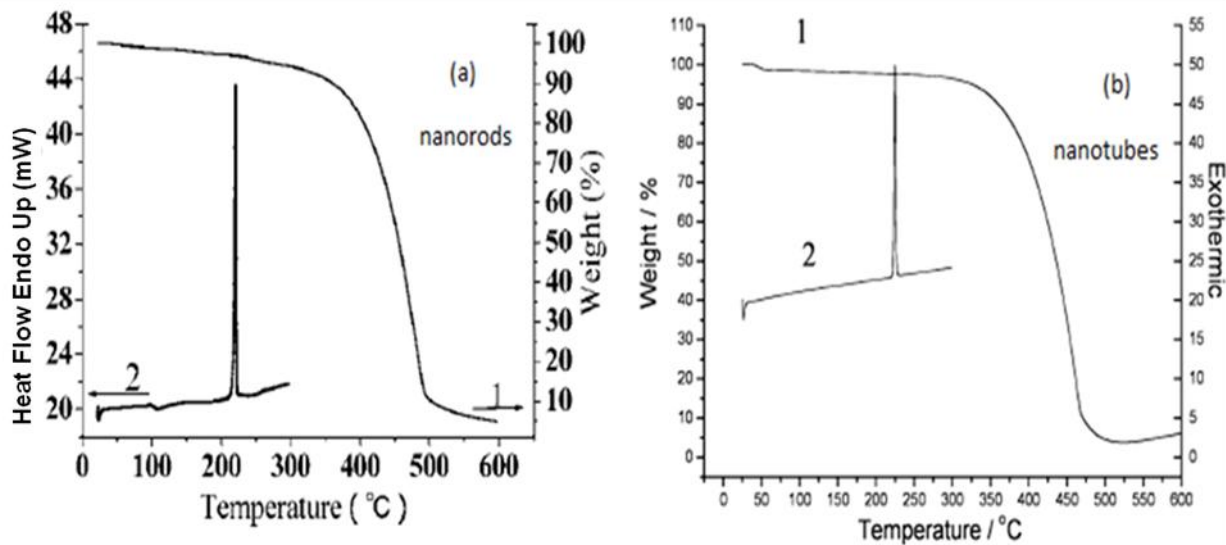


Figure 32. TGA (1)/DSC (2) curves of the (a) selenium nanorods and (b) nanotubes. [Reprinted with permission from ref. (159), Chen Z, Shen Y, Xie A, Zhu J, Wu Z, Huang F. 9: 1327-33, 2009; © American Chemical Society, 2009].

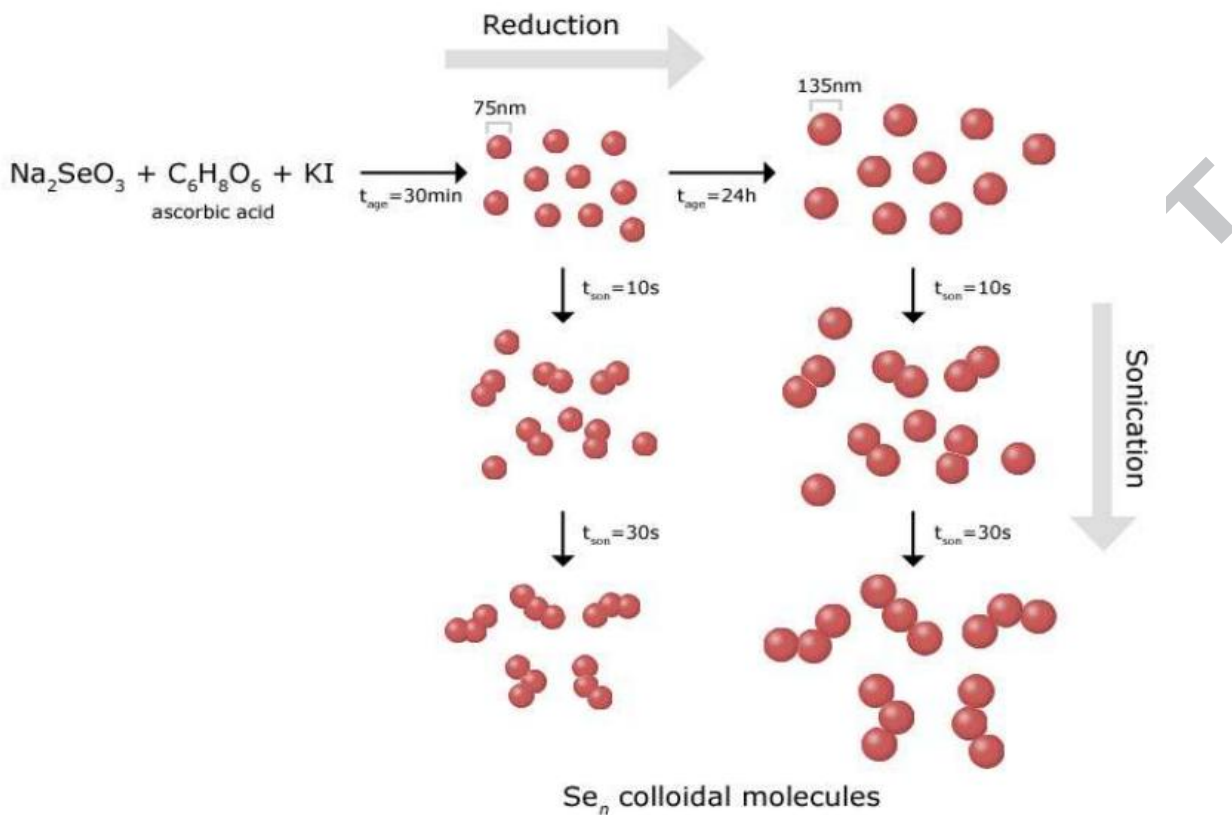


Figure 33. Schematic representation of the pathways for the preparation of Se colloidal aggregates. [Reprinted with permission from ref. (343), Ng CHB, Fan WY, 2014; 30: 7313-18, 2014 @ American Chemical Society, 2014].

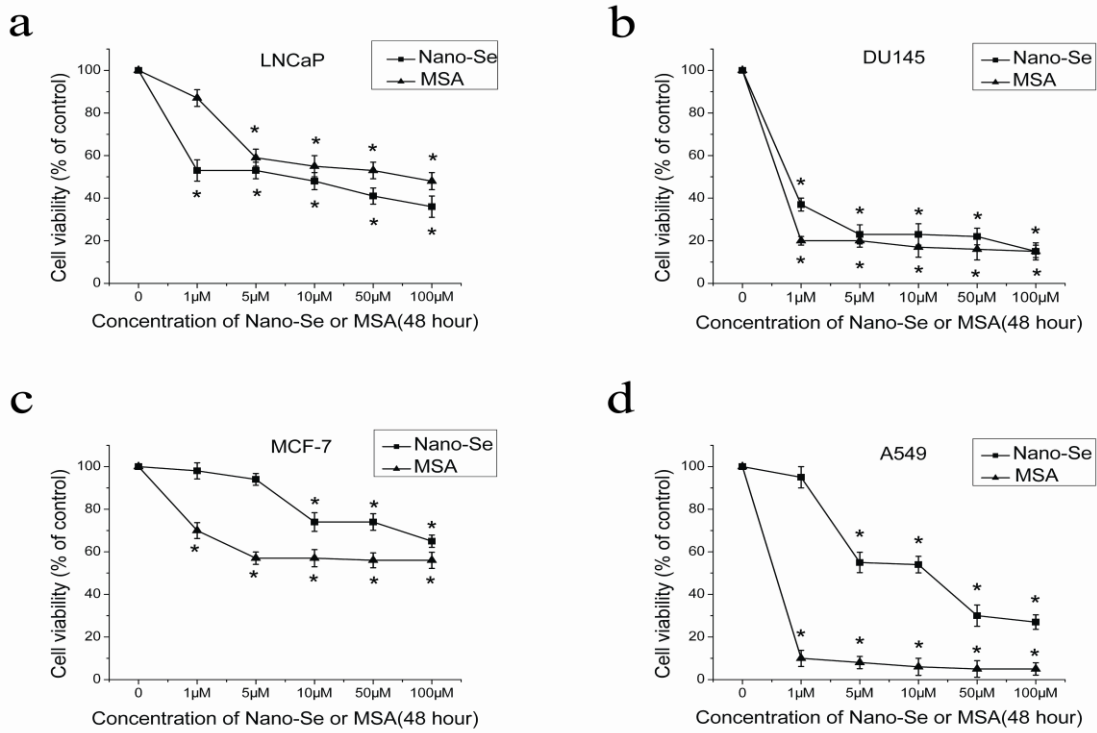


Figure 34: Growth suppression of human cancer cell lines by nano-Se and MSA. LNCaP (**A**), DU145 (**B**), MCF-7 (**C**) and A549 (**D**) cells were treated with nano-Se or MSA (0–100 μ M) for 48 h. Data were shown as mean \pm standard error from three independent experiments. * denotes $p < 0.05$. [Reprinted with permission from ref. (357), Kong L, Yuan Q, Zhu H, Li Y, Guo Q, Wang Q, Bi X, Gao X. 32: 6515-22, 2011; @ Elsevier, 2011].

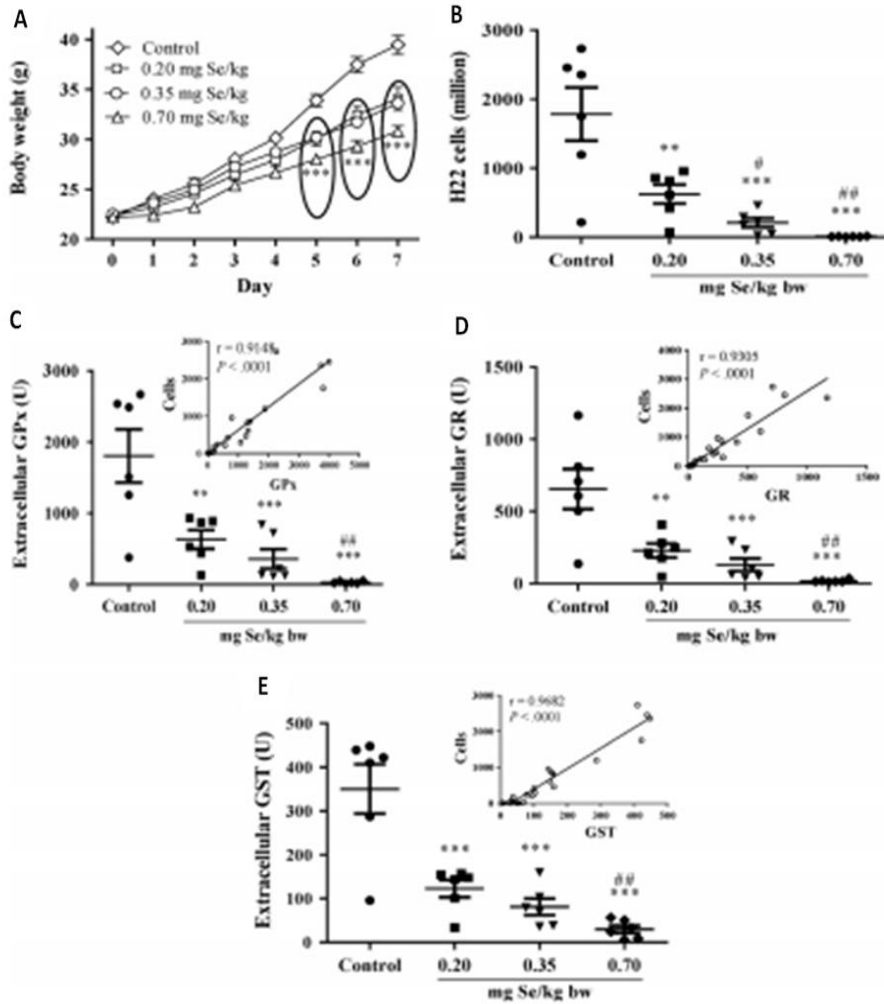


Figure 35: Dose effect of Se nanoparticles administered intraperitoneally on H22 cell proliferation. Mice ($n = 6$ /group) were intraperitoneally inoculated with 2 million H22 cells only once on day 0, and at 1-h post-inoculation, Se nanoparticles were administered intraperitoneally at the indicated doses once daily for seven consecutive days. (A) Body weight. (B) H22 cell number. (C–E) Extracellular total activity of GPx, GR and GST, respectively, in the peritoneal cavity and their correlations with H22 cells. [Reprinted with permission from ref. (365), Wang X, Sun K, Tan Y, Wu S, Zhang J, 72:1-10, 2014; @ Elsevier, 2014].

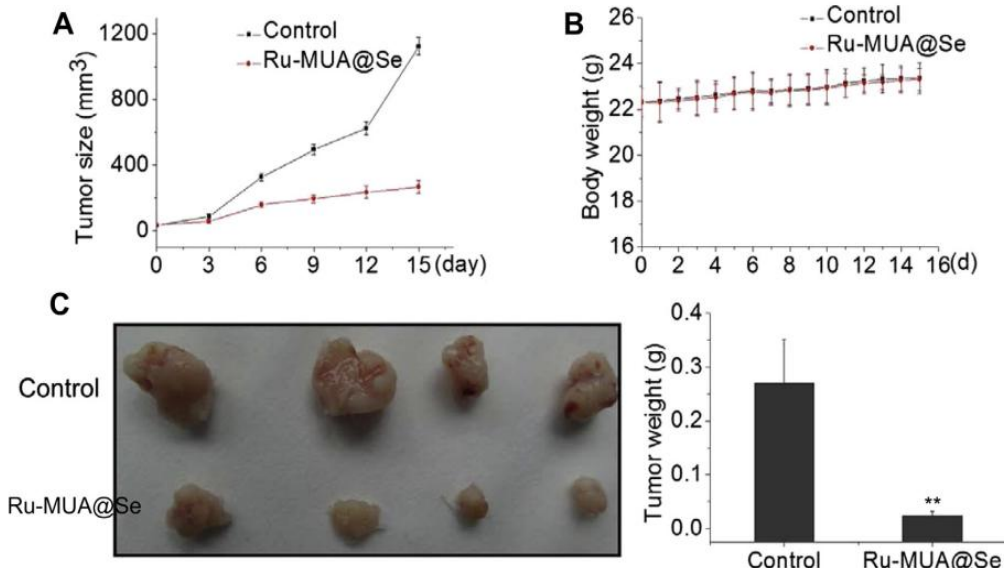


Figure 36. Inhibition of tumour growth by Ru-MUA@Se in vivo. HepG2 cells were injected s.c. (1×10^7 cells per mouse) into the 5- to 6-week-old SCID male mice. After the tumours had been established ($\sim 50 \text{ mm}^3$), the mice were injected with or without 3 mg/kg/day of Ru-MUA@Se. After 2 weeks, the mice were sacrificed and tumours were removed, whose images are captured by a high-resolution camera. (A) tumour size of the control and treated groups; (B) the average mouse body weight of the control and treated groups; (C) tumours of the mice from Ru-MUA@Se-treated group were significantly smaller than those of the control group. [Reprinted with permission from ref. (367), Sun D, Liu Y, Yu Q, Qin X, Yang L, Zhou Y, Chen L, Liu J, 35:1572-1583, 2014; @ Elsevier, 2014].

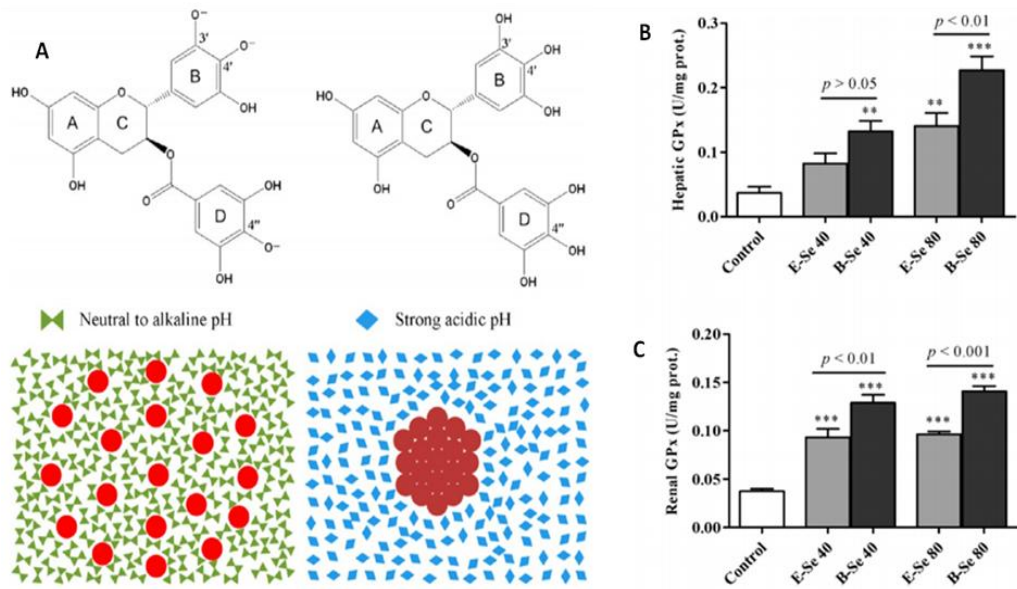


Figure 37: (A) Schematic illustration of the formation of E-Se at different pH values. Bioavailabilities of E-Se and B-Se mice orally administered with a dose of 40 or 80 µg of Se/kg once daily for 7 consecutive days. (B) Hepatic GPx activity. (c) Renal GPx activity. [Reprinted with permission from ref. (368), Wu S, Sun K, Wnag X, Wang D, Wan X, Zhang J, 61:7268–7275, 2013; @ American Chemical Society, 2013]

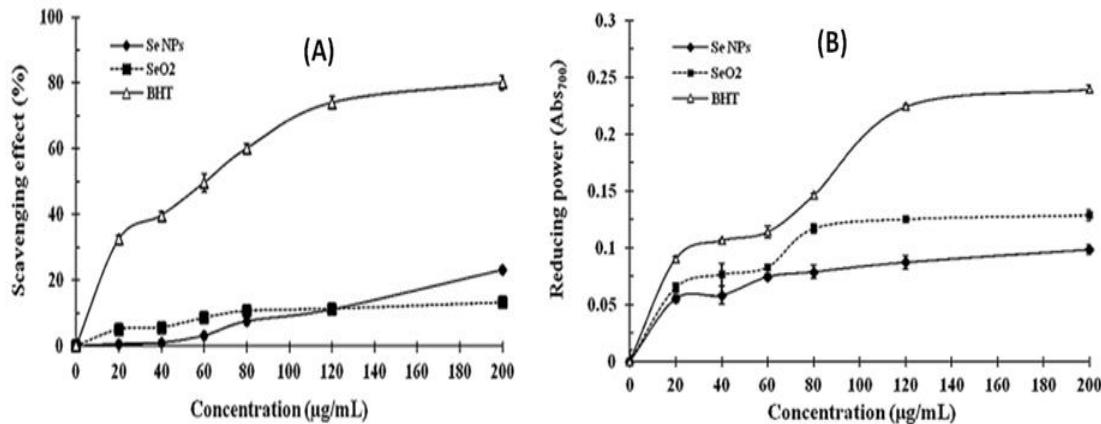


Figure 38: (A) Scavenging effects of biogenic SeNPs and SeO_2 on DPPH free radicals and (b) reducing power of the biogenic SeNPs and SeO_2 compared with BHT as a standard control. Data are mean of triplicate experiments. [Reprinted with permission from ref. (369), Forootanfar H, Adeli-Sardou M, Nikkhoo M, Mehrabani M, Amir-Heidari B, Shahverdi AR, Shakibaie M, 28: 75-79, 2014; @ Elsevier, 2014]

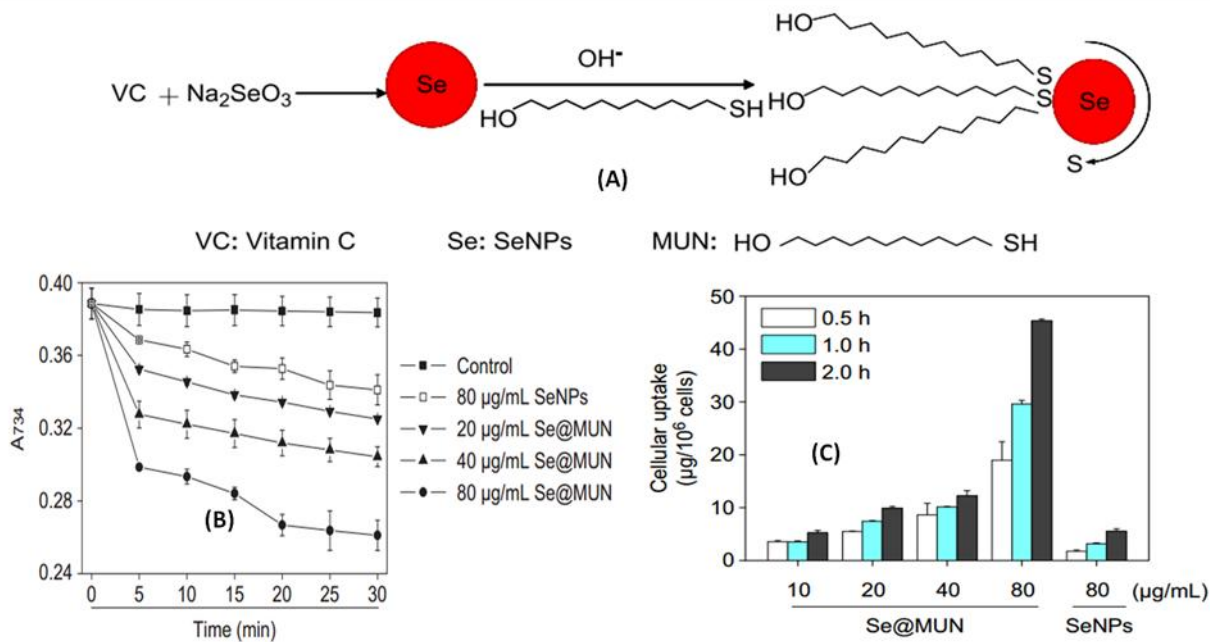


Figure 39. (A) Schematic of the formation of Se@MUN and (B) antioxidant activities, (C) cellular uptake efficiency of 6-coumarin-loaded Se@MUN and SeNPs by HK-2 cells after 0.5, 1.0 and 2.0 h of incubation, respectively. [Reprinted with permission from ref. (375), Li Y, Li X, Wong YS, Chen T, Zhang H, Liu C, Zheng W, 32:9068-9076, 2011; @ Elsevier, 2011].

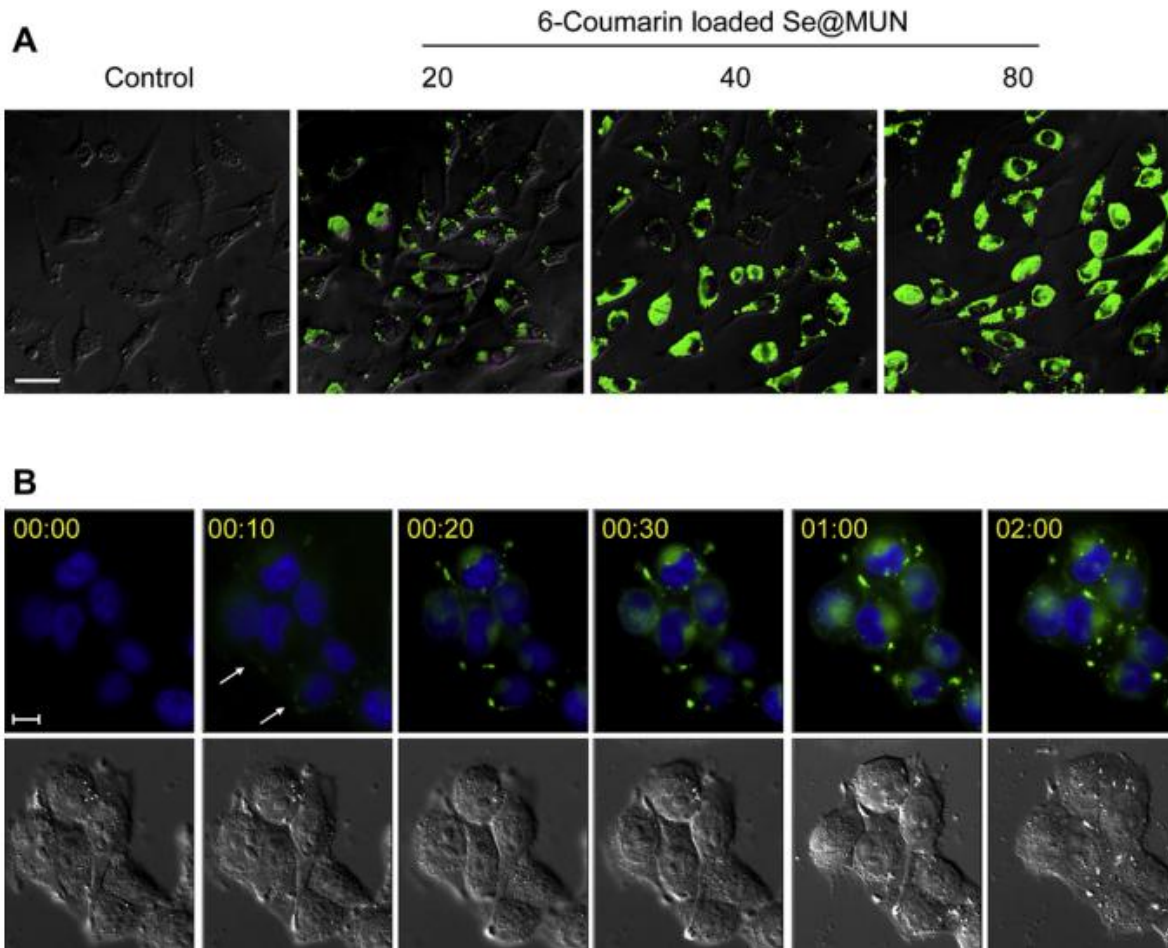


Figure 40. Cellular uptake of Se@MUN. (A) Fluorescence microscope images show the internalization of 6-coumarin-loaded nanoparticles (green fluorescence) in HK-2 cells after 2 h of incubation. (B) Real-time imaging of the same HK-2 cells treated with 20 mg/ml of 6-coumarin-loaded nanoparticles. The cell morphology was captured by a differential internal reflection (DIC) microscope. The nanoparticles and cell nucleus were visualized by green and blue fluorescence, respectively. The upper panel is the merged images of nanoparticles and the nucleus and the lower panels are DIC images. Scale bar: 10 mm. Time presented as h:min. [Reprinted with permission from ref. (375), Li Y, Li X, Wong YS, Chen T, Zhang H, Liu C, Zheng W, 32:9068-9076, 2011; @ Elsevier, 2011].

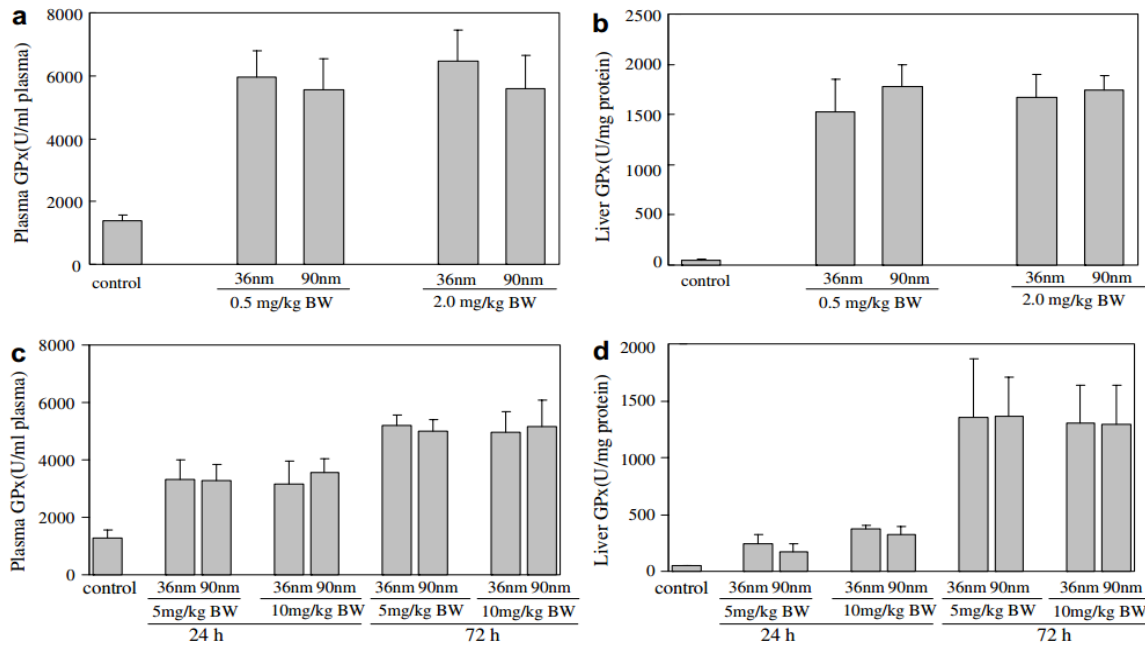


Figure 41. Effect of two sizes of nano-Se on GPx activity. (a) GPx in liver in a short-term model. (b) GPx in plasma in a short-term model. (c) GPx in liver in a single-dose model. (d) GPx in liver in a single-dose model. [Reprinted with permission from ref. (377), Peng D, Zhang J, Liu Q, Taylor EW 101: 1457-63, 2007; @ Elsevier, 2007].

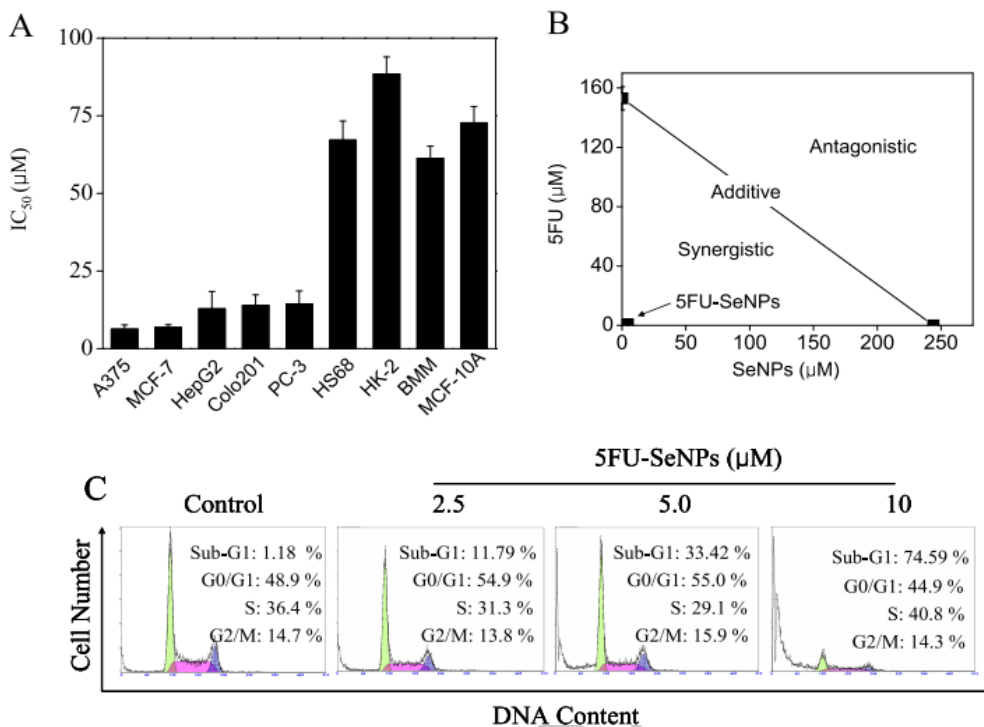


Figure 42. Induction of apoptotic cell death by 5FU-SeNPs. (A) Growth inhibition of 5FU-SeNPs on selected cancer and normal cells (72 h). Cell viability was determined by a colorimetric MTT assay. (B) Isobologram analysis of the anti-proliferative effects of 5FU and SeNPs on A375 cells. (C) Flow cytometric analysis of A375 cells exposed to 5FU-SeNPs for 72 h. [Reprinted with permission from ref. (381a), Liu W, Li X, Wong YS, Zheng W, Zhang Y, Cao W, Chen T. 6: 6578-91, 2012; @ American Chemical Society, 2012].

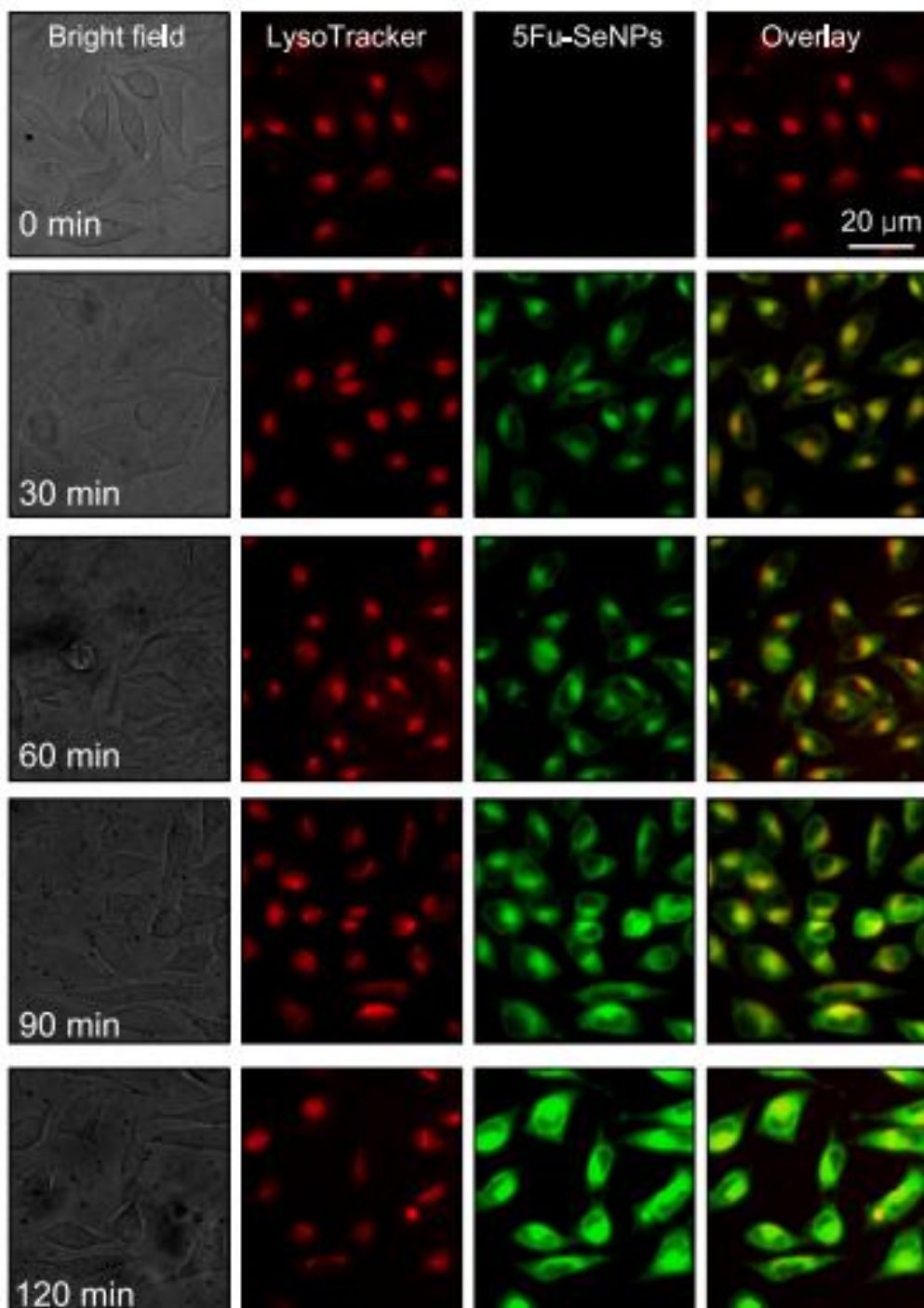


Figure 43. Co-localization of 5FU-SeNPs (green fluorescence) and lysosomes (red fluorescence) in A375 cells. The cells were treated with 40 $\mu\text{g}/\text{mL}$ of 6-coumarin-loaded nanoparticles for different periods of time and visualized under a fluorescence microscope. [Reprinted with permission from ref. (381a), Liu W, Li X, Wong YS, Zheng W, Zhang Y, Cao W, Chen T. 6: 6578-91, 2012; @ American Chemical Society, 2012].

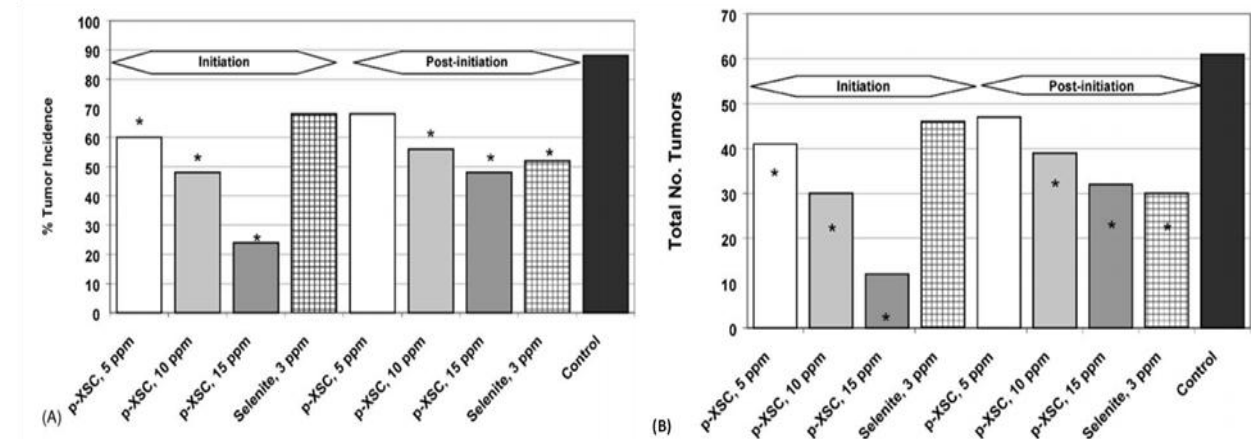


Figure 44. Effect of p-XSC on DMBA-induced mammary cancer. (A) Tumour incidence. (B) Total tumour yield. Supplementation was given 2 weeks prior until 1 week after DMBA administration (initiation) or 1 week after until 25 weeks after DMBA administration (post-initiation). (*) $p < 0.05$. [Reprinted with permission from ref. (395), El-Bayoumy K, Sinha R. 551:181-97; 2004 @ Elsevier, 2004].

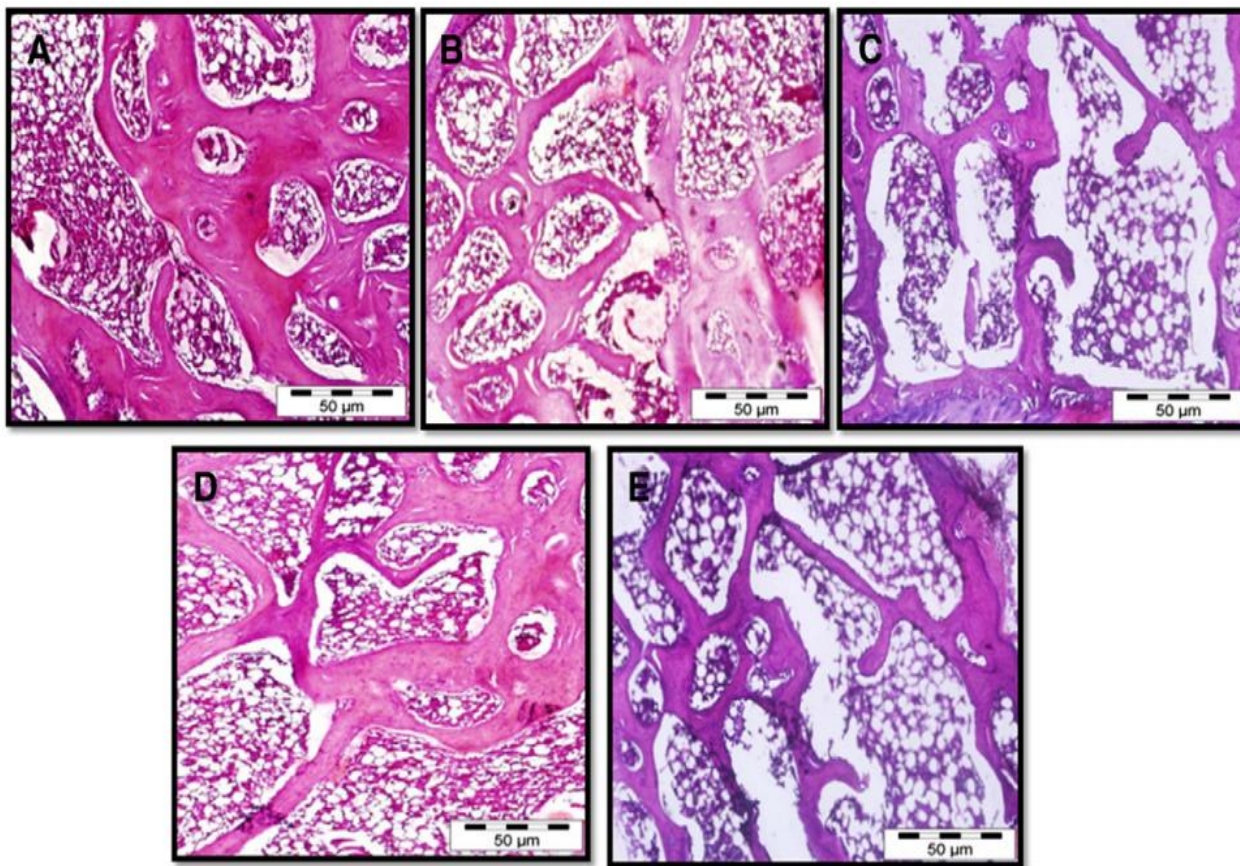


Figure 45. Histopathological examination of rat femur. (A) Normal control, (B) anastrozole control, (C) anastrozole with SeNP low dose (0.25 mg/kg), (D) anastrozole with SeNP medium dose (0.5 mg/kg) and (E) anastrozole with SeNP high dose (1 mg/kg). [Reprinted with permission from ref. (398), Vekariya KK, Kaur J, Tikoo K, 268:212-220; 2013 @ Elsevier, 2013].

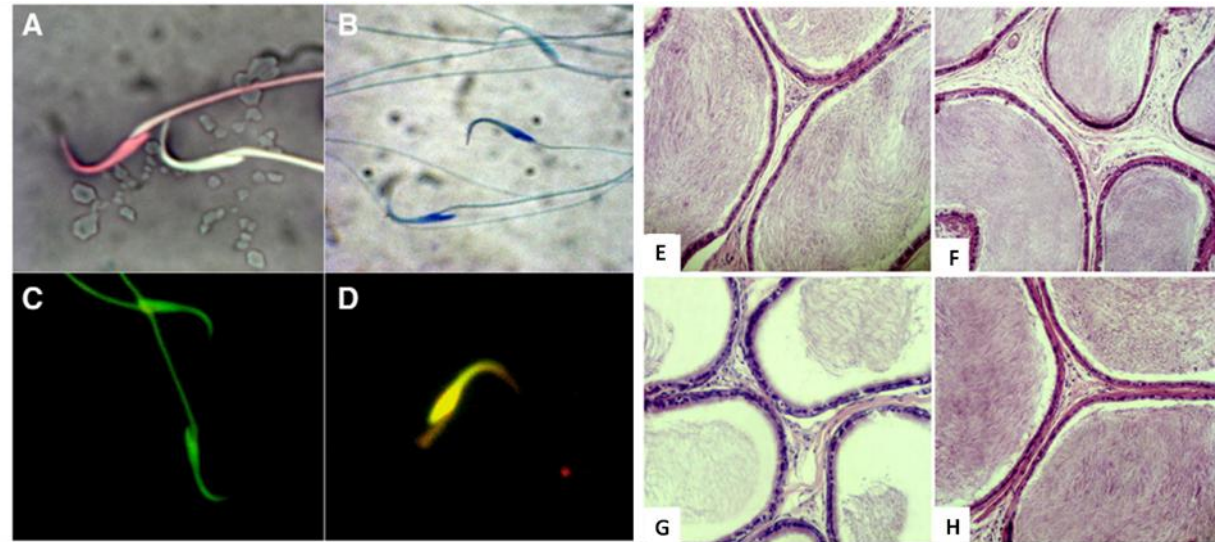


Figure 46. Representation of sperm quality. (A) Eosin-Y staining, dead sperms appear pink and live sperms were not stained. (B) Aniline blue staining for assessment of sperm chromatin quality. Mature sperms are detected as light blue and immature sperms are detected as dark blue. (C) Acridine orange (AO) fluorescent staining for assessment of DNA integrity of cauda epididymal spermatozoa. Normal sperm with intact DNA (double stranded) detected as green (C) and damaged DNA (fragmented) detected as yellow (D). Histopathological feature of sperm concentration in cauda epididymis sections from control group (E), nano-Se (F), CIS (G) and nano-Se+CIS (H). [Reprinted with permission from ref. (399), Rezvanfar MA, Shahverdi AR, Ahmadi A, Baeeri M, Mohammadirad A, Abdollahi M, 266:356-365, 2013; @ Elsevier, 2013].

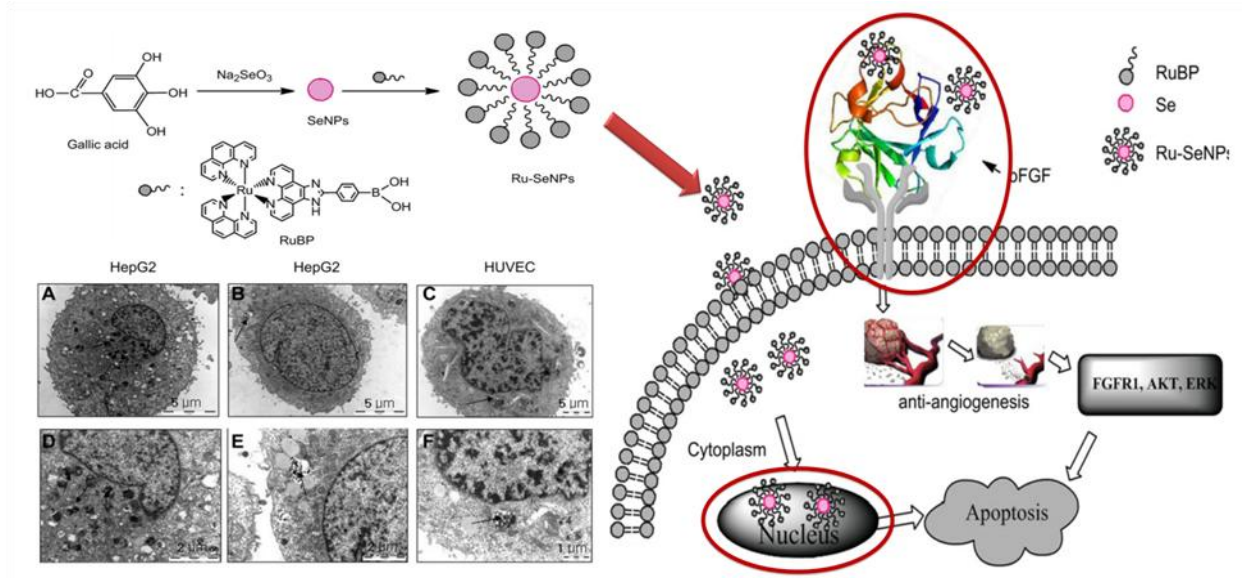


Figure 47. Schematic of the synthesis and mechanistic role of ruthenium-modified selenium nanoparticles (Ru-SeNPs). Representative TEM images showing the ultra-structure of HepG2 cells (A and B) and HUVEC cells (C) treated with 20 mg/mL of Ru-SeNPs for 12 h. Arrows indicate Ru-SeNPs. [Reprinted with permission from ref. (367), Sun D, Liu Y, Yu Q, Qin X, Yang L, Zhou Y, Chen L, Liu J, 35:1572-1583, 2014; @ Elsevier, 2014].

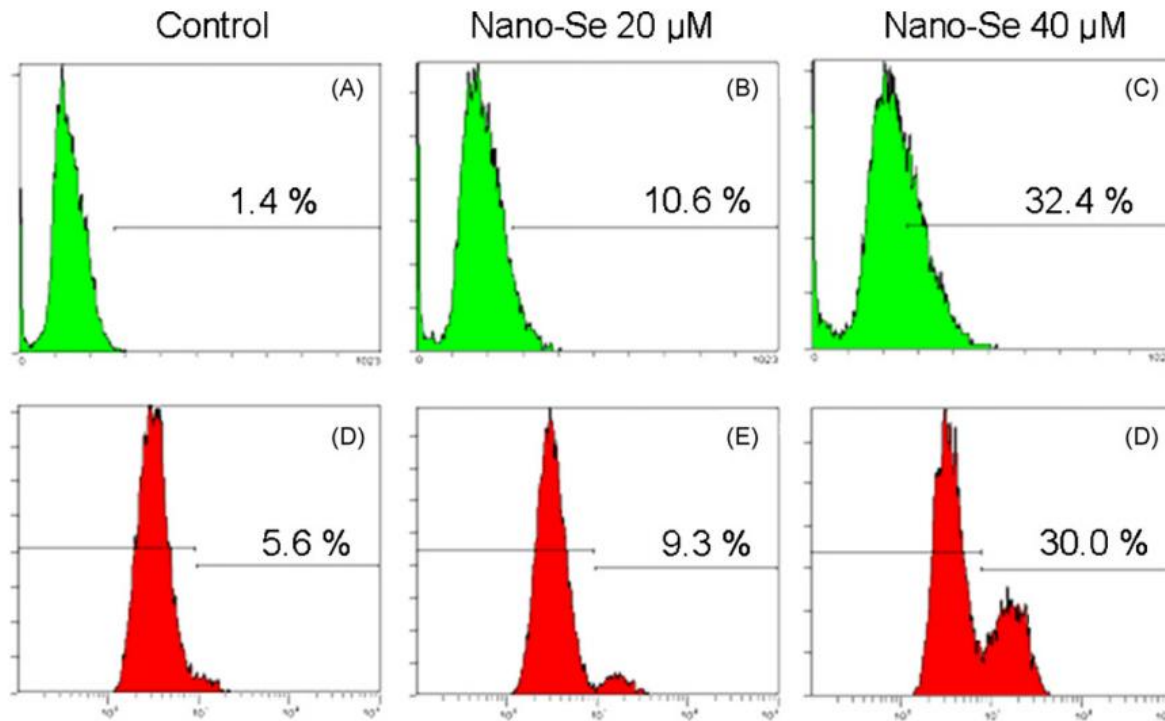


Figure 48. Oxidative stress (A–C) and depletion of mitochondrial membrane potential (D–F) in A375 cells induced by nano-Se. Cells were treated with nano-Se for 24 h. (A–C) Intracellular ROS generation was determined by measuring the fluorescence intensity of an oxidation-sensitive fluorescein DCFH-DA on a flow cytometer. (D–F) Cells after treatment were stained with a mitochondria-selective dye JC-1 and analyzed by flow cytometry. The number indicated in each histogram represents the percentage of cells that emit green fluorescence due to the depletion of mitochondrial membrane potential. [Reprinted with permission from ref. (400), Chen T, Wong YS, Zheng W, Bai Y, Huang L, 67:26-31, 2008; @ Elsevier, 2008].

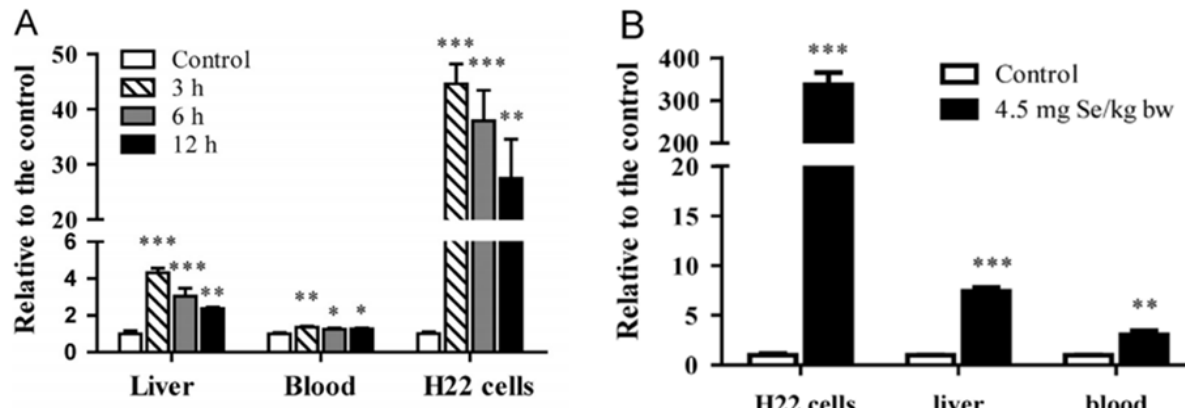


Figure 49. Se distribution in the liver, blood and H22 cells (A) 0.7 mg Se/kg bw intraperitoneally (B) after 1 h post-Se treatment. [Reprinted with permission from ref. (366), Wang X, Sun K, Tan Y, Wu S, Zhang J, 72:1-10, 2014; @ Elsevier, 2014].

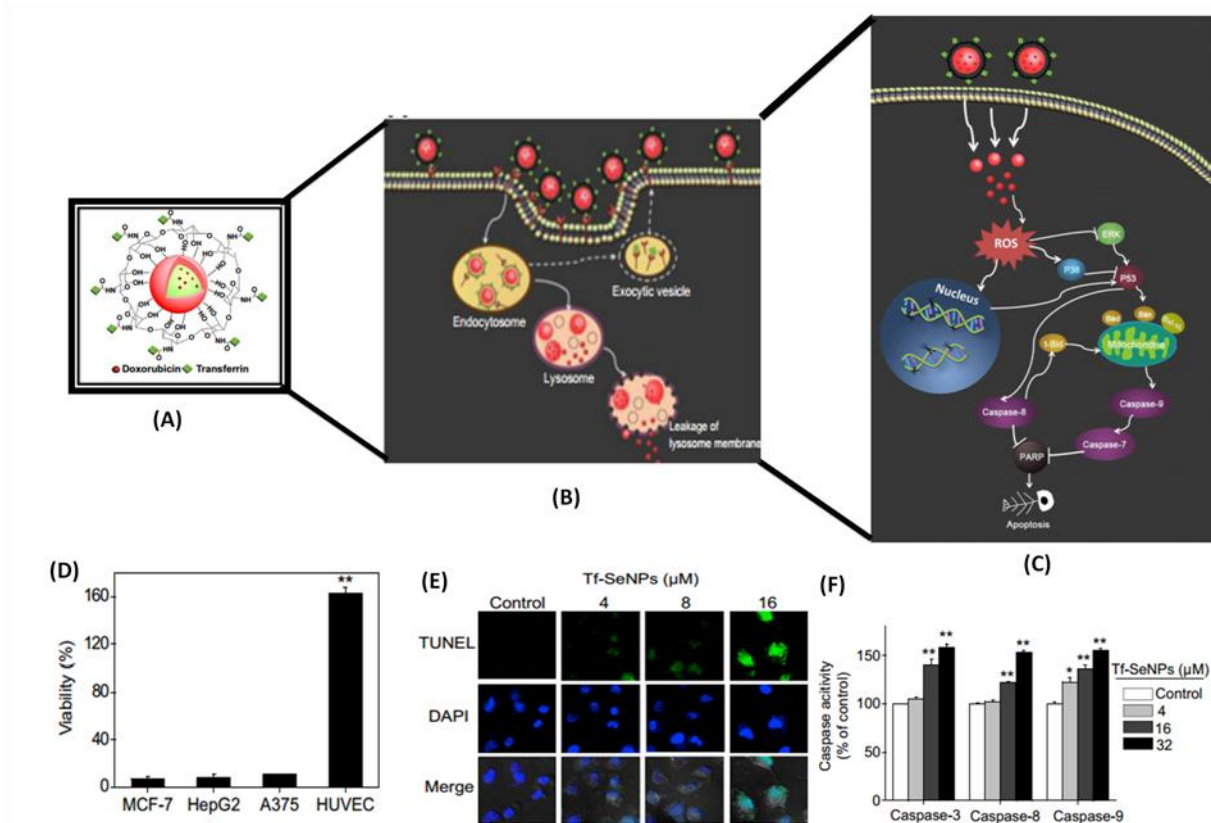


Figure 50. Schematic of doxorubicin-loaded Tf-Se nanoparticles (A) with selective uptake and intracellular localization (B) and (C) apoptosis signalling pathways of Tf-SeNPs. (D) Growth inhibition effect of TF-Se in different cell lines. (E) DNA fragmentation and respective (F) caspase activity of Tf-Se nanoparticles. [Reprinted with permission from ref. (402), Huang Y, He L, Liu W, Fan C, Zheng W, Wong YS, Chen T 34:7106-7116, 2013; @ Elsevier, 2013].

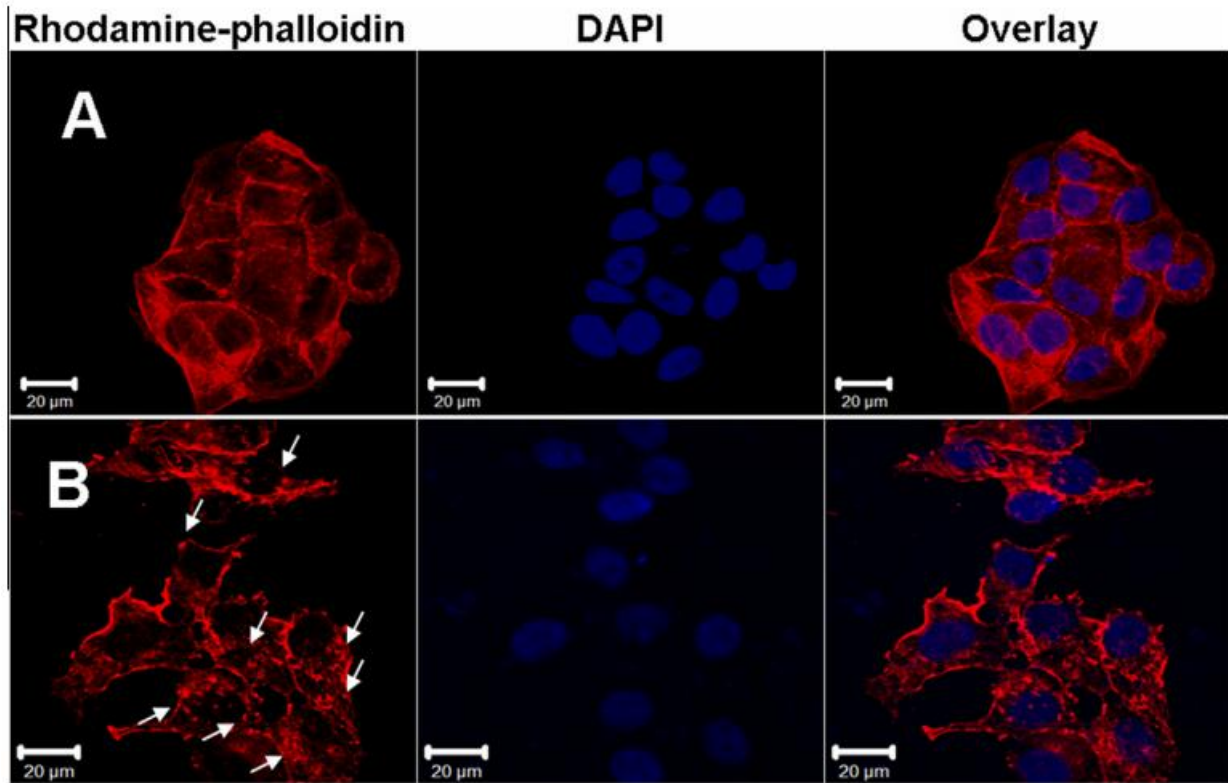


Figure 51. Effects of SeNPs on the structures and amounts of F-actin in MCF-7 cells. Fluorescence staining of F-actin structures of (A) control and (B) 5 1 g/mL SeNP-treated MCF-7 cells; dot-like structures of F-actin are indicated by white arrows. [Reprinted with permission from ref. (403), Kong L, Yuan Q, Zhu H, Li Y, Guo Q, Wang Q, Bi X, Gao X, 32:6515-6522, 2011; @ Elsevier, 2011].

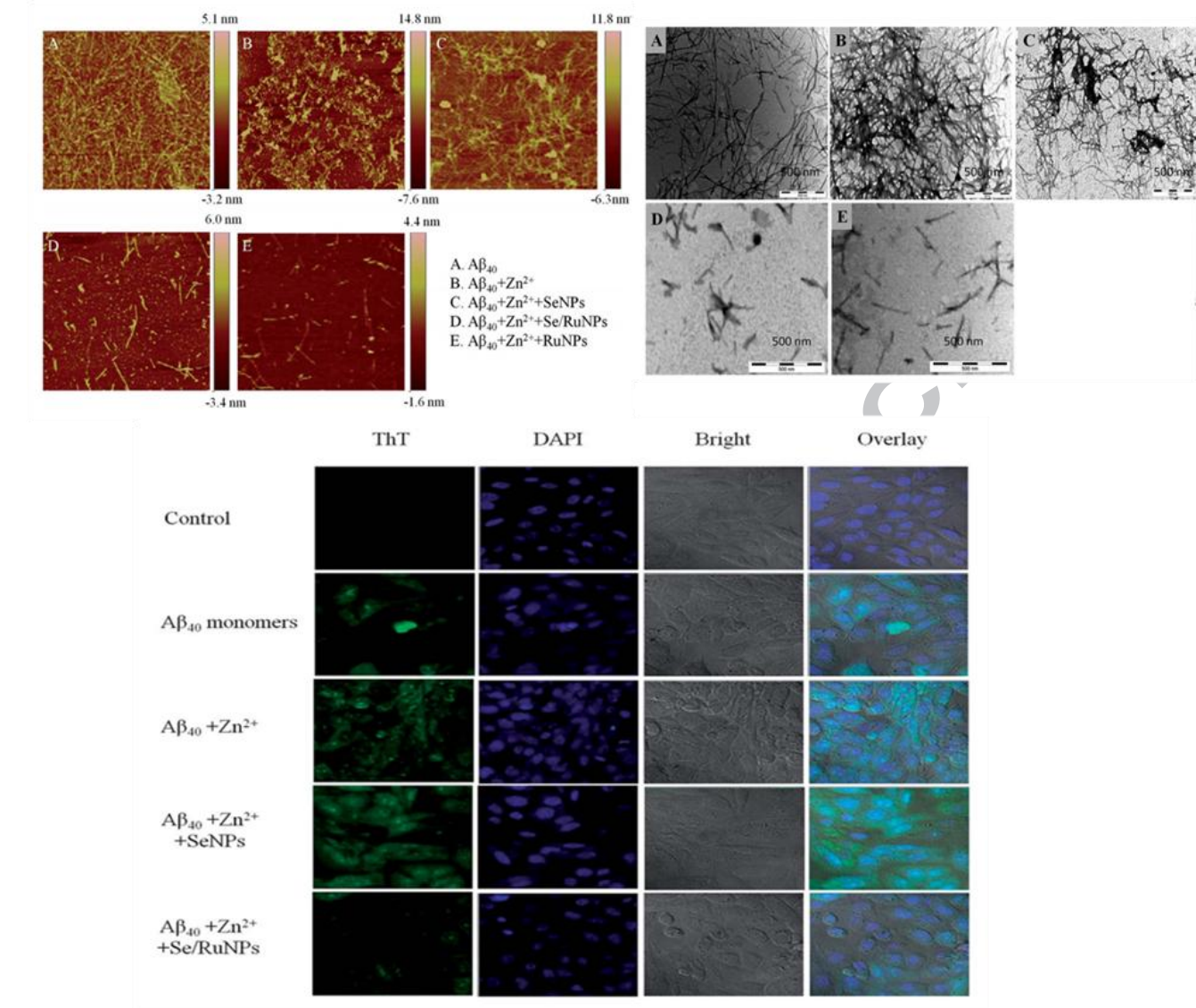


Figure 52. AFM and TEM images of the morphologies of $\text{A}\beta_{40}$ fibrillization. $\text{A}\beta_{40}$ were incubated with (a) and without Zn^{2+} (b) and/or SeNPs (c), Se/RuNPs (d) and RuNPs (e) for 3 days, respectively. $\text{A}\beta_{40} = 30 \text{ mM}$, $[\text{A}\beta_{40}]:[\text{Zn}^{2+}] = 1:2$, NPs = $60 \mu\text{g ml}^{-1}$. The corresponding Se/RuNPs inhibited intracellular $\text{A}\beta_{40}$ aggregates at different conditions. Reprinted with permission from [370], Yang L, Chen Q, Liu Y, Zhang J, Sun D, Zhou Y, Liu 2, 1977–1987, 2014, @ 2014, RSC.

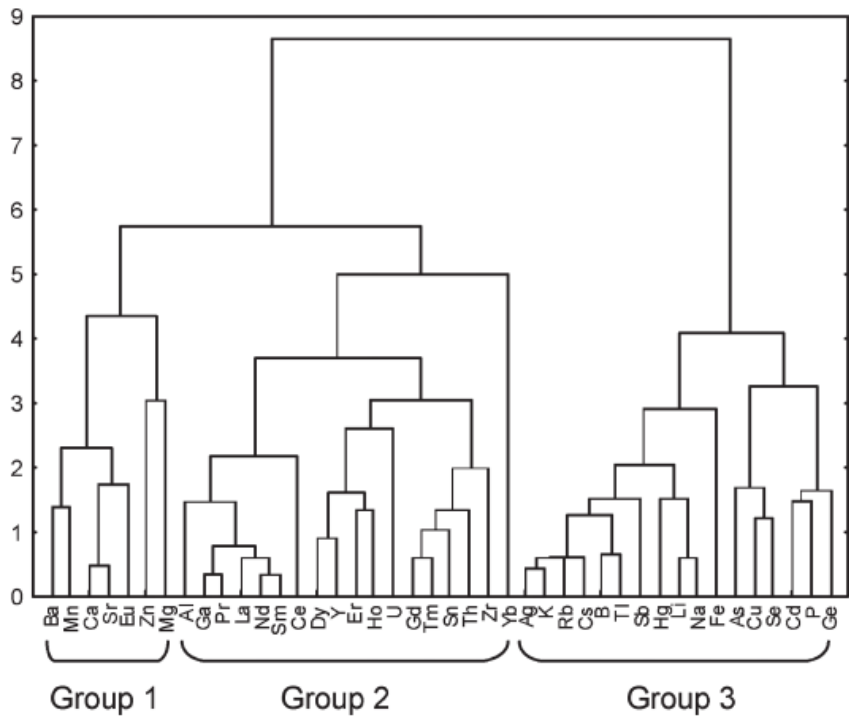


Figure 53: Cluster analysis (Euclidean distance, complete linkage) of the elements based on accumulation behavior during the development and ripening of berries. [Reprinted with permission from ref. (432), Bertoldi D, Larcher R, Bertamini M, Otto S, Concheri G, Nicolini G, 2011:59:7224–7236.; @ ACS, 2011].

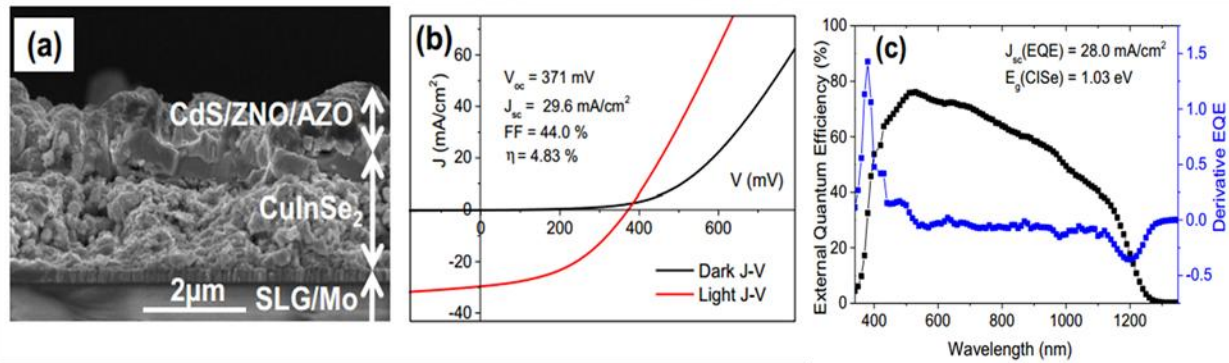


Figure 54. Cross-sectional SEM image of the SLG/Mo/CuInSe₂/CdS/ZnO/AZO solar cell, with the printed CuInSe₂ absorber layer (a) current–voltage curve of the device under dark and light conditions (b) and external quantum efficiency (EQE) of the device as a function of wavelength (c). [Reprinted with permission from ref. (446), Zaghi AE, Buffière M, Brammertz G, Batuk M, Lenaers N, Kniknie B, Hadermann J, Meuris M, Poortmans J, Vleugels J, 2014,25:1254-1261. 2014; @ Elsevier, 2014].

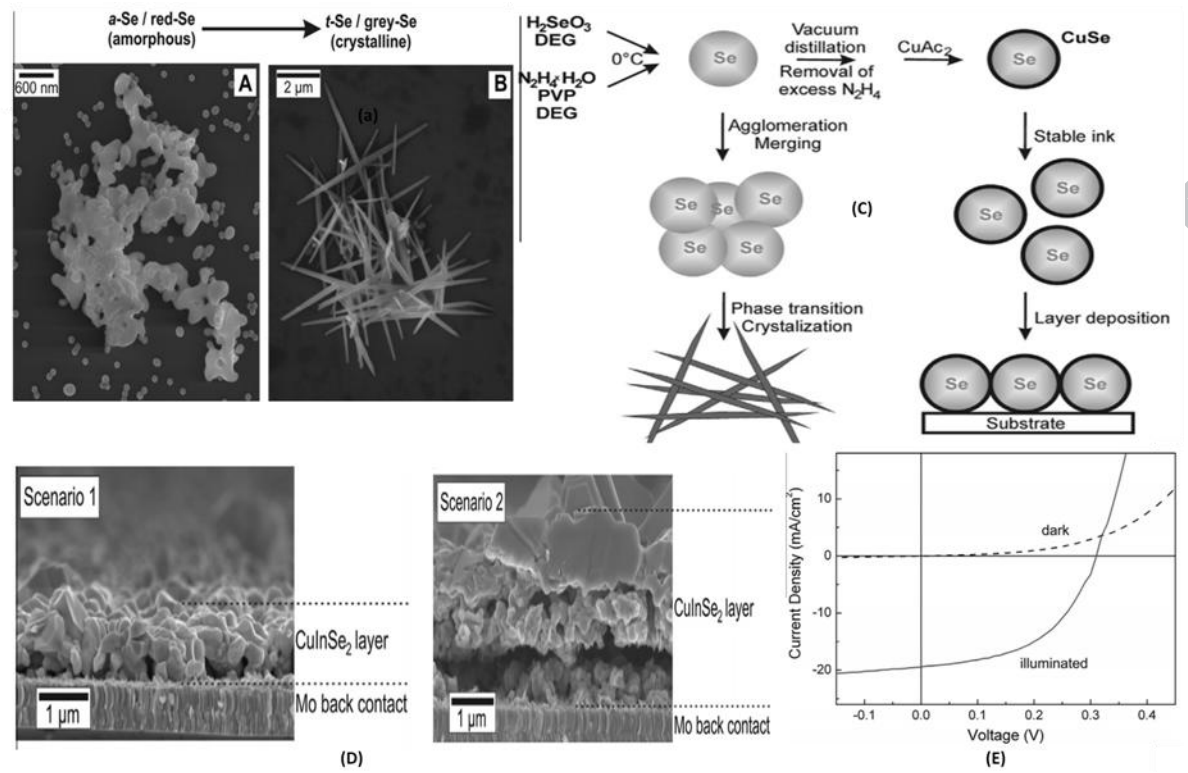


Figure 55. The corresponding SEM images (A–B) showing phase transitions of Se nanoparticles. (C) Schematic illustration of the formation of thin-layer solar cells. (D) Selenization behaviour of Se-modified thin-layer solar cells and (E) current voltage characteristic of the as-synthesized solar cells of Se nanoparticles. [Reprinted with permission from ref. (447), Dong H, Quintilla A, Cemernjak M, Popescu R, Gerthsen D, Ahlswede E, Feldmann C, 415:103-110, 2014; @ Elsevier, 2014].

Table. 1. The obtained diameter of Se⁰ nanoparticles with different saccharides.

| Concentration Of Se ⁰ ($\mu\text{mol/L}$) | Average diameter (nm) | Major distribution range of diameter (nm) | Average diameter (nm) | Major distribution range of diameter (nm) |
|---|-----------------------------|---|-----------------------------|---|
| Se⁰ | | | | |
| 1.07 | 74 | 71 | 69-83 | 68 |
| 10.7 | 343 | 321 | 314-359 | 336 |
| 21.4 | 379 | 351 | 308-395 | 376 |
| 32.2 | 413 | 417 | 344-447 | 386 |
| 42.8 | 574 | 585 | 469-583 | 582 |
| Se⁰ -40% Glucose | | | | |
| 1.07 | 74 | 23 | 22-23 | 19 |
| 10.7 | 343 | 30 | 27-41 | 31 |
| 21.4 | 379 | 40 | 34-51 | 38 |
| 32.2 | 413 | 52 | 40-67 | 51 |
| 42.8 | 574 | 63 | 55-71 | 61 |
| 107 | 1086 | 160 | | 138 |
| 268 | | | | 457 |
| Se⁰ -1.0% Sucrose | | | | |
| 1.07 | 74 | 23 | 22-23 | 19 |
| 10.7 | 343 | 30 | 27-41 | 31 |
| 21.4 | 379 | 40 | 34-51 | 38 |
| 32.2 | 413 | 52 | 40-67 | 51 |
| 42.8 | 574 | 63 | 55-71 | 61 |
| 107 | 1086 | 160 | | 138 |
| 268 | | | | 457 |
| Se⁰ -0.1% Chitosan | | | | |
| 1.07 | 74 | 1 | 1-2 | 2 |
| 10.7 | 343 | 8 | 7-11 | 12 |
| 21.4 | 379 | 15 | 13-22 | 39 |
| 32.2 | 413 | 13 | 13-22 | 46 |
| 42.8 | 574 | 20 | 20-28 | 51 |
| 107 | 31 | 30-36 | | 65 |
| 268 | 72 | 59-89 | | 71 |
| 536 | 172 | 140-175 | | 112 |
| 1072 | 180 | 134-238 | | 139 |
| Se⁰ -0.021% ESSP | | | | |
| 1.07 | 74 | 1 | 1-2 | 2 |
| 10.7 | 343 | 8 | 7-11 | 12 |
| 21.4 | 379 | 15 | 13-22 | 39 |
| 32.2 | 413 | 13 | 13-22 | 46 |
| 42.8 | 574 | 20 | 20-28 | 51 |
| 107 | 31 | 30-36 | | 65 |
| 268 | 72 | 59-89 | | 71 |
| 536 | 172 | 140-175 | | 112 |
| 1072 | 180 | 134-238 | | 139 |
| 120-138 | | | | |

Table 2 Summary of various approaches for Se nanostructure synthesis.

| Structure type | Size of the particles | Growth reagent | Growth conditions | Reference |
|----------------|---|---|--|-----------|
| Se nanospheres | 60–110 nm | Na ₂ SeO ₃ , H ₄ SiW ₁₂ O ₄₀ , H ₃ PW ₁₂ O ₄₀ | Photolysis of aqueous solution | [63] |
| | >100 nm | H ₂ SeO ₃ , H ₂ SeO ₄ , HCOOH | Photolysis by 200W Hg lamp at pH 3.5 | [70] |
| | ~150 nm | Metallic Se, W(CO) ₆ , Co ₄ (CO) ₁₂ | Electrochemical oxidation | [118] |
| | ~300 nm | Na ₂ SeO ₃ , sodium lactate, | Biosynthesis via Se respiring bacteria | [124] |
| | 100–200 nm | H ₂ SeO ₃ , PVP, Sodium acrylate | Polymeric template method | [199] |
| | 40–3000 Å | H ₂ SeO ₃ , N ₂ H ₄ | AOT microemulsion method | [212] |
| Se nanorods | Length = 487 nm Width = 59 nm | H ₂ SeO ₃ , N ₂ H ₄ , H ₆ TeO ₆ , | Reflux at 100°C for 2 h | [96] |
| | Length = 10 μm Width = 20 to several hundred nms | Se powder | Nd:YAG laser of 1064-nm wavelength | [77] |
| | Diameter = 40–120 nm Length = 1–2.5 μm | SeO ₂ , EG | Microwave polyol method at 195°C for 30 min | [225] |
| Se nanowires | Diameter = 6–20 nm Length = 1–30 μm | Se powder | 355 nm beamed laser | [85] |
| | Diameter > 100 nm | Se powder | Chemical vapour deposition method | [99] |
| | Diameter = 180–250 nm Length = 1–2 cm | SeO ₂ , NH ₃ | Autoclave at 180–200°C for 72 h | [157] |
| | Diameter = 60 nm Length = 6 μm | SeO ₂ , EG | Microwave polyol method | [225] |
| Se nanotubes | Width = 200–500 nm | Se powder, NH ₃ , ethanol | Hydrothermal process at 200°C with subsequent sonication of 30 min | [160] |
| | Thickness = 120 nm | SeO ₂ , Tween 20, N ₂ H ₄ .H ₂ O | Micellar method | [214] |
| Se nanobelts | Diameter ~ 80 nm Thickness ~ 25 nm | SeO ₂ , glucose, PVP, ethanol, NH ₃ | Autoclave at 160°C for 20 h | [161] |
| | Width = 100–300 nm Thickness = 30 nm | Na ₂ SeSO ₃ , Brij 78, C ₁₂ EO ₁₀ | Micellar method | [216] |
| Se nanoribbons | Thickness ~ 15 nm Width = 50–300 nm | Metallic Se powder | Vapor liquid solid process | [101] |
| Se nanofilms | Thickness = 100–200 nm | SeO ₂ , N ₂ H ₄ | Room temperature reduction | [93] |
| Se bamboo raft | Width ~ 2 μm | SeO ₂ , ethylene alcohol, cellulose acetate | Autoclave at 160°C for 36 h | [251] |
| Se QDs | Diameter > 5 nm | Se nanopowder with avg size 69 nm | Nd:YAG laser | [86] |

Table 3. Determination of water-extractable Se in medicinal plants (lg/g) by microwave-assisted extraction (ME) as compared to that obtained by conventional extraction (CE)

| Plant sample (local common names) | Part used | Conventional method | Microwave method | % Recovery |
|--|-----------|---------------------|------------------|------------|
| <i>Apium graveolens</i> (Ajmod) | Seeds | 1.59 ± 0.13 | 1.55 ± 0.143 | 97.4 |
| <i>Asparagus racemosus</i> wild (satavara) | Roots | 1.26 ± 0.114 | 1.23 ± 0.116 | 97.6 |
| <i>Avicennia alba</i> blume (Tivar) | Fruits | 1.12 ± 0.098 | 1.09 ± 0.0784 | 97.2 |
| <i>Cassia senna</i> (Sena makki) | Leaves | 1.68 ± 0.131 | 1.65 ± 0.165 | 98.2 |
| <i>Corchorus trilocularis</i> (Mundheri) | Leaves | 1.64 ± 0.124 | 1.59 ± 0.11 | 96.9 |
| <i>Emblica officinalis</i> (Amla) | Fruit | 2.22 ± 0.183 | 2.18 ± 0.165 | 98.2 |
| <i>Aegle marmelos</i> (Bilva) | Fruits | 2.05 ± 0.191 | 2.04 ± 0.116 | 98.0 |
| <i>Mentha arvensis</i> (Podina) | Leaves | 1.90 ± 0.136 | 1.86 ± 0.125 | 97.8 |
| <i>Plantago asiatica</i> (Bartung) | Seeds | 1.66 ± 0.132 | 1.62 ± 0.118 | 96.3 |
| <i>Portulaca oleracea</i> (khurfa) | Seeds | 1.26 ± 0.102 | 1.22 ± 0.087 | 96.7 |
| <i>Withania somnifera</i> (Dunal) | Roots | 1.50 ± 0.112 | 1.45 ± 0.102 | 96.6 |
| <i>Xanthium strumarine</i> (Chota gokhru) | Fruit | 2.21 ± 0.135 | 2.17 ± 0.132 | 98.1 |

Table 4. Sample preparation conditions and band gap variation of selenium nanoparticles.

| No. | [Se] ($\times 10^{-3}$ M) | Stabilizer S | [S] (M or wt%) | Synthesis Temperature (°C) | Eg (eV) |
|----------|-------------------------------|-----------------|--------------------|-------------------------------|---------|
| | | | 0 | | 1.67 |
| 1 | 1.0 | Gelatin | 0.1 | 25 | 1.75 |
| | | | 1.0 | | 1.70 |
| | | | 10.0 | | 1.65 |
| | | | | 4 | 1.85 |
| 2 | 1.0 | Gelatin | 0.1 | 27 | 1.75 |
| | | | | 45 | 1.67 |
| | | | | 80 | 1.66 |
| | | | | 90 | 1.65 |
| | | SDS | 0.1 | | 1.68 |
| | | CPyCl | 0.1 | | 1.47 |
| 3 | 1.0 | SPPh | 5×10^{-3} | 25 | 1.55 |
| | | PVP | 0.1 | | 1.55 |
| | | PEG600 | 0.1 | | 1.44 |

E_g determination error is ± 0.01 .

Table 5. Summary of the shapes, absorption peaks and methods for the synthesis of Se nanostructures

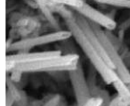
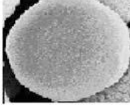
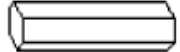
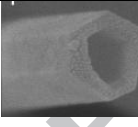
| Shape | Illustration | Absorption Peak (nm) | Method of Synthesis | Reference |
|--------------------|---|----------------------|---|---------------------------------------|
| Sphere |  | 260–600 | Laser method, polymer method | 70,172,164,190 |
| Nanowire |  | 350–650 | Laser ablation method, Thermal evaporation, electrochemical, hydrothermal | 42-48,69,84,87-91,109,130-131,180,187 |
| Nanotubes |  | ~680 | Surfactant method, electrochemical, electrodeposition, hydrothermal | 92,94,127,182,186,89, 224 |
| Nanobelts |  | 300–600 | Surfactant-mediated method, hydrothermal, solvothermal | 117-123,128,180 |
| Microsphere |  | 380–620 | Polymer biosynthetic approach, hydrothermal | 193,198 |
| Nanorods |  | 347–586 | Microwave polyol method, hydrothermal, electro-deposition method | 94,129,135,189 |
| Microtubes |  | 385–780 | Sonication method | 224 |

Table 6. Variation of size and band gap energy with laser ablation time.

| S.No | Ablation time (min) | Band gap E_g (eV) | $\Delta E_g = E_g - E_b$ (eV) | Diameter (nm) |
|------|---------------------|---------------------|-------------------------------|------------------|
| 1 | 0 | 1.72 ± 0.04 | 0.00 ± 0.04 | 69.0 ± 1.5 |
| 2 | 2 | 1.82 ± 0.08 | 0.10 ± 0.12 | 10.5 ± 3.62 |
| 3 | 4 | 2.50 ± 0.10 | 0.78 ± 0.14 | 3.76 ± 1.13 |
| 4 | 6 | 2.63 ± 0.05 | 0.91 ± 0.09 | 3.48 ± 0.336 |
| 5 | 8 | 2.76 ± 0.12 | 1.04 ± 0.16 | 3.25 ± 0.26 |
| 6 | 10 | 2.98 ± 0.06 | 1.26 ± 0.10 | 2.96 ± 1.07 |
| 7 | 15 | 3.19 ± 0.08 | 1.47 ± 0.12 | 2.74 ± 2.32 |

Table 7A. Estimation of TRAP levels in anastrozole and SeNP (0.25, 0.5 and 1 mg/kg)-treated SD rats.

| Parameters | TRAP (U/L) | |
|-------------------------------------|-----------------------|---|
| Groups | Treatment | |
| | Before SeNP treatment | After SeNP treatment |
| Normal control | 7.30±0.31 | 7.32±0.21 |
| Anastrozole control | 9.7±1.15 *** | 13.93±1.45 *** |
| Anastrozole + SeNPs (0.25 mg/kg) | 8.37±0.33 | 8.94±0.48 ** Vs anastrozole control |
| Anastrozole + SeNPs (0.5 mg/kg) | 9.29±0.31 | 7.87±0.24 *** Vs anastrozole control |
| Anastrozole + SeNPs (1 mg/kg) | 9.20±0.19 | 7.21±0.27 *** Vs anastrozole control |

Table 7B. Estimation of TRAP levels in ovariectomized and SeNP (1 mg/kg)-treated SD rats.

| Parameters | TRAP (U/L) | |
|----------------------------|-----------------------|------------------------------------|
| Groups | Treatment | |
| | Before SeNP treatment | After SeNP treatment |
| Normal control | 7.30±0.31 | 7.32±0.21 |
| Ovariectomized | 10.24±0.31 ** | 16.41±0.70 *** |
| Se NPs + ovariectomized | 9.92±0.83 | 9.19±1.29 *** Vs ovariectomized |

Table 8. Effect of functionalization on the *in vitro* anticancer activity of HepG2 and R-HepG2 cells.

| Concentration ($\mu\text{g/ml}$) | Percentage Cell viability | | |
|---------------------------------------|--------------------------------------|--------------|----------------------------|
| | PEG-modified silica nanoparticles | PEG200 alone | Se with no modification |
| 1 | | | 83.5 |
| 2 | 75.2 | | 81.2 |
| 4 | 34.97 | | 76.2 |
| 8 | 17.76 | 94.8 | |
| 16 | 14.8 | 88.9 | |